PETROPHYSICAL EVALUATION OF LITHOLOGY AND MINERAL DISTRIBUTION WITH AN EMPHASIS ON FELDSPARS AND CLAYS, MIDDLE AND UPPER WILLIAMS FORK FORMATION, GRAND VALLEY FIELD, PICEANCE BASIN, COLORADO

by

JEREMY DANIEL RING

B.A., University of Colorado at Boulder, 2008

A thesis submitted to the

Faculty of the Graduate School of the

University of Colorado in partial fulfillment

of the requirement for the degree of

Master of Science

Department of Geological Sciences

2014

This thesis entitled:

Petrophysical evaluation of lithology and mineral distribution with an emphasis on feldspars and clays, middle and upper Williams Fork Formations, Piceance Basin, Colorado

Written by Jeremy Daniel Ring

has been approved by the Department of Geological Sciences

____

Matthew J. Pranter

____

Gus Gustason, III

____

Penny E. Patterson

Date ____________________

The final copy of this thesis has been examined by the signatories, and we find that both the content and the form meet acceptable standards of scholarly work in the above mentioned discipline.

ABSTRACT

Ring, Jeremy Daniel (M.S. Geology [Department of Geologic Sciences])

Petrophysical evaluation of lithology and mineral distribution with an emphasis on feldspars and clays, middle and upper Williams Fork Formations, Piceance Basin, Colorado.

Thesis directed by Professor Matthew J. Pranter

Understanding accessory mineralogy occurrence and distribution is critical to evaluating the reservoir quality and economic success of tight-gas reservoirs, since the occurrence of iron-rich chlorites can decrease resistivity measurements and the occurrence of potassium feldspar increases gamma-ray measurements, resulting in inaccurate water saturation and net-to-gross calculations, respectively. This study was undertaken to understand the occurrence and distribution of chlorite and potassium feldspar in the middle and upper Williams Fork Formations of the Piceance Basin at Grand Valley Field.

Eight lithofacies are identified in core based on grain-size, internal geometry, and sedimentary structures. Four architectural elements (channel fill, crevasse splay, floodplain, and coal) were determined from lithofacies relationships, and then associated with well-log responses. Logs and models were used to determine the occurrence and distribution of lithology, architectural elements, chlorite and potassium feldspar, as well as the relationships between minerals and lithology and architectural elements. Net-to-gross ratios vary stratigraphically, from 8% to 88%, with a higher average in the middle Williams Fork Formation (58.3%) than in the upper Williams Fork

Formation (48.5%). Volumetric proportions vary stratigraphically for both channel fills (18- 75%) and crevasse splays (1-7%).

The average volume percent of chlorite and potassium feldspars are both <1%, with P_{50} values of 1.3% and 7%, respectively. Chlorite is pervasive at the base of the middle Williams Fork Formation: almost 90% of the sandstones in sand-rich intervals contain chlorite. The distribution of chlorite did not vary between reservoir architectural elements, with 70% of both crevasse splays and channel fills containing chlorite.

The results of this study show that, for the middle and upper Williams Fork Formations at Grand Valley Field, 1) there are eight lithofacies and four architectural-element types identified from core; 2) the occurrence and distribution of accessory minerals (<10%) of chlorite and potassium feldspar can be accurately estimated from limited core and well-log data; 3) chlorite occurrence does not vary significantly between reservoir architectural elements; 4) the abundance of chlorite near completion intervals and the occurrence of potassium feldspar in calculated mudstone lithologies indicate a need to re-evaluate the utilization of saturation models and lithology calculations in reservoir-quality evaluations.

DEDICATION

This thesis is dedicated to my parents, Danny and Diane. I love you both for being there for me while also allowing me to fail, learn from my mistakes, and become the person I am today.

ACKNOWLEDGMENTS

I would like to thank Marc Connolly for his time, knowledge and guidance throughout this process and Gabriela Keeton for being the crazy to my calm. I would like to also thank Gus Gustason, Rex Cole, and Penny Patterson for helping me more than I could have asked for. I would be remiss to not thank Matthew Pranter for the opportunity, guidance, and support he has provided to me and the lessons that I have learned from him.

This work would not have been possible without the financial and technical support through the Reservoir Characterization and Modeling Laboratory (RCML) of the Geological Sciences Department at the University of Colorado at Boulder and Matthew Pranter. The following sponsors of the Williams Fork consortium - Phase V are also to thank for their financial, educational, and data contributions: Williams Petroleum, iReservoir.com, Inc., Anadarko Petroleum Corporation, Marathon Oil Company, Bill Barrett Corporation, Newfield Energy, Chevron Corporation, Occidental Petroleum Corporation (Oxy), ConocoPhillips, ExxonMobil, Suncor Energy, Fugro-Jason and Schlumberger.

Last, but not least, I would like to whole-heartedly thank Molica Taing for everything she has done for me and everything she has meant to me. I would never have been able to get through all of this on my own. Her help and support has kept me going when I wanted to give up, smiling when I felt nothing but sadness. I could never express how much I truly appreciate everything she has done for me.

CONTENTS

LIST OF TABLES

LIST OF FIGURES

INTRODUCTION

The Piceance Basin, located in northwestern Colorado, produces natural gas from numerous reservoirs of the Upper Cretaceous Mesaverde Group (Figure 1). Most production is from isolated sandstone reservoirs within the Williams Fork Formation. The reservoirs are interpreted to be the result of meandering- and braided-river deposits, separated from each other by floodplain deposits within coastal-plain and alluvial-plain depositional settings (Johnson, 1989; Hettinger and Kirschbaum, 2002, 2003). Recent research that has focused on evaluating and estimating the spatial distribution and connectivity of the fluvial sandstone reservoirs, both in outcrop and the subsurface include Pranter et al., (2007, 2008, 2009), Yurewicz et al., (2008), Hewlett, (2010), Baytok, (2010), Pranter and Sommer (2011). The high heterogeneity and low static connectivity of the reservoirs has lead to well spacing being reduced from 20 to 10 ac (933 to 660 ft [284 to 201 m]) (Pranter, et al., 2007; Pranter and Sommer, 2011).

General studies by Pitman et al. (1989), Crossey and Larsen (1992), and Webb et al. (2004) have focused on controls and quality of petrophysical properties, while more recent studies have examined the correlation of diagenetic variations of the Williams Fork Formation with core petrophysics and well-log responses (Ozkan et al., 2011). These studies have aided in relating mineralogy and diagenesis to reservoir quality. In particular, chlorite has been observed to be primarily authigenic, based on textures observed in thin sections (Crossey and Larsen, 1992). Chlorite is found as both a pore-fill and a coating around quartz grains in Mesaverde sandstones (Pitman et al., 1989). The relatively small amounts of chlorite are difficult to identify in thin sections, but X-ray diffraction analysis suggests that most chlorite is iron-bearing (Crossey and

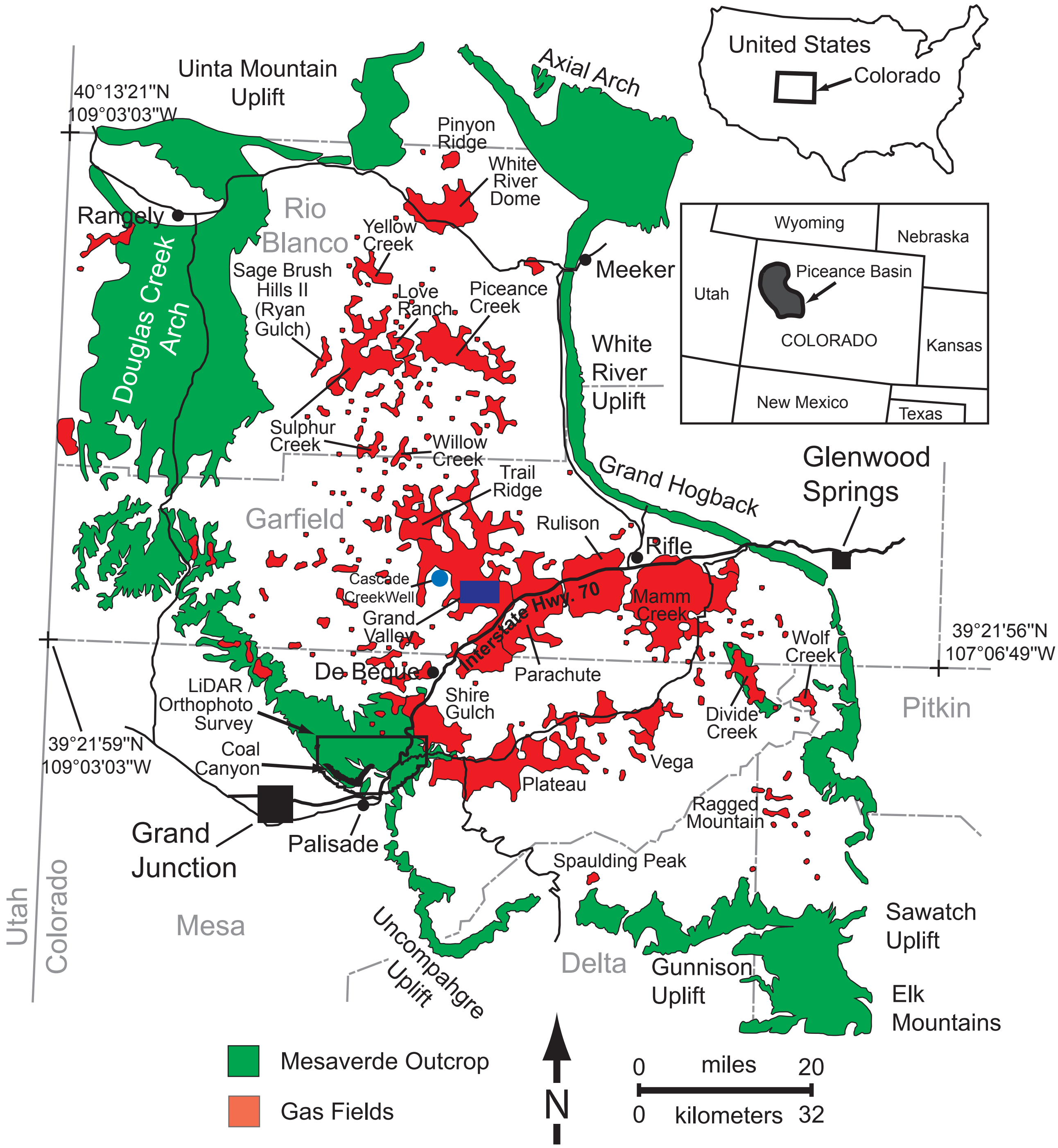

Figure 1. Location map of the Piceance Basin. Current Mesaverde gas fields are shown in red and outcrops of the Mesaverde Group that occur on the margins of the basin are shown in green. The location of the Cascade Creek 697-20-28 well (blue circle) and study area (blue box) within Grand Valley Field are shown. The Cascade Creek 697-20-28 well was used to build and calibrate the petrophysical model.From Pranter et al. (2009). Modified from Johnson (1989), Tyler and McMurry (1995), and Hoak and Klawitter (1997).

Larsen, 1992). Iron-bearing chlorite is of particular interest as it can lower electric-log resistivity considerably due to the high conductivity of the iron (Bowen, 2005).

This study focuses on the spatial distribution of lithology, chlorite, and potassium feldspar within the middle and upper Williams Fork Formations for a portion of Grand Valley Field. Potassium feldspar and chlorite occurrences were calculated from log analysis, and their distributions were compared to lithology and architectural-element type. Because water-saturation calculations rely on accurate resistivity readings, the suppression of resistivity values by iron-bearing chlorite can result in an over-estimation of water saturation for sandstones with iron-bearing chlorite (Durand et al., 2001). Some of the highest reservoir quality in the Williams Fork Formation is observed in the sandstones with grain-coating chlorite (Ozkan et al., 2011), furthering the need to accurately model the saturations of these intervals. The interest in potassium feldspar is due to the increased gamma-ray response caused by the presence of the radioactive potassium (Ozkan et al., 2011), which can decrease the calculated proportions of sandstone (net-to-gross ratio) based on the gamma-ray logs.

This study develops a better understanding of the spatial variability of sandstone deposits of the middle and upper Williams Fork Formations with respect to lithofacies, fluvial architectural elements, and specific mineralogic constituents. Three key research questions that are addressed include: (1) What are the key lithofacies, lithofacies associations, and architectural elements and how are they expressed in log signatures? (2) What is the occurrence of chlorite and potassium feldspar, and how does it vary spatially? (3) Is there a relationship between interpreted reservoir architectural-element types and the distribution of these accessory minerals?

TECTONIC AND STRATIGRAPHIC SETTING

The Piceance Basin is an asymmetrical northwest-southeast-elongated basin bounded by numerous uplifts which developed during the Laramide Orogeny from Late Cretaceous through the Eocene (~75-40 Ma): the Axial Arch on the north, the White River Uplift on the east, the Sawatch Uplift and Elk Mountains on the southeast, the Gunnison Uplift on the south, the Uncompahgre Uplift on the southwest, the Douglas Arch on the west, and the Uinta Mountain Uplift on the northwest (Tweto, 1975; Johnson, 1989). Basement-cored, high-angle reverse-fault uplifts during the Laramide orogeny partitioned the larger Rocky Mountain Foreland Basin system into the multiple basins present today (Johnson and Flores, 2003; DeCelles, 2004). Sediments shed from the Early Cretaceous tectonic uplift of the Sevier highlands in the west were transported towards the Western Interior Seaway by fluvial systems within alluvial- and coastal-plain settings (Hettinger and Kirschbaum, 2002, 2003).

The Mesaverde Group was deposited during Campanian time along the western margin of the seaway (Johnson, 1989), and contains the Iles Formation, Williams Fork Formation, and Ohio Creek Member (Figure 2). Underlying and intertounging with the Mesaverde Group is the Mancos Shale, a marine shale deposited during major incursions of the Western Interior Seaway.

The Williams Fork Formation is composed primarily of strata deposited by fluvial systems in the western portion of the Piceance Basin, with decreasing marine influence over time and towards the west. The Williams Fork Formation is approximately 5000 ft (1524 m) thick near the Grand Hogback on the eastern margin of the basin and thins to

Figure 2. Type-log for Grand Valley Field

GM 522-3 Well (API 05045102210000)

The type log (on the following page) is shown to associate the various intervals used throughout the study. The gamma-ray (GR) log is colored based on lithology, progressing from yellow for sandstone to grey for shale.

GR units are gAPI; Density-Porosity (DPHI) and Neutron-Porosity (NPHI) units are decimal percent. The petrophysical model tops, ROL+X', are surfaces X ft above the Rollins Sandstone Member (ROL).

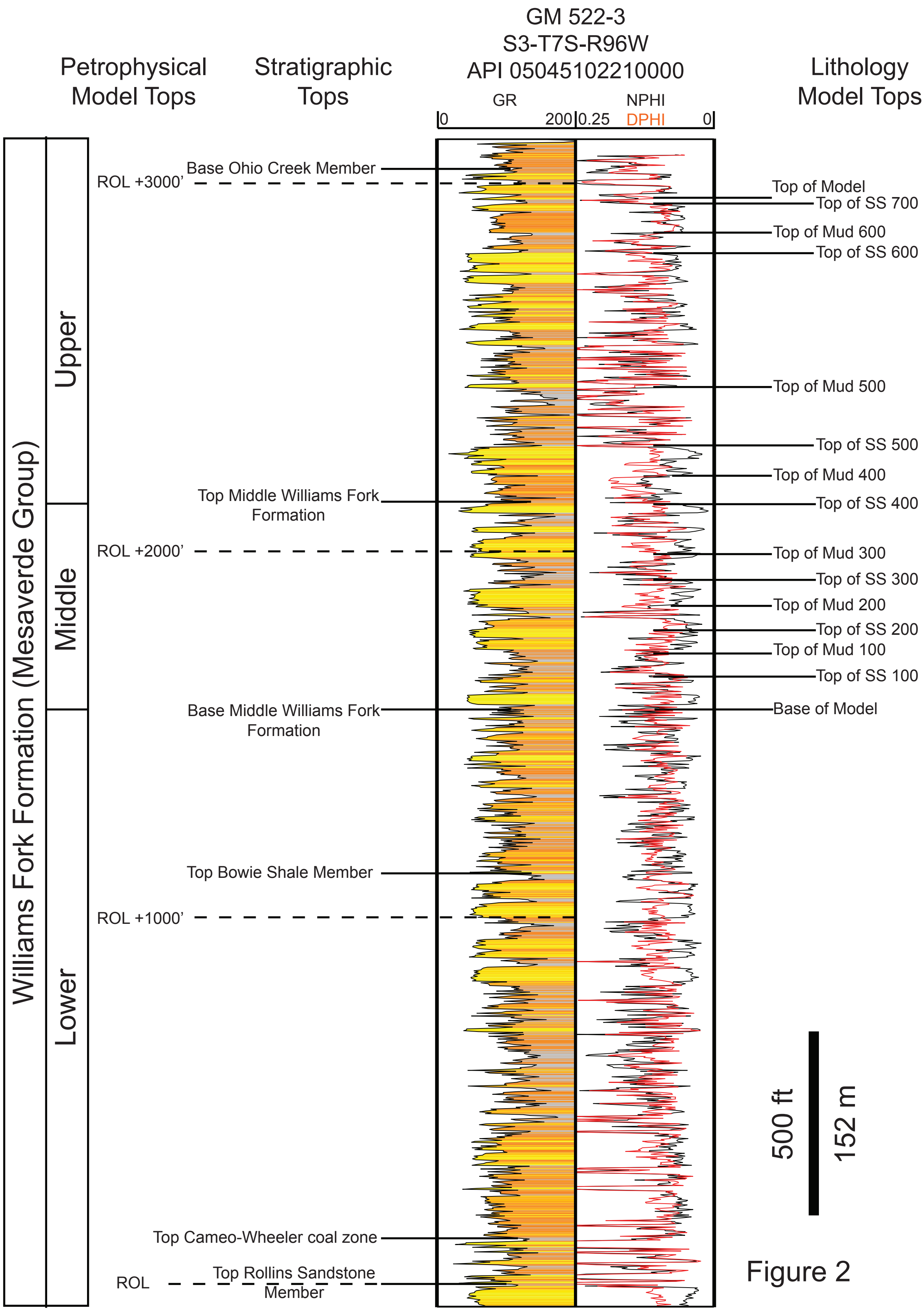
GM 522-3
S3-T7S-R96W
API 05045102210000
Petrophysical Model Tops
Stratigraphic Tops
Lithology Model Tops
GR
0
200
NPHI
0.25
DPHI
0
Williams Fork Formation (Mesaverde Group)
Upper
Middle
Lower
ROL +3000'
ROL +2000'
ROL +1000'
ROL
Base Ohio Creek Member
Top Middle Williams Fork Formation
Base Middle Williams Fork Formation
Top Bowie Shale Member
Top Cameo-Wheeler coal zone
Top Rollins Sandstone Member
Top of Model
Top of SS 700
Top of Mud 600
Top of SS 600
Top of Mud 500
Top of SS 500
Top of Mud 400
Top of SS 400
Top of Mud 300
Top of SS 300
Top of Mud 200
Top of SS 200
Top of Mud 100
Top of SS 100
Base of Model
500 ft
152 m

Figure 2

approximately 1200 ft (365 m) thick at the Colorado-Utah state line (Hettinger and Kirschbaum, 2002, 2003).The Williams Fork Formation is divided into the lower (sandstone-poor), middle and upper (sandstone-rich) Williams Fork Formations (Cole and Cumella, 2005). The uppermost portion of the Williams Fork Formation includes the Ohio Creek Member (or Conglomerate), identified as a white kaolinitic zone which may or may not contain conglomeratic lenses (Johnson and May, 1980). Kaolinite is formed by weathering or hydrothermal alteration of aluminosilicate minerals, and rocks rich in feldspar commonly weather to kaolinite. The Ohio Creek Member is separated from the rest of the Williams Fork Formation by an extensive unconformity, and has been interpreted as lowstand deposits formed by braided-fluvial rivers (Patterson et al., 2003).

The lower Williams Fork Formation was deposited within anastomosing to meandering river systems within a coastal-plain setting (Lorenz, 1987; Johnson, 1989; Hemborg, 2000; Patterson et al., 2003; Cole and Cumella, 2005). In the southeastern Piceance Basin near Mamm Creek Field, the lower Williams Fork Formation consists of offshore, distal to proximal lower shoreface and upper shoreface strata deposited during multiple transgressive-regressive cycles (Shaak, 2010). The middle and upper Williams Fork Formations are interpreted as having been deposited by a low-to-moderate sinuosity braided river system within an alluvial-plain setting (Patterson et al., 2003; Cole and Cumella, 2005; German, 2006). This interpretation has primarily been based on the low-to-moderate range of paleocurrents, the paucity of sandstones with distinct lateral accretion surfaces, and the relatively higher net-to-gross ratio for the middle and upper Williams Fork Formations as well as the observations that the sandstones are highly amalgamated and sheetlike with high width-to-thickness ratios (8:1–100:1; average: 34:1) (German, 2006). Keeton (2012) recognized deposits in outcrop (Plateau Creek Canyon) that support dividing the upper Williams Fork formation into a lower meandering-fluvial system (Flaco interval) and an overlying braided-fluvial system (Ges interval).

The Piceance Basin is a basin-centered gas system as defined by Law (2002): a regionally pervasive gas accumulation that is gas saturated, abnormally pressured, lacks a downdip water contact, and has low-permeability reservoirs. The high pressures created during hydrocarbon generation forced water out of the pores of the sandstones, resulting in an inversion of fluid contacts compared to those encountered in conventional reservoirs: gas-saturated sandstones are located down-dip of gas-water transition zones and water-saturated sandstones (Yurewicz, 2005). The inversion of fluid contacts is an important consideration in saturation and petrophysical modeling.

DATASET AND METHODOLOGY

Grand Valley Field is located in the central area of the Piceance Basin in western Colorado, north of the town of Parachute. The area of interest for this study consisted of approximately 8 mi^2 (20.7 km^2) within Grand Valley Field (Figure 3). This location was selected due to the availability of core and subsurface data, which was utilized for stratigraphic and mineralogical analysis. A 329-well database of logs was analyzed to determine the distribution of lithology and architectural elements. Additional well logs from a 27-well subset were used in conjunction with x-ray diffraction data and core to analyze the occurrence and distributions of potassium feldspar and chlorite.

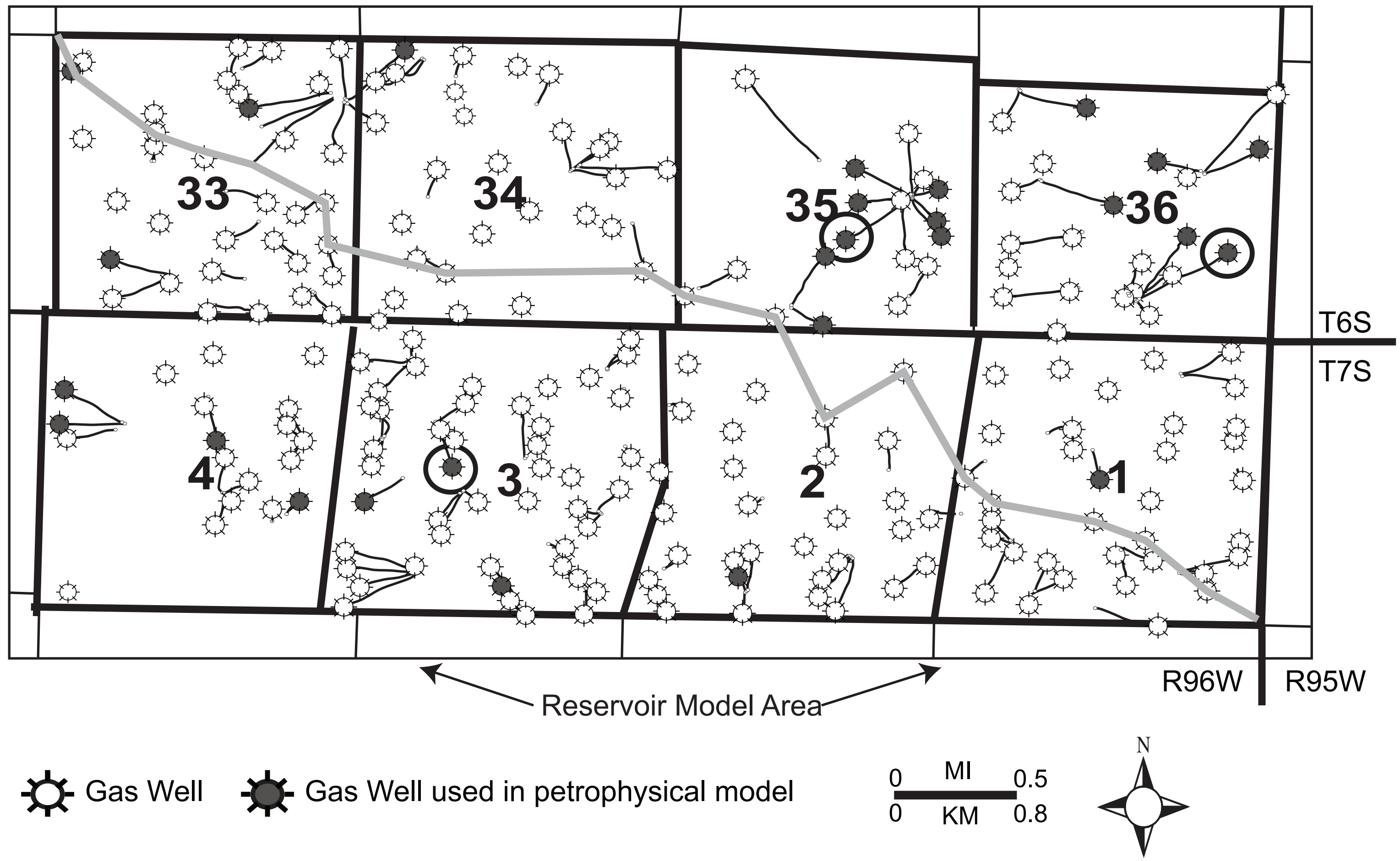

Figure 3: Wells locations (N=329) within the study area in Grand Valley Field, Piceance Basin, Colorado used in the three-dimensional model. The wells with grey in-fill (N=27) were used in the petrophysical model, along with the Cascade Creek 697-20-28 well and core (Figure 1). Circles denote wells for type log (section 3; figure 2), GR standard log (section 36), and NPHI standard log (section 35). The path for the cross-section (Figure 16) is shown.

To understand the sedimentary deposits of the middle and upper Williams Fork Formations at Grand Valley Field, 354 ft (107.9 m) of core from the Cascade Creek 697-20-28 well were described to determine lithology, lithofacies and lithofacies associations (architectural elements). Core observations were compared to their corresponding shale volume (v-shale) logs to determine characteristic log signatures for lithology and architectural elements. The v-shale log measures the proportion of shale, derived from a linear relationship to the normalized gamma ray log.

In order to investigate the stratigraphic distribution of minerals, specifically chlorite and potassium feldspar, petrophysical lithology and saturation models were developed and analyzed. The well-log calculations and subsequent petrophysical (mineralogical) modeling were accomplished using standard industry processes and software.

The petrophysical model was developed for the Cascade Creek 697-20-28 well, which was the closest cored well (6.5 mi; 10.4 km away) to the Grand Valley field study area. The measured weight percent of chlorite and potassium feldspar from the core were compared to the modeled mineral percentages, and the model's input parameters were adjusted until the percentages matched to within a 3% range. The input parameters were subsequently used to model petrophysical properties in the 27 wells within the study area, and mineral proportions and fluid saturation values were calculated for each well.

Three-dimensional (3-D) models were developed in order to understand the stratigraphic variability of lithology and architectural elements within the middle and upper Williams Fork Formations. Additionally, 3-D models of chlorite and potassium feldspar constrained to the petrophysical model results (chlorite and potassium-feldspar proportion logs) were produced to understand the relationships between architectural elements and the occurrence of chlorite and potassium feldspar.

Using sequential-indicator simulation, a lithology model was created to evaluate the spatial distribution of lithology within the middle and upper Williams Fork Formations. The distributions of both chlorite and potassium-feldspar percent were also modeled and constrained independently to the lithology model and upscaled architectural-element logs. As both minerals of interest in this study are generally <10% of the total rock volume, the models were further refined using cutoff values to highlight the areas where a greater relative concentration of each mineral existed within the reservoirs, with higher concentrations of the minerals defined as anything above their P_{50} distribution value. Volumetric calculations for the “high concentration” models were subsequently completed to quantify the significance of the minerals.

LITHOFACIES AND ARCHITECTURAL-ELEMENT ANALYSIS

Types, Characteristics, and Occurrences

Lithofacies, lithofacies associations, and architectural elements were determined from core observations to understand the sedimentary deposits of the middle and upper Williams Fork Formations. Eight lithofacies are identified in the core: contorted mudstone (F_C), laminated mudstone (F_L), contorted sandstone (S_C), planar-laminated sandstone (S_L), ripple-laminated sandstone (S_R), wavy-laminated sandstone (S_{WL}) structureless sandstone (S_S), and coal (C) (Table 1). The eight lithofacies identified in the core are grouped into four lithofacies associations (architectural elements). Lithofacies associations (architectural elements) include channel fill, crevasse splay,

Table 1: Summary of Facies

Facies Name	Facies Code	Description	Interpretation	Picture	Color-Code
Contorted Mudstone /Siltstone	F_C	Description: Dark-to-light grey mudstone and/or siltstone with soft-sediment deformation. Grain-size is predominantly mudstone, but can vary up to very-fine-grained sandstone. Contact: Sharp with sandstones, gradational with mudstones Thickness: 0.5' - 3.5' Internal Geometry: Contorted, structureless; vertical and horizontal bioturbation	Floodplain deposit or top of upward-fining channel-fill sequence.		
Planar-Laminated Mudstone	F_L	Description: Dark-to-light grey mudstone, composed of silt-sized material. Faint to strong laminations, or fissile. Contact: Both sharp and gradational with all other facies. Thickness: 0.5' - 10' Internal Geometry: structureless to planar- and wavy-laminated. Laminations darker than surrounding rock.	Floodplain deposit or top of upward-fining channel-fill sequence.		
Contorted Sandstone	S_C	Description: Very-fine- to medium-grained sandstone, with up to 50% interbedded mudstone. Contorted and bioturbated. Contact: Seemless into other sandstone facies, gradational into mudstones. Thickness: 1.0' to 4.0' Internal Geometry: Sedimentary structures present, but distorted. Convoluted laminations, bioturbation.	Crevasse splay or channel fill sandstone with post-depostional deformation.		
Planar-Laminated Sandstone	S_L	Description: Very-fine- to medium-grained sandstone with planar laminations and clasts of mud/coal Contact: Erosional and gradual with other sandstones, gradational into mudstones. Thickness: 1.0' - 16' Internal Geometry: Parallel laminations of varying apparent inclination, basal clasts of mudstone and coal(?).	Channel fill	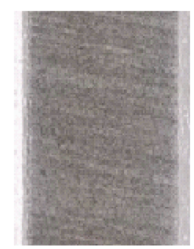	

Table 1: Summary of Facies (Continued)

Facies Name	Facies Code	Description	Interpretation	Picture	Color-Code
Ripple-Laminated Sandstone	S_R	Description: Very-fine- to upper-fine-grained sandstone with interbedding with mudstones. Contact: Gradational from sandstones and into mudstones. Thickness: 0.5' - 3.0' Internal Geometry: Asymmetric ripples, mud drapes on top of ripples	Top of crevasse splay or portion of channel fill		
Wavy-Laminated Sandstone	S_{WL}	Description: Very-fine- to upper-fine-grained sandstone with laminations and containing carbonaceous debris. Contact: Primarily gradational with both mudstones and sandstones. Thickness: 1.0' - 4.0' Internal Geometry: Wavy, semi-parallel laminations with occasional mud draping on the laminations.	Top of crevasse splay or portion of channel fill		
Structureless Sandstone	S_S	Description: Upper-fine- to medium-grained sandstones with rip-up clasts. Contact: seemless to erosional with sandstones, denoted by basal rip-up clasts. Thickness: 1.0' - 4.0' Internal Geometry: No discernable sedimentary structures, but basal clasts of mudstones and coal(?) are present.	Channel fill		
Coal	C	Description: Coal and coal streamers. Contact: Sharp Thickness: N/A in interval; 0.5' - 12' below interval Internal Geometry: Contorted, structureless.	Marsh/floodplain		

Table 2: Summary of Architectural Elements

Architectural Element Name	Description	Interpretation	Color-Code
Channel Fill	Overall fining upward, 1' - 13' sequence including all facies other than coal	Point Bar or Channel Bar	
Crevasse Splay	Overall coarsening upward, 1' - 6' sequence. Sandstone facies transitioning into mudstone facies	Crevasse Splay	
Floodplain	Mudstones isolated between sandstone bodies or unassociated with any other facies	Floodplain	
Coal	Carbonaceous black coal	Floodplain	

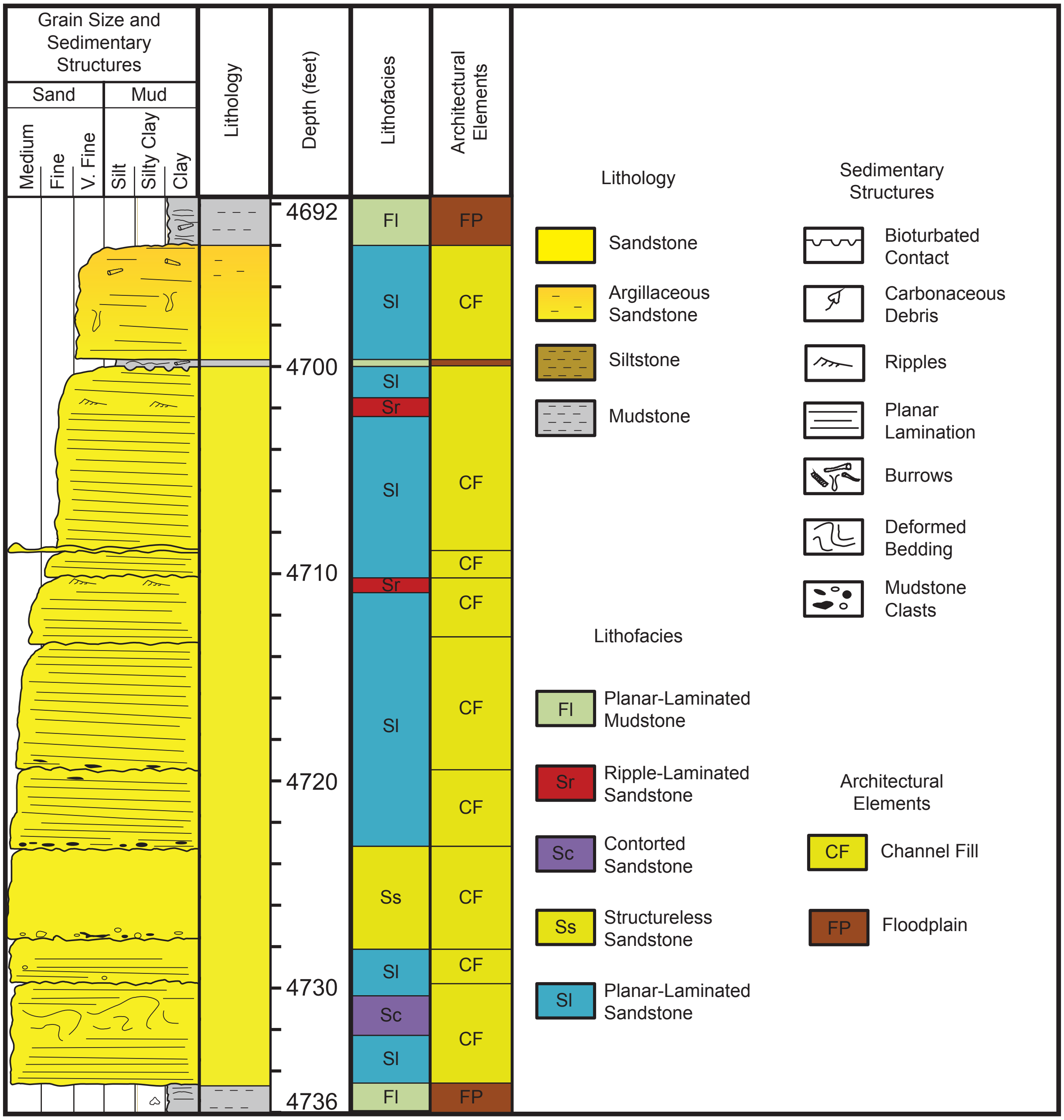

Figure 4. Fining-upward succession of deposits from the upper Williams Fork interval of the Cascade Creek 697-20-28 well, including core description, lithology, and interpretation of lithofacies and architectural elements.

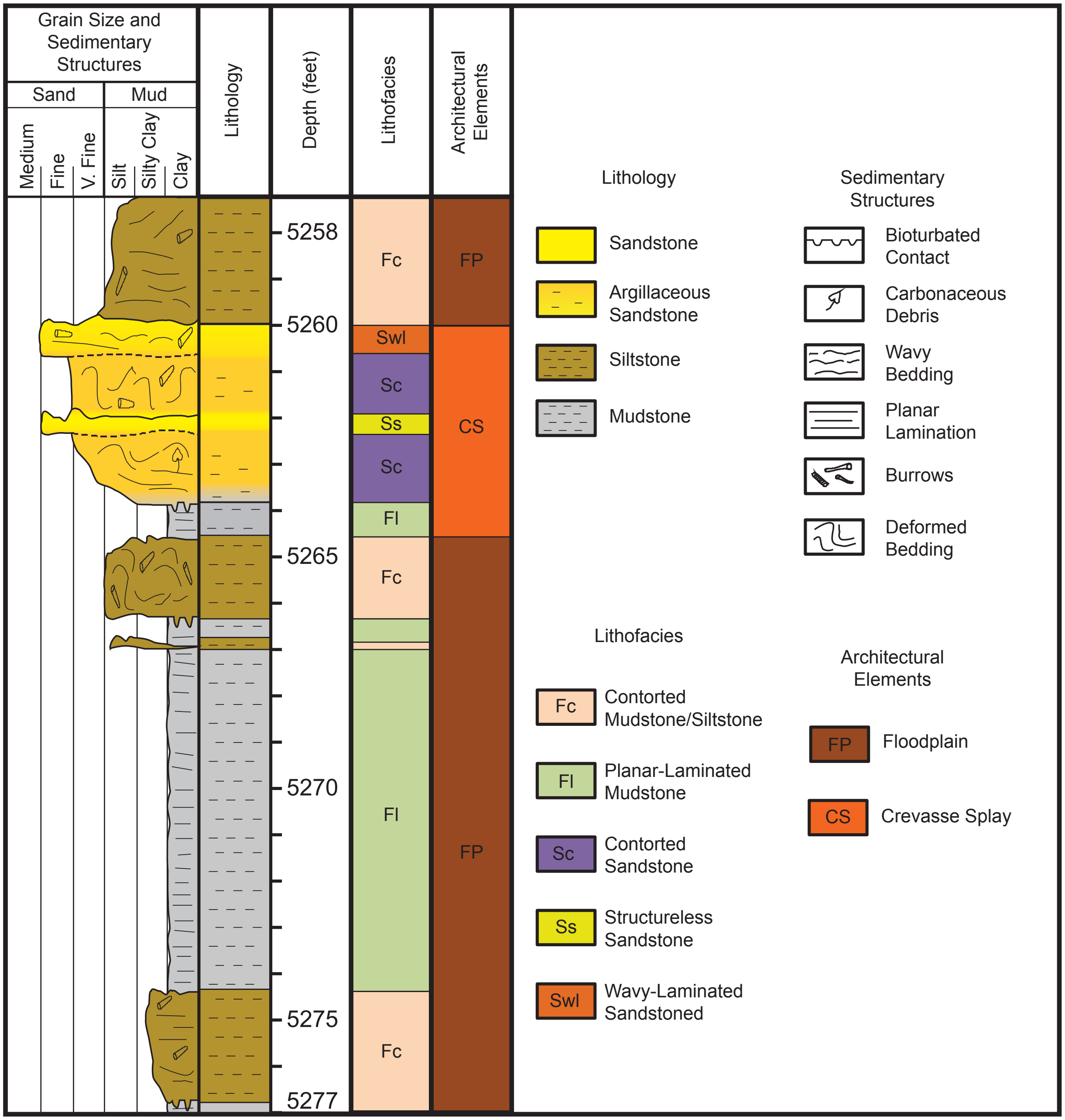

Figure 5. Coarsening-upward succession of deposits from the middle Williams Fork interval of the Cascade Creek 697-20-28 well, including core description, lithology, and interpretation of lithofacies and architectural elements.

floodplain, and coal (Table 2, Figures 4 and 5). Channel fill refers to the undifferentiated sands interpreted to have been deposited by fluvial processes within the levees of the channel. There was no further interpretation made to define depositional style of these sands.

Overall, the core primarily consists of the S_L and M_L lithofacies (38.6% and 28%, respectively), with channel-fill architectural elements (52.3%) being much more prevalent than crevasse splays (15%) (Figure 6).

Correlation to Well-log Signatures

The stratigraphic variability of lithology and fluvial deposits (architectural elements) within the middle and upper Williams Fork Formations was evaluated by calibrating well-log responses of fluvial sandstones to the lithofacies and architectural element analysis of the core and outcrop statistics. Core from the Cascade Creek 697-20-28 well and characteristics and statistics of fluvial sandstone-bodies were used to establish v-shale well-log cutoffs and log signatures corresponding to lithology and architectural elements (Appendix C: Cole and Cumella, 2005; Pranter et al., 2009; Pranter and Sommer, 2011). Once criteria were established, lithology logs were calculated and architectural-element logs were interpreted within sandstone intervals. Sandstone was calculated using a v-shale cutoff of < 0.25, mudrock having values of ≥ 0.25, and coal having values of normalized gamma-ray < 70 gAPI units, deep resistivity values of > 40 ohm-m and normalized bulk density of less than 2.2 g/cm^3 (Jon Cantwell, personal communications, 2010). Cut-off values for sandstone and mudstone were created based on comparison of the v-shale log values to a gamma-ray value of 85 gAPI units and core.

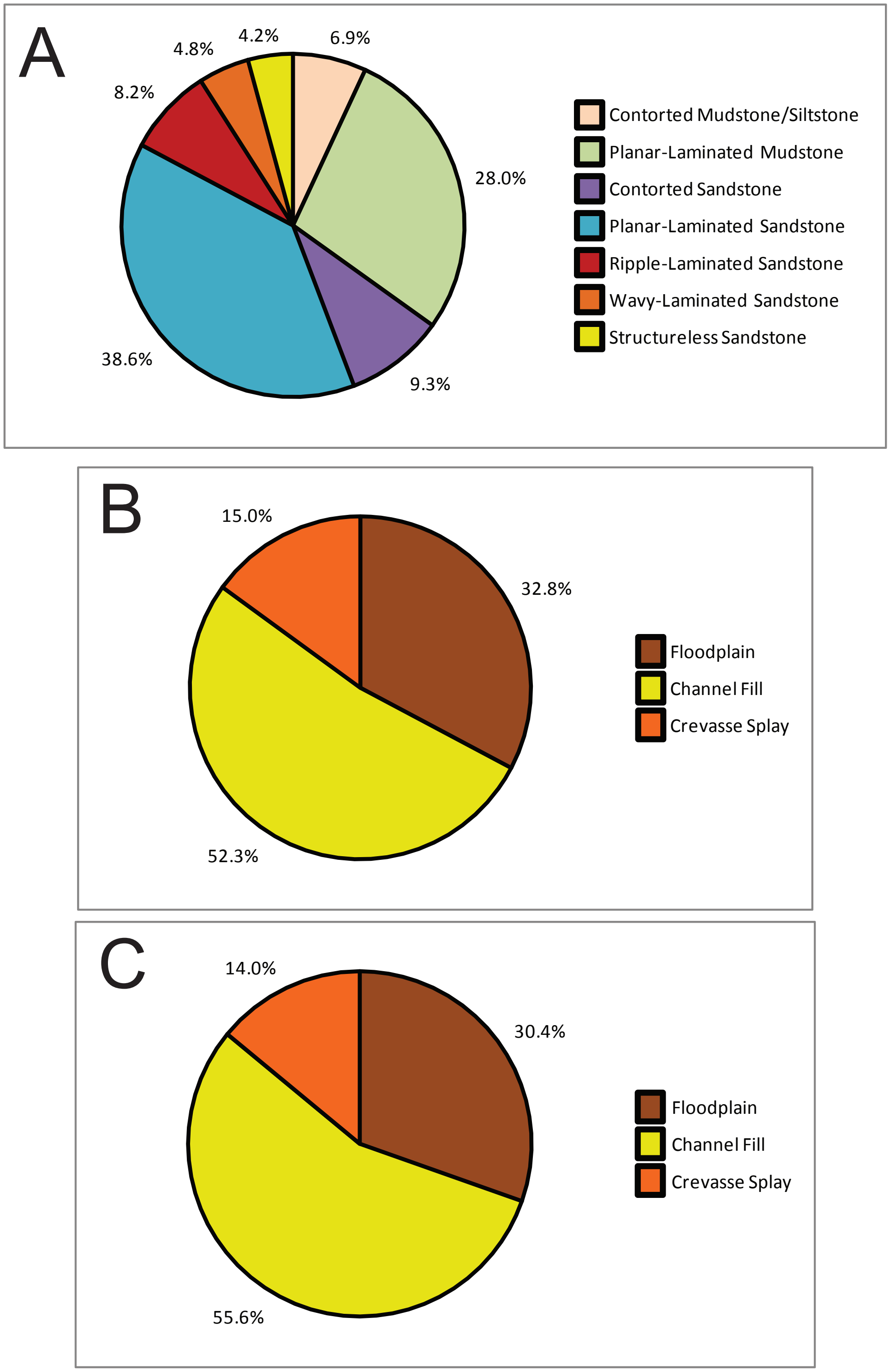

Figure 6. Proportions of (A) lithofacies and (B) architectural elements observed in the Cascade Creek 697-20-28 core (354 ft (107.9 m)), compared to the (C) architectural elements interpreted in well logs (463,348 ft (141,228 m)).

Channel fills and crevasse splays were interpreted using criteria similar to Cole and Cumella (2005), Pranter et al. (2009), Pranter and Sommer (2011), and Hewlett (2010) and originally discussed by Rider (2002). Channel fills were interpreted for the sandstone portions of the middle and upper Williams Fork Formations based on the following criteria: a v-shale value of < 0.25, either a blocky or fining-up, “bell-shaped” (Rider, 2002) v-shale response, a sharp basal contact, and thickness range of 2-30 ft (0.6-9 m) (Pranter et al., 2009; Hewlett 2010) (Figure 7A).

Crevasse-splays were interpreted as having a v-shale value of < 0.25 with coarsening-up or “funnel-shaped” (Rider, 2002) v-clay log responses. Thickness ranges were between 0.7 and 15 ft (0.2 and 4.5 m), and commonly were 10 ft (3 m) or less in thickness (Figure 7B).

The calculated lithology logs and interpreted architectural-element logs were used to evaluate the stratigraphic variability of lithology and architectural elements through vertical proportion curves (VPC’s). The VPC’s show the proportion of lithology or architectural elements versus depth. Vertical proportion curves were created for both the lithology and architectural element logs from the base of the middle Williams Fork Formation to the top of the Mesaverde Group, approximately 1,300 to 1,520 ft (396 to 463 m) (Figure 8). The lithology VPC was analyzed to determine intervals of higher and lower net-to-gross ratio, resulting in eight intervals of high net-to-gross ratios and seven intervals of low net-to-gross ratios, relative to the average net-to-gross (~70%) of the total interval. Overall, the VPC’s for both the lithology and architectural elements display similar stratigraphic variability (net-to-gross ratio) for the proportion of mudrock versus sandstone. The net-to-gross ratio over the entire interval varies from 18 to 78%, with the

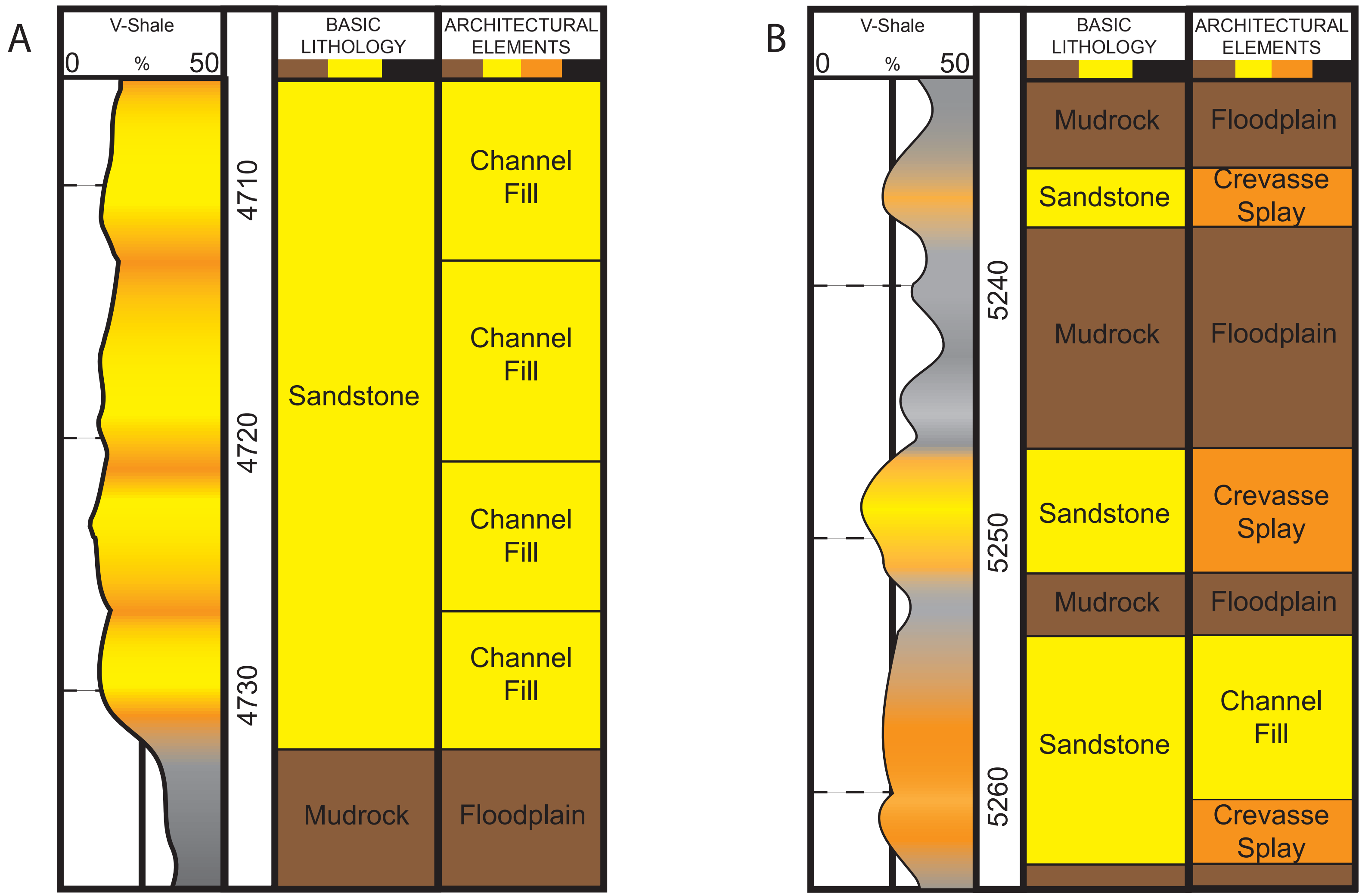

Figure 7. Interpretation of lithology and architectural elements from v-shale logs, based on criteria developed from core observations. (A) Stacked channel fill architectural elements. (B) Crevasse splay architectural elements. Well shown is the Cascade Creek 697-20-28. Depth is in feet.

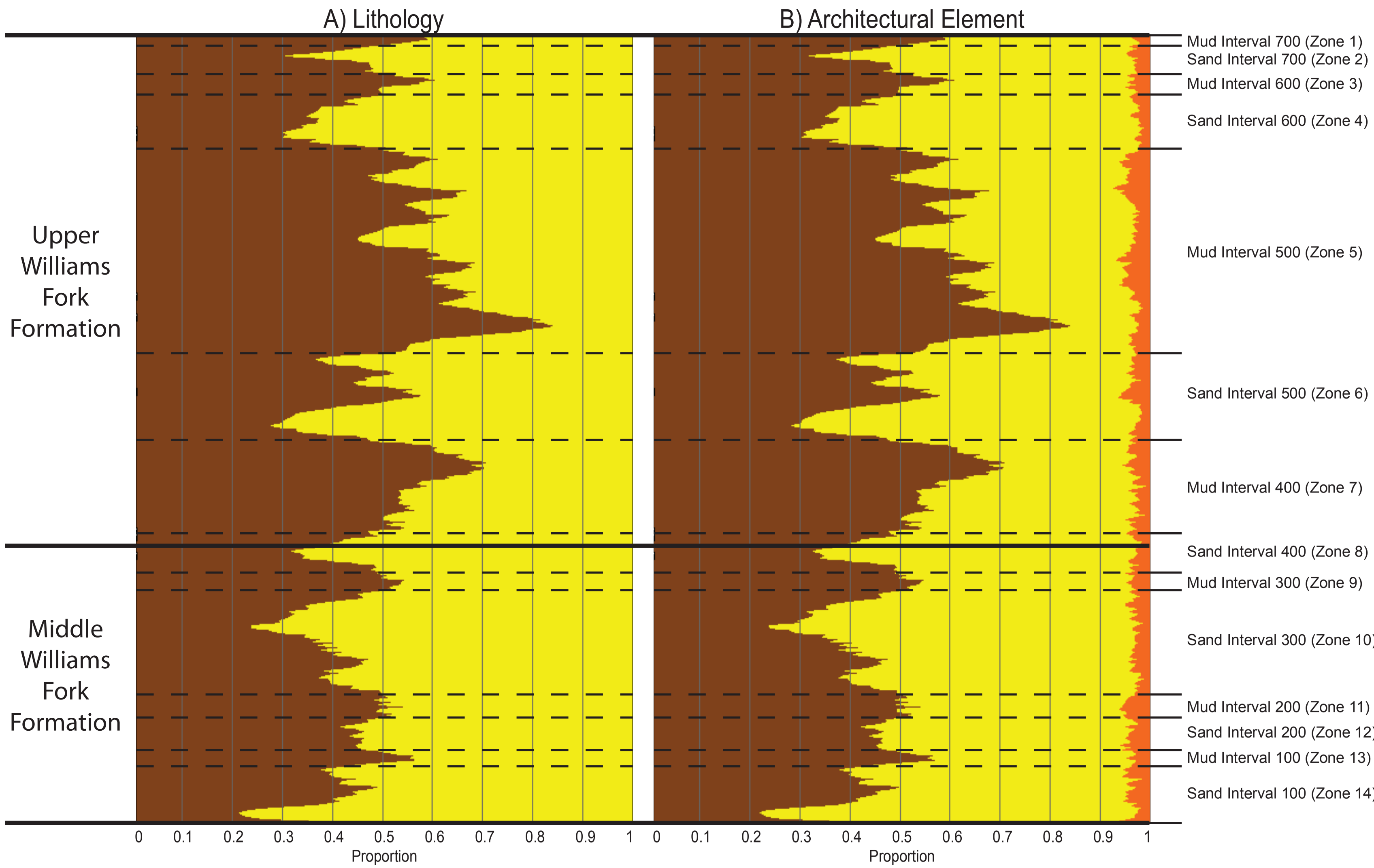

Figure 8: Vertical proportion curves (VPCs), derived from the original (input) logs, showing the proportion of lithology and architectural element by layer. Layers here are approximately 4 ft (1.2 m) thick. A) Lithology VPC where brown is mudrock and yellow is sandstone; and B) architectural element VPC, where brown is mudrock, yellow is channel bar, and orange is crevasse splay. Mud- and sand-prone intervals are highlighted, as well as model zones.

middle Williams Fork Formation exhibiting a higher, narrower range (43-78%) of stratigraphic variability than that of the upper Williams Fork Formation (18-70%).

The VPC for architectural elements shows that most of the sandstone in the middle and upper Williams Fork Formations is comprised of channel-fill deposits. Only a minor percentage of the net-to-gross ratio is interpreted to be associated with crevasse splays. The occurrence of crevasse splays has a narrow, low range (1-7%) when compared to channel-fill deposits (18-75%). The middle Williams Fork Formation averages 37% channel fill and 20% crevasse splays, while the upper Williams Fork Formation averages 68% channel fill and 10% crevasse splays, resulting in an increase in the ratio of channel fills to crevasse splays (CF:CS) from 1.9:1 in the middle Williams Fork Formation to 6.7:1 in the upper Williams Fork Formation.

QUANTITATIVE MINERAL ANALYSIS

Stratigraphic Variability

Petrophysical lithology and saturation models were developed in order to analyze the stratigraphic distribution of minerals, specifically chlorite and potassium feldspar. Two sets of data were required to develop the model: 1) a triple-combo well-log suite consisting of gamma-ray (GR), resistivity (RILD), neutron-porosity (PHIN), bulk density (RHOB), and photoelectric factor (PE) logs in digital format and 2) x-ray diffraction data of mineralogical volumes from core (in volume %). The petrophysical model can be conceptually explained through a diagram (Figure 9) representing the total bulk volume of a rock divided into a hierarchy of the various constituents, with the goal to accurately model specific mineral volumes and fluid saturations from log responses.

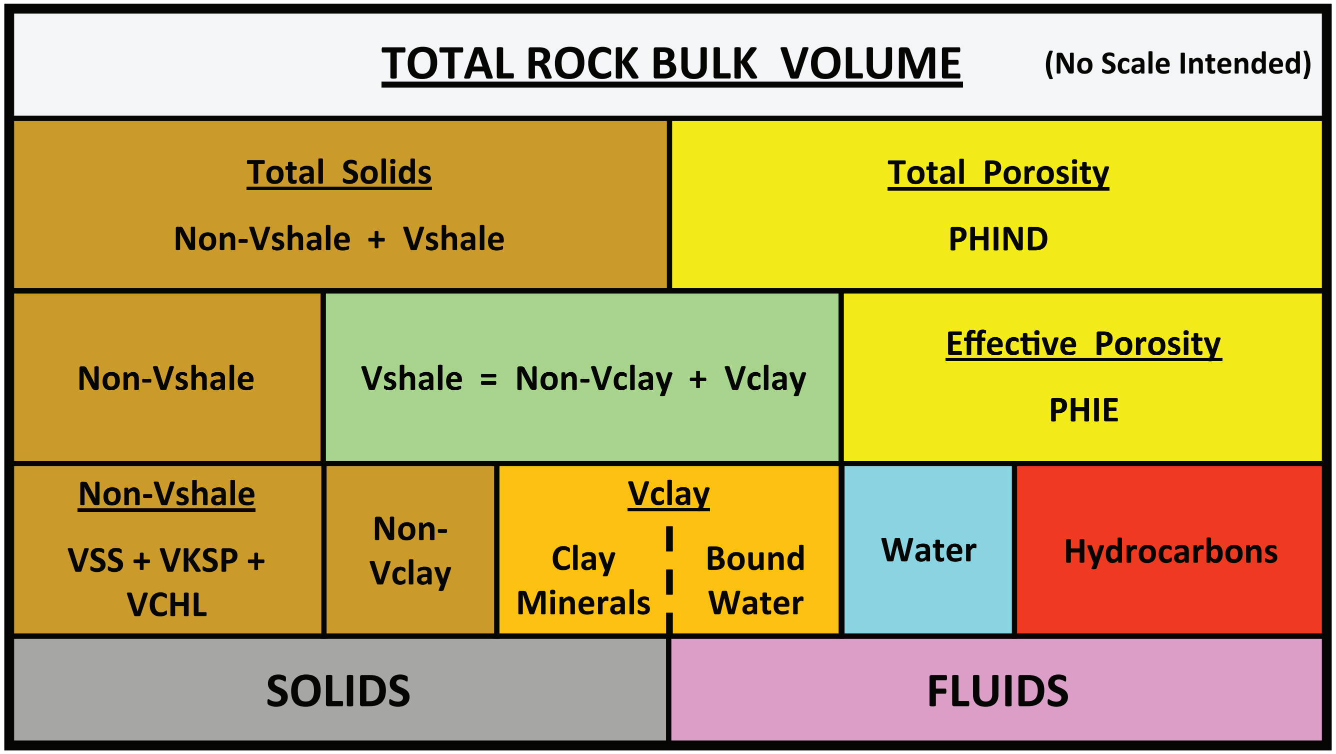

Figure 9: Total rock bulk volume is divided into solid and porosity (fluid) components. Shale and non-shale volumes comprise the solid fraction. The shale volume includes clay and non-clay constituents where clay consists of both clay minerals and associated bound water. The non-shale volumes include silica (VSS), potassium feldspar (VKSP), and chlorite (VCHL), which are calculated through the petrophysical-lithology model. The model also calculates total porosity (PHIND) and effective porosity (PHIE). Total porosity consists of both movable fluids and immovable (clay-bound) water. Effective porosity consists of free water, irreducible water, and hydrocabons, excluding clay-bound water.

The petrophysical methods used in this study are well documented (Crain, 1986), though elaboration is necessary on key points where less common methods were used. The gamma-ray (GR) and neutron-porosity (PHIN) logs were normalized against standard wells to compensate for log variations due to differences caused by variations in vendor tool, calibration, and data processing. No other curve data was normalized, as the process of log normalization changes the actual data values for a given log, and as such, was used sparingly and only on well-logs which exhibited large data ranges relative to the standard well. The standard well used for normalization of the gamma-ray logs was selected based on evaluation of histogram distributions of gAPI units, for all wells in the study area. The standard well, Williams GM 43-36 (API 05045141350000), is located in the southeast quarter of section 36 in the study area (Figure 3). The gamma-ray well-log histogram showed two distinct peaks in the frequency distribution of the data, one at approximately 60 gAPI and the other at approximately 120 gAPI. The peak around 60 gAPI represents the log responses caused by sandstones while the peak at 120 gAPI represents the log responses caused by shale. This bimodal distribution of gAPI values are common in wells drilled in locations dominated by quartz sandstones and shales as in the Piceance basin (Marc Connolly, personal communication, 2011).

The standard well for neutron-porosity-log normalization was selected in a similar manner. A histogram distribution of porosity values, in percent, for each well was evaluated, and the standard well was selected from the data set. The neutron-porosity histograms display a single peak, or mode, at approximately 0.12 decimal porosity. This matches historical values and trends of the neutron-porosity in the area indicating good quantity data (Marc Connolly, personal communication, 2011). These values and trends are observed in the Federal GM 432-35 well (API 05045116090000), located in the northeast quarter of section 35 in the study area (Figure 3).

Calculated logs include coal indicator flags (COAL), temperature gradient (TEMP), chloride gradient (NACL), and shale volume (v-shale) logs. Cross-plot analysis was used to determine formation water-resistivity (R_W), total porosity (PHIND), apparent-grain-density (RHOMAND), and clay volume (v-clay) logs.

Formation water-resistivity (R_w) gradients were developed from analysis utilizing Pickett plots. The Pickett plot is a graphical representation of the Archie equation, which calculates water saturation (S_w) from formation-water resistivity (R_w), porosity (ϕ), true formation resistivity (R_t), and empirical factors derived from formation evaluation: The tortuosity factor (*a*) represents the pore geometry of the rock. The cementation exponent (*m*) is interpreted as the rate of change of the connectedness with porosity and connectivity. The saturation exponent (*n*) represents the relationship between water saturation and resistivity:

$$S_w = \left[\frac{a * R_w}{\phi^m * R_t}\right]^{\frac{1}{n}}$$

A Pickett plot is a cross plot of porosity (Y-axis) vs. resistivity (X-axis), both on logarithmic scales. In this study, log data used are density porosity (PHID) and deep induction resistivity (RILD). Water saturation (S_w) can be determined based on an analysis of the Pickett plot data and application of the Archie equation. A water saturation (S_w) grid can be created on the Pickett plot and is dimensionally controlled by the coefficients in the Archie equation, where the tortuosity factor (*a*) controls the y-intersection for the 100% water saturation line, the cementation exponent (*m*) controls the slope of the lines of equal water saturation, and the saturation exponent (*n*) controls the spacing between the lines of constant water saturations. Due to the lack of core data necessary for experimental determination of the coefficients, values of *a=1*, *m=2,* and *n=2* were used as reasonable approximations for the study area (Asquith et al., 2004). Formation porosity and resistivity both control water saturation on the Pickett plot, with the highest water saturations being calculated from the lowest porosities and resistivities and the lowest water saturations being calculated from the highest porosities and resistivities.

Pickett plots were built for three 1000-ft (304-m) stratigraphic intervals. The three intervals, from deepest to shallowest, are: 1) Rollins to ROL+1000', 2) ROL+1000' to ROL+2000', and 3) ROL+2000' to ROL+3000' (Figure 2). The surfaces are named such that ROL+X' refers to a location X feet above the top of the Rollins Sandstone member (ROL). This was done in order to examine vertical trends in formation water-resistivity. Water saturation values were obtained by identifying a trend in each Pickett plot that represented either 100% water-saturation in water-saturated intervals or irreducible water saturation in gas-saturated intervals. In this study, the trends on the Pickett plots demonstrate that the lower two intervals (Rollins to ROL+1000' and ROL+1000' to ROL+2000') are primarily gas-saturated, and the upper interval (ROL+2000' to ROL+3000') is water-saturated.

In the upper interval, the 100% water saturation trend was interpreted where the density of data points on the Pickett plot began to decrease as the porosity (PHID) and resistivity (RILD) reached their smallest measured values. The water saturation grid was overlain on the Pickett plot, with the line representing 100% water saturation aligned

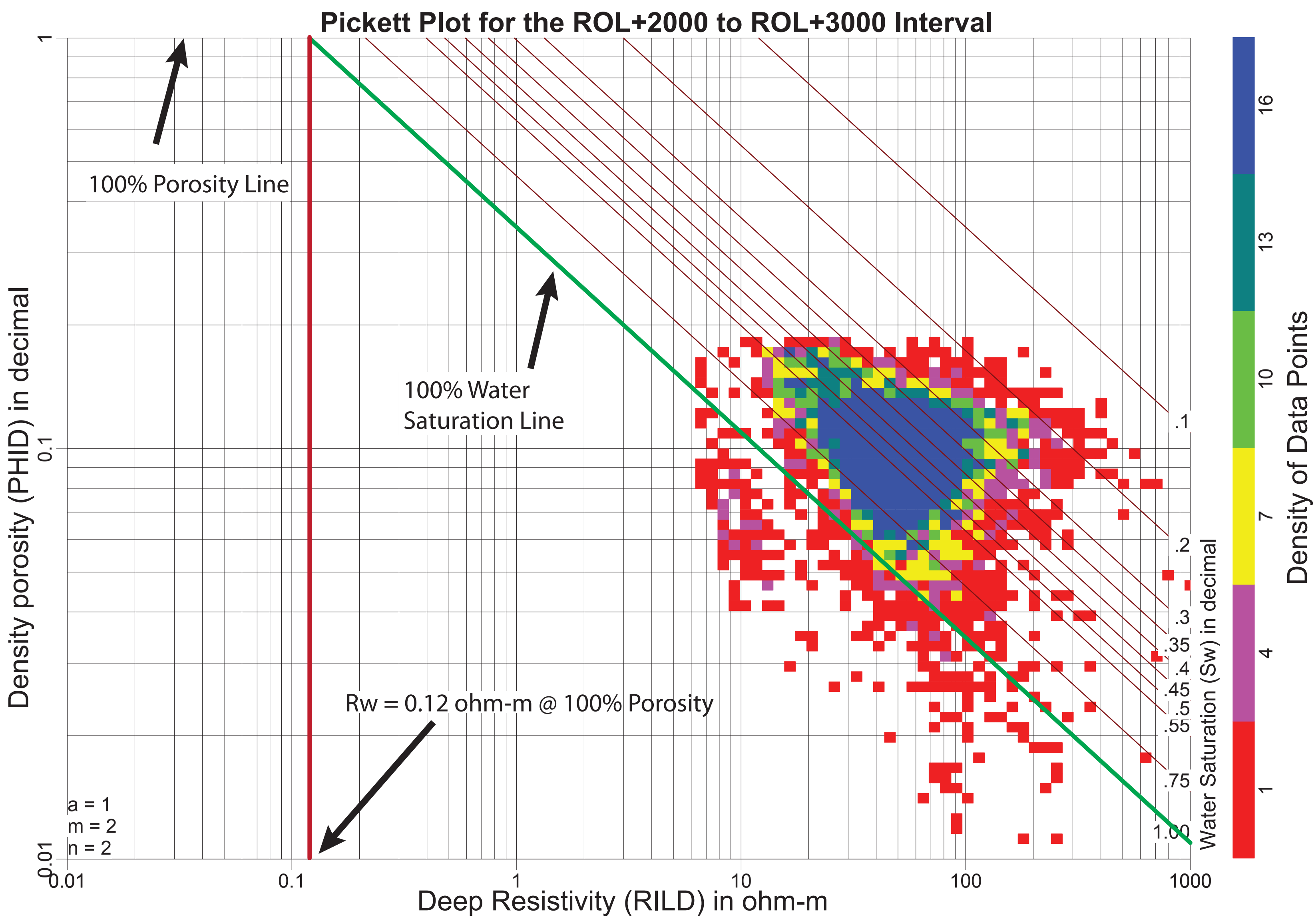

Figure 10: Pickett plot for the upper stratigraphic interval, 2000 ft above the Rollins to 3000 ft above the Rollins, in which the lowermost extent of the data represents the 100% water saturation line (green), which intersects 100% porosity at a resistivity of 0.12 ohm-m (red line).

along this 100% water saturation trend. The R_w value for the interval was interpreted as being equal to the resistivity value (x-axis) where the 100% water saturation line intersected the 100% porosity value (y-axis) (Figure 10).

The technique for determining formation water-resistivity was modified for the lower two intervals where there are no sands having 100 percent water saturation. If the irreducible water saturation value is known, a trend for it can be identified on the Pickett plot, and water saturation and formation water-resistivity can still be calculated. Because clay-bound water accounts for approximately 25% of the total water saturation in reservoirs like those in the Piceance Basin (Cluff and Byrnes, 2010), data points on a Pickett plot can be interpreted as being in a fully gas-saturated interval where irreducible water saturation (S_{wirr}) equals 25% (or 0.25). The irreducible water-saturation trend was interpreted where the density of data points on the Pickett plot began to decrease as the porosity (PHID) and resistivity (RILD) reached their largest measured values, as data along this trend exhibits higher gas saturations and immovable water saturations (Figure 11). The water-saturation grid was overlain on the Pickett plot, with the line representing 25% water saturation aligned along this irreducible water-saturation trend. The R_w value for the interval was interpreted as being equal to the resistivity value (x-axis) where the 100% water-saturation line intersected the 100% porosity value (y-axis).

Results from Pickett plot analysis indicate formation-water resistivity decreases with depth. In descending stratigraphic order, average formation-water-resistivity values of 0.12, 0.085, and 0.060 ohm-m were determined for the three intervals. The data

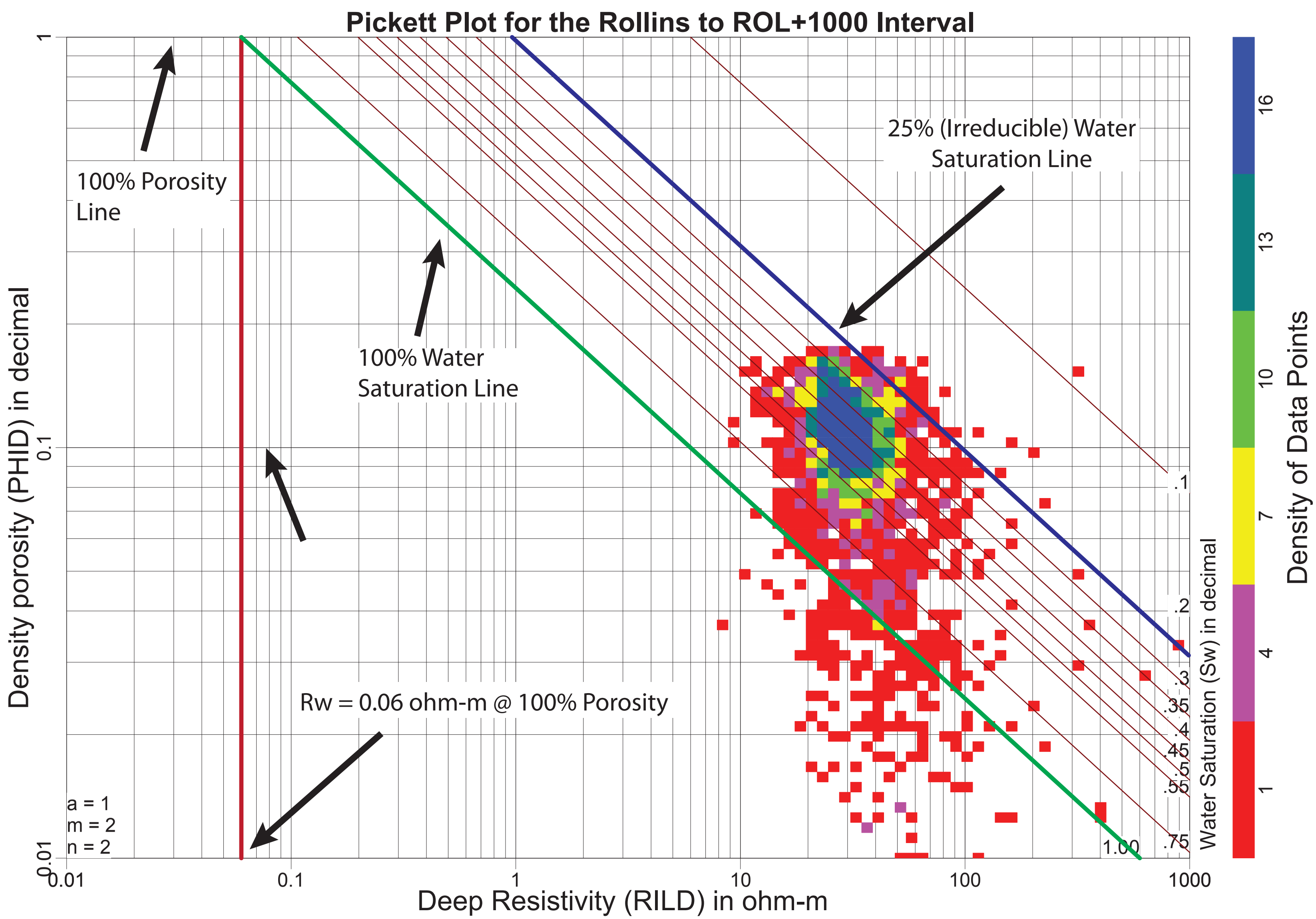

Figure 11: Pickett plot for the lowermost stratigraphic interval, from the Rollins to 1000 feet above the Rollins, in which the uppermost extent of the data represents the clay-bound (irreducible) water of 25% water saturation (blue line). The 100% water saturation line (green) intersects 100% porosity at a resistivity of 0.06 ohm-m (red line).

points and the stratigraphic distance between intervals (1000 ft [304.8 m]) were used to develop a linear gradient to calculate R_w at a given depth above the Rollins:

$$R_w = (\text{Measured Depth of Rollins} - \text{Given Depth}) * 0.0003 + 0.045$$

The equation coefficient represents the slope (0.0003 ohm-m/ft), and the constant represents the y-intercept (0.045 ohm-m) of a linear regression through the three R_w data points.

V-shale and v-clay logs were calculated and used to define the relative proportions of shale- and clay-sized particles at a given depth, identify the intervals dominated by shale and clay, and exclude those intervals from subsequent modeling. The v-shale log is the volume of shale at a given depth expressed as a decimal fraction or percentage and is a linear calculation from the normalized gamma-ray log (Crain, 1986; Asquith et al., 2004). To calculate the v-shale log, gamma-ray values representing 100% shale (GR_shale) and 0% shale (GR_sand) are established based on histogram analysis of the normalized gamma-ray logs. This analysis was done for each of the twenty-seven wells, and the following average values were used for all subsequent v-shale calculations: GR_sand = 43 gAPI and GR_shale = 135 gAPI units. V-shale logs were then calculated for each well from the normalized gamma-ray (GR_NM) log using the equation:

$$\text{V-shale} = (\text{GR\_NM} - \text{GR\_sand}) / (\text{GR\_shale} - \text{GR\_sand}).$$

Any gamma-ray reading lower than the GR_sand value or higher than the GR_shale value defaulted to a v-shale value of 0% or 100% shale, respectively. As a final step, a coal flag was then used to exclude the intervals of coal. Anywhere that coal was calculated was assigned a null value for shale. An interval was flagged as coal when the density (RHOB) log was between 0 and 2 g/cc and the resistivity (RILD) log was greater than 20 ohm-m.

The v-clay log is the volume of clay expressed as a decimal or percentage, and was calculated based on a normalized neutron-porosity (PHIN_LSN) versus bulk-density (RHOB) cross plot (Figure 12). A clay volume grid was created by selecting three data points on the neutron-density cross plot, with each data point establishing a boundary condition for the grid. Two data points, referred to as the sandstone points represent 0% clay. A line defined by the two sandstone points is the sandstone line where any point along or above the line has 0% clay. The two sandstone points were PHIN_LSN=0, RHOB=2.5 and PHIN_LSN=0.15, RHOB=2.25, which were selected using known points from the Schlumberger chart book (2009). PHIN_LSN values are in decimal or fraction and RHOB values are in g/cm^3.

The clay point represents neutron porosity and density values representative of average clay values found in the Williams Fork formation (Marc Connolly, personal communication, 2011; Debra Patskowski, personal communication, 2011). A line running parallel to the sandstone line and through the clay point, referred to as the clay line defines the 100% clay line of the grid, where any location along or below the line has 100% clay. The clay point was at PHIN_LSN=0.35, RHOB=2.5, determined from clay point parameter estimations (Schlumberger, 2009). The v-clay grid was then

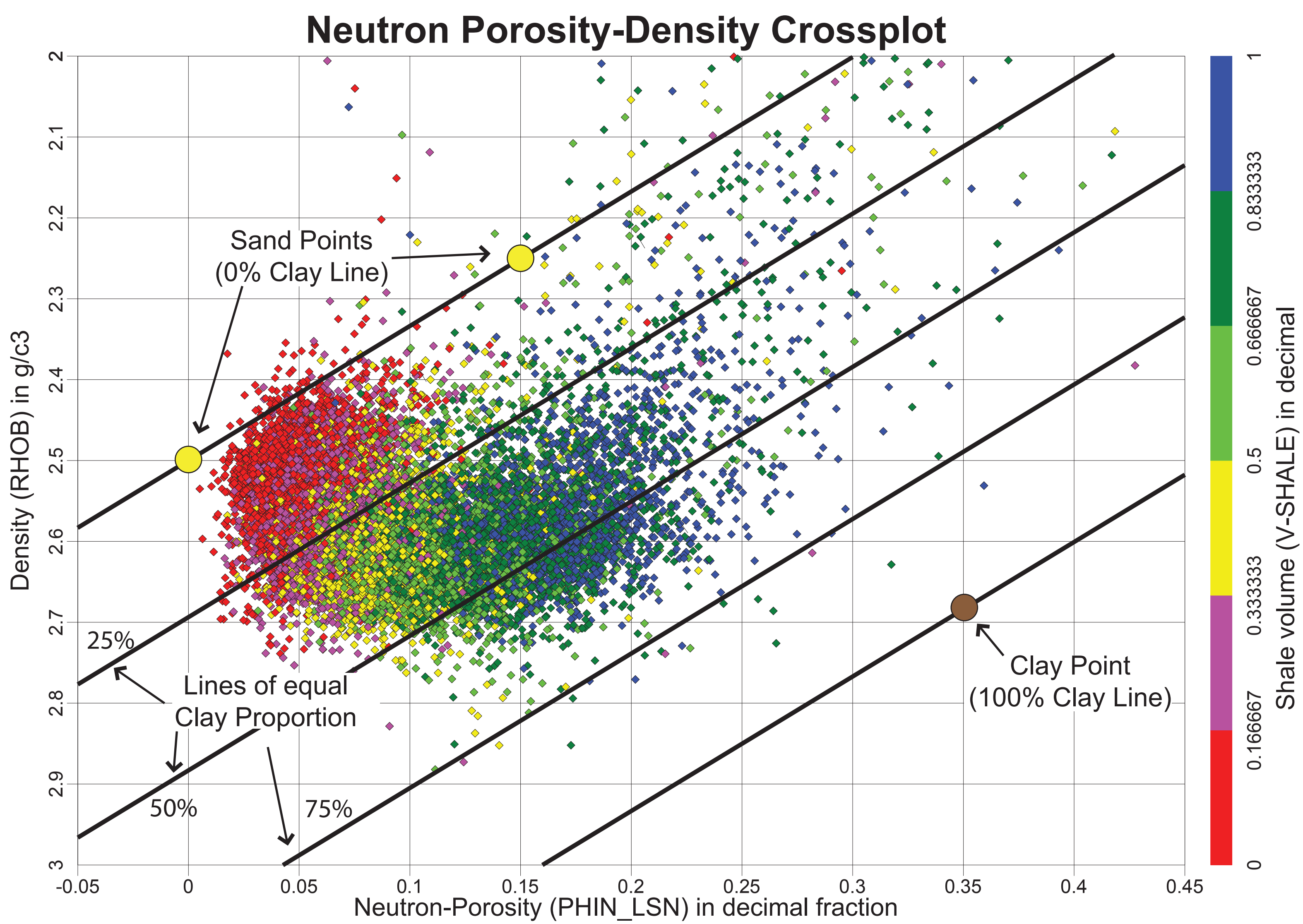

Figure 12: Neutron-Porosity versus Density cross plot of all 27 wells in the petrophysical study. The black line connecting the 0% clay points (yellow circles) provides the slope for equal clay-proportion lines across the grid, and the 100% clay point (brown circle) provides the distance between 0% clay and 100% clay within the grid. Lines of equal clay proportion are distributed along a linear gradient between the sand and clay lines.

created between the sandstone line and clay line, with v-clay increasing linearly from 0% at the sandstone line to 100% at the clay line. All values on the neutron-density cross plot were then assigned a clay volume percentage based on their location relative to the grid, resulting in a v-clay log for each of the 27 wells in the study area.

The neutron-density cross-plot porosity (PHIND) logs and apparent-grain-density (RHOMAND) values were assigned using the same methodology as the v-clay log: the data points were plotted on a cross plot of neutron-porosity versus density and assigned values for both PHIND and RHOMAND were established based on the known distribution of values on the cross plot (Figure 13). The primary difference in methodology from the v-clay log is the non-linear relationship of PHIND and RHOMAND to the cross plot. Every data point was assigned both a neutron-density value and apparent grain density value based on their location within the cross plot. These values, along with the depth log, were used to generate the neutron-density-porosity and apparent-grain-density logs.

In developing the petrophysical model for the Cascade Creek 697-20-28 well (Figure 14), the core-measured x-ray diffraction values of chlorite and potassium feldspar were used to calibrate the calculated mineral proportions (volumes) of the petrophysical model. The main controls in calibrating the mineral proportions were the matrix densities (RHOMA, g/cm^3) and cross-sectional photoelectric values (UMA, $barns/cm^3$) for each mineral. The RHOMA and UMA values do not represent the true values for each mineral, but rather the apparent values that the well logs have recorded. Therefore, these values were adjusted individually and the petrophysical model was iterated until a combination of all UMA and RHOMA values was found where the

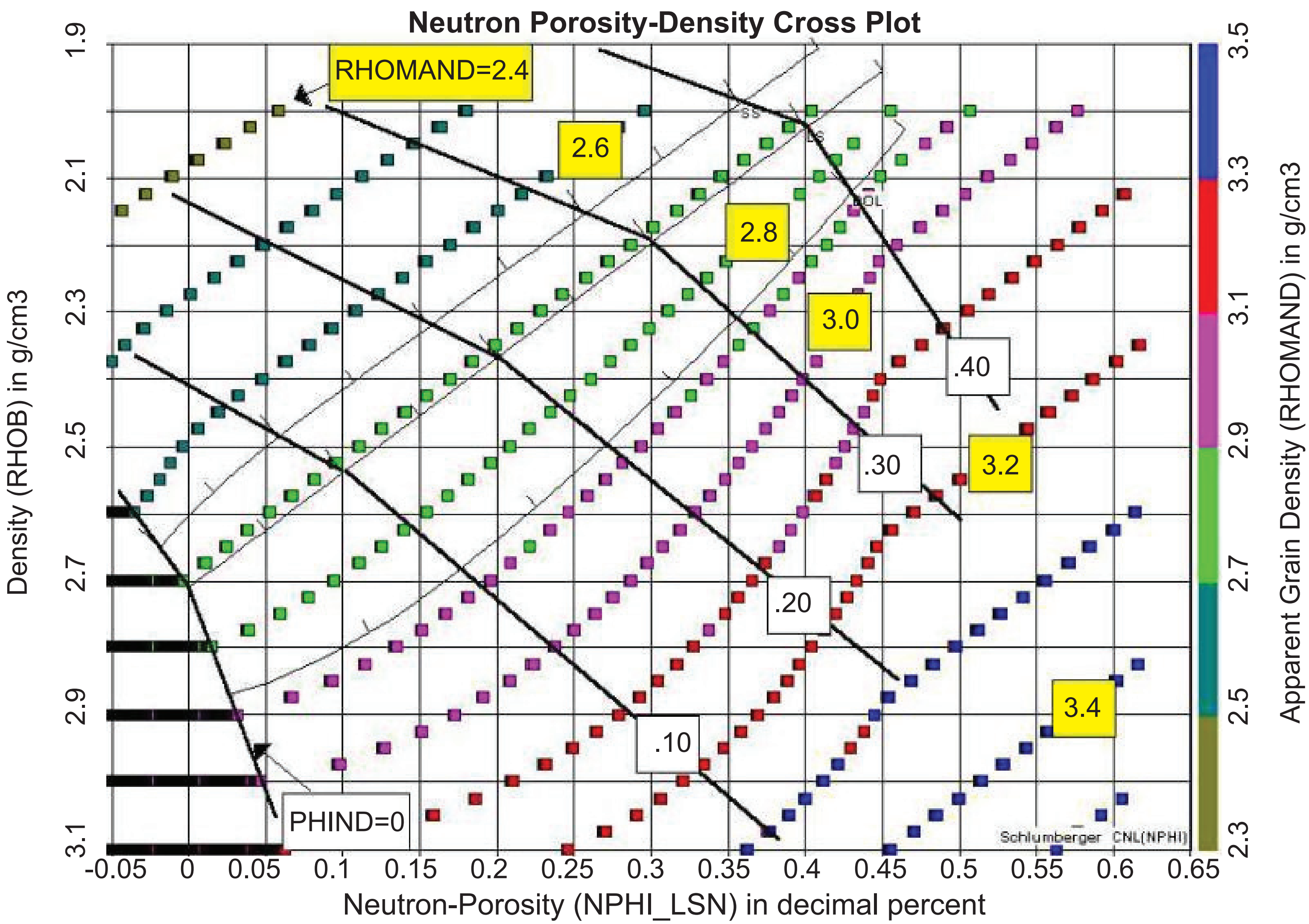

Figure 13: Diagramatic Neutron-Porosity versus Density cross plot showing how neutron-density porosity (PHIND) and apparent grain density (RHOMAND) logs are generated. The square dots are lines of equal apparent grain density and the thick black lines are lines of equal neutron-density porosity. Edited From Powerlog (2011).

Figure 14. Petrophysical Model for the Cascade Creek 697-20-28 Well

The well log display (on following page) shows the log inputs, core measurements with locations, and results for the petrophysial modeling from the core of the Cascade Creek 697-20-28 well in the Piceance Basin. Key with units and scales is shown below.

GR	CALI	TEMP RW NACL	Core Measurements	Mineral Proportions	BVW BVG	VCHL	VKSP	RHOB PE	Depth Core Plugs	RILS RILD	PHID PHIN
Gamma Ray 0 to 200 (gAPI) Fill where < 100 (Illustrative Sand Indicator)	Caliper 6 to 16 (inches) Fill where > 8.5 inches (Drillbit size)	TEMP 50-250 (deg F) RW Formation Water Resistivity 0 to 0.2 (ohm-m) NACL Chloride Content 0 to 80000 (ppm)	Clay Quartz Plagioclase Calcite Dolomite Chlorite Potassium Feldspar	Clay Non-Clay Sandstone Chlorite Potassium Feldspar Coal Effective Porosity	BVW Bulk Volume Water 0 to 20 (Volume %) BVG Bulk Volume Gas 0 to 20 (Volume %)	Chlorite 25 to 0 (Volume %)	Potas-sium Feldspar 0 to 25 (Volume %)	RHOB Density 2 to 3 (g/cm3) PE Photoelectric Factor 0 to 10 (B/E)	Depth (ft) Core Plug Location	RILS Shallow Resistivity 1 to 1000 (ohm-m) RILD Deep Resistivity 1 to 1000 (ohm-m) Fill where >10 ohm-m	PHID Density-Porosity 0.5 to -0.1 (Decimal %) PHIN Neutron-Porosity 0.5 to -0.1 (Decimal %)

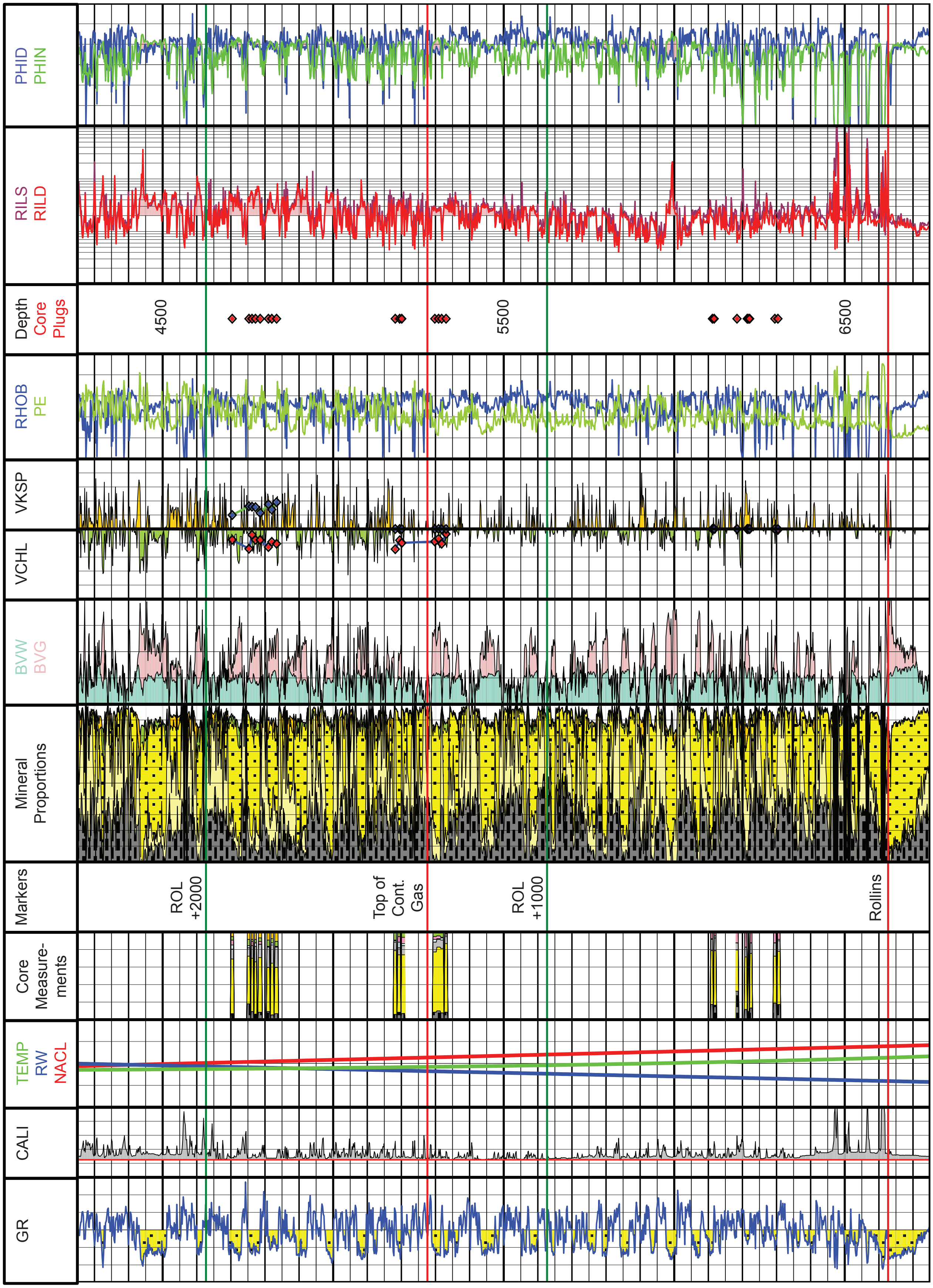
PHID
PHIN
RILS
RILD
Depth
Core
Plugs
4500
5500
6500
RHOB
PE
VKSP
VCHL
BVW
BVG
Mineral
Proportions
Markers
ROL
+2000
Top of
Cont.
Gas
ROL
+1000
Rollins
Core
Measure-
ments
TEMP
RW
NACL
CALI
GR

calculated values for the minerals closely matched the core measured values (Chlorite volumes had a correlation coefficient (R^2) of 0.865 after removal of two shale measurements (VSH>80%) at 4810' and 4820').

A blind study was completed to validate the parameters of the model. The MWX (Multi-Well Experiment) public dataset was utilized for this blind study, specifically logs and point-count measurements from the MWX-2 well (API 0504560011) were used, courtesy of The Discovery Group Inc. Chlorite volumes were calculated using the same apparent RHOMA and UMA values determined from the Cascade Creek 697-20-28 well in seven intervals with point-count and Photoelectric (PE) log measurements. The chlorite log volumes correlated to the chlorite point-count results with a correlation coefficient (R^2) of 0.896, after removal of one measurement in shale (VSH >80%) at 5846' (Appendix M).

The RHOMA and UMA input parameters were calibrated to the cored well (Cascade Creek 697-20-28), and then applied to the 27 wells in the study area. Mineral proportions and fluid saturations were calculated throughout each well. No additional x-ray diffraction data or mineralogy measurements were available within the study area, so no further calibration of the calculated results could be accomplished. It is important to note that this modeling technique resulted in a non-unique solution, such that other combinations of RHOMA and UMA could give similar, reasonable results.

The range of calculated mineral proportions was 0-30% for potassium feldspar, and 0-21% for chlorite. Calculated proportions for both the chlorite and potassium feldspar increased stratigraphically, from 0% at the base of the Williams Fork Formation up to their respective maximums near the top of the Mesaverde Group.

SPATIAL DISTRIBUTION OF CHLORITE AND POTASSIUM FELDSPAR

Three-dimensional lithology models were developed to investigate the spatial distribution of chlorite and potassium feldspar, and architectural-element logs were used to investigate the distribution of these minerals among architectural elements. The area of the model encompasses the eight-section study area (Figure 3). The thickness of the model varies from 1,300 to 1,520 ft (396 to 463 m), and the interval includes the middle and upper Williams Fork Formations. The fourteen intervals defined from the stratigraphic-log correlations and analysis of the vertical proportion curves were used in constructing the framework of the model, resulting in a three-dimensional model with fourteen zones: seven zones representing sandstone-rich intervals and seven zones representing relatively sandstone-poor intervals within the middle and upper Williams Fork Formations (Figure 15).

Upscaled discrete logs (i.e., lithology and architectural element) and continuous logs (i.e., potassium feldspar and chlorite) were treated as hard data and honored in the three-dimensional models. Lithology vertical proportion curves and percentages were used as vertical constraints in the three-dimensional lithology models to honor the stratigraphic changes in the lithology percentages, based on the upscaled lithology logs.

An average lithology model was created from thirty lithology realizations. The average lithology model approximates the mapped distribution of lithology based on kriging. Each of the 14 zones was modeled independently, using a corresponding vertical proportion curve specifically generated on a zone by zone basis, while coal was modeled deterministically.

Sequential indicator-based simulation (SIS) was utilized to build these models. SIS is a cell- or pixel-based modeling method that simulates the spatial distribution and

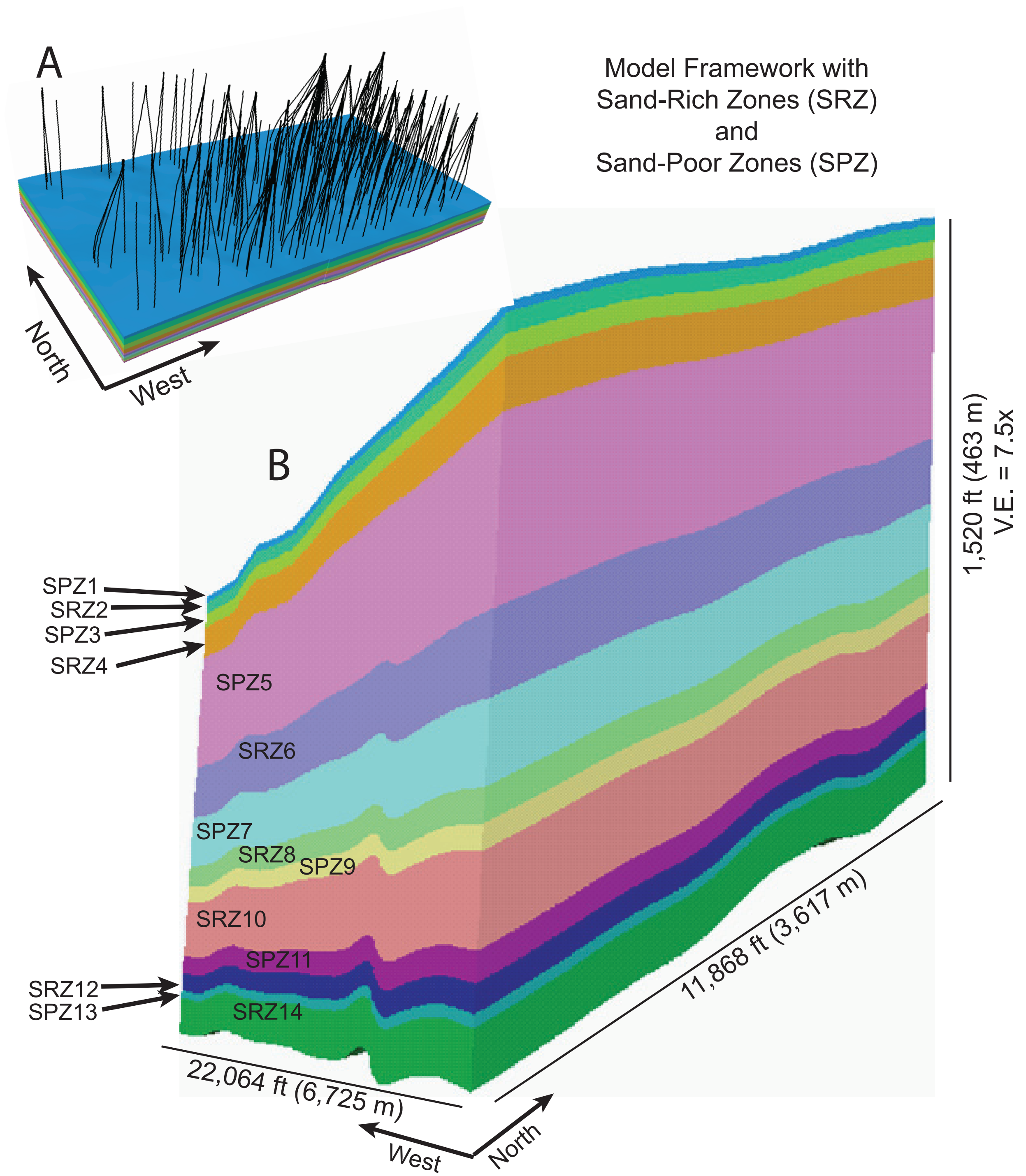

Figure 15: Three-dimensional model framework from the base of the middle Williams Fork formation to the top of the Mesaverde Group. (A) Location of 329 wells intersecting the model, with no vertical exaggeration. (B) Model consists of 14 zones, denoted as either Sand-Rich (SRZ) or Sand-Poor (SPZ) zones. The model is approximately 9.4 sq mi (24.3 sq km) and varies in thickness from 1,300 to 1,520 ft (396 to 463 m). The model contains 350 proportional layers that are each approximately 4 ft (1.2 m) thick. Cell dimensions are 40 by 40 ft (12.2 by 12.2 m) aerially, resulting in 57.3 million cells.

continuity of discrete and continuous data (e.g., lithology or v-clay, respectively) through the use of variograms to control any trends in the distribution of the data. All layers and zones were modeled using the same isotropic, spherical variogram (dip of 0, nugget of 0, major and minor ranges of 5000, and a vertical range of 1). Indicator-based simulations populate the model, cell by cell, by first assigning well data (lithology based on the v-clay log) to the grid cell closest to the well (Deutsch and Journel, 1998). A random order of cells is established in which every cell is visited once, and is assigned a simulated value based on the conditional probabilities (the stratigraphic lithology percentages derived from the VPCs) (Deutsch and Journel, 1998). Nearby data and previously simulated values, starting at the well, are evaluated, and the conditional probabilities are constructed by kriging. The resulting three-dimensional model will honor the input data, global proportions of the property, and variograms, if established (Deutsch and Journel, 1998).

Average models for chlorite and potassium feldspars were also created from thirty realizations of each. The models were conditioned to the chlorite and potassium feldspar proportion logs as well as frequency histograms of the mineral volume percentages based on the upscaled logs. The models were further refined using cutoff values of chlorite and potassium feldspar to highlight the areas where a greater relative concentration of each mineral (chlorite or potassium feldspar) existed within the model, resulting in discrete-mineral-concentration models for chlorite and potassium feldspar. The modeled P_{50} values of both chlorite (P_{50} = 1.3%) and potassium feldspar (P_{50} = 7%) were used as the cutoff values for areas of higher concentrations of the minerals. Any area with a volume percentage equal to or greater than the P_{50} value was considered to be a high concentration, while any area with a volume percentage less than the P_{50} value was considered to be a low concentration. Volumetric calculations for the discrete-mineral-concentration models were subsequently completed to quantify the significance of the minerals.

The values of the discrete-mineral-concentration models were extracted and used to create pseudo-well logs along the 327 wellbores in which architectural element logs had previously been interpreted. These pseudo-well logs of mineral concentrations were then used to analyze the distribution of the mineral concentrations as they related to the interpreted architectural elements.

Analysis of the lithology model shows how the distribution of sandstone varies spatially within the middle and upper Williams Fork Formations (Figure 16A). The highest net-to-gross ratios in the middle and upper Williams Fork Formations are statistically similar (84% versus 88%, respectively). The lowest net-to-gross ratios are much more contrasting (36% versus 8%, respectively). The average net-to-gross ratio for the middle Williams Fork Formation is 58.3%, while the average net-to-gross for the upper Williams Fork Formation is 48.5%, with a combined net-to-gross ratio of 50.2%.

The volumetric proportion of chlorite ranges from 0 to 21% of all model cells, while only averaging 1% distribution across the entire model. The proportion of potassium feldspar ranges from 0% to 30% of all model cells, and also averages 1% distribution for the entire model. Statistically, zone 10 had the highest average chlorite proportion (2%) while zones 2 and 10 had the highest average potassium feldspar proportion (3%). The P_{50} values for chlorite and potassium feldspar are calculated as 1.3% and 7%, respectively.

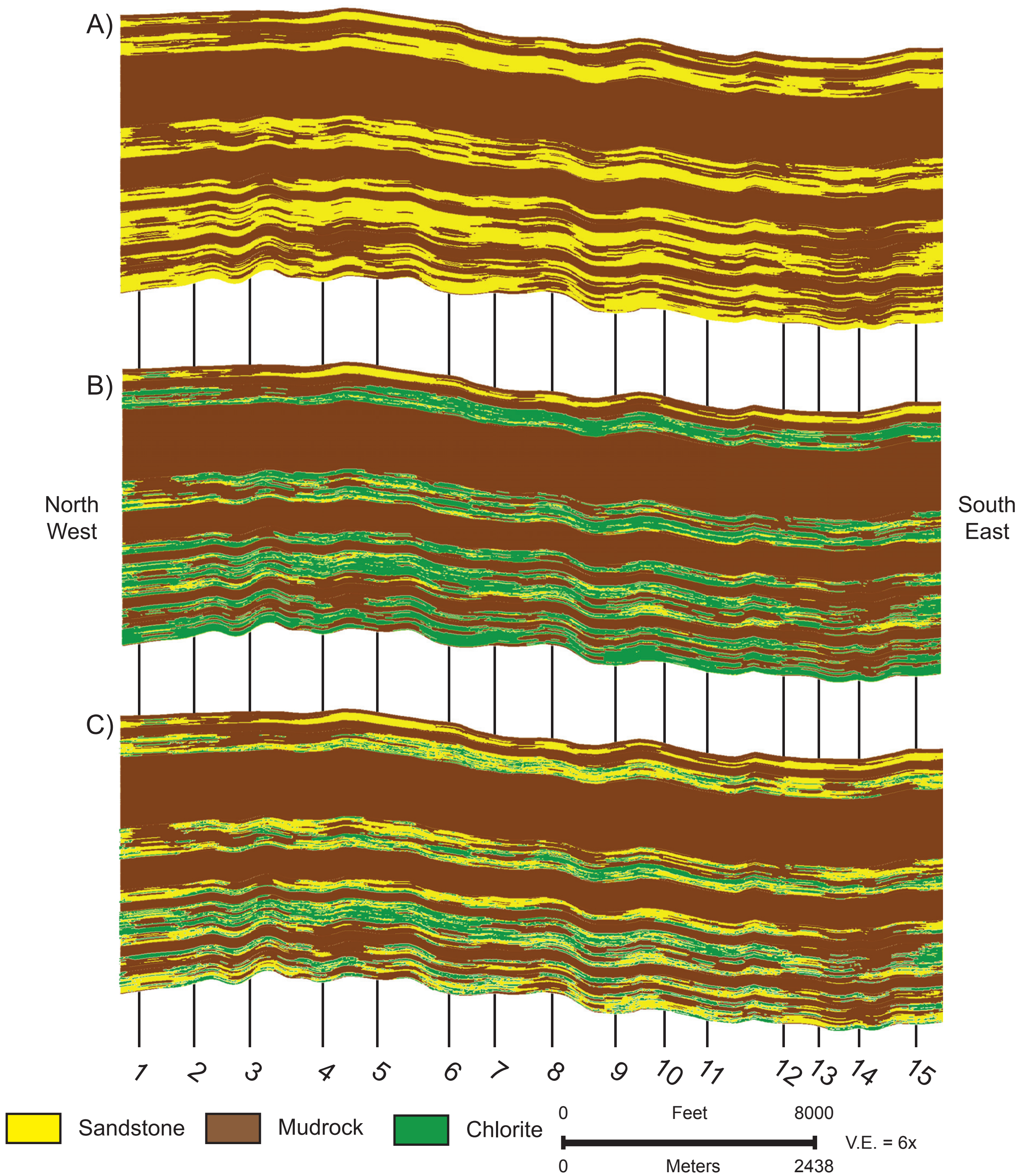

Figure 16: Stratigraphic cross-section of lithology and chlorite distribution models. (A) Lithology constrained to the sandstone-rich intervals. (B) Occurrence of chlorite constrained to sandstones. (C) Occurrence of high-concentration chlorite (>1.3%). See Figure 3 for location of cross-section. APIs of wells intersected (1-15) are 05045128320000, 05045095550000, 05045079000000, 05045078880000, 05045077140000, 05045104650000, 05045103760000, 05045114250000, 05045115020000, 05045079780000, 05045124900000, 05045144680000, 05045144690000, 05045073710000, and 05045133370000.

The distribution of the chlorite did not vary significantly between reservoir architectural elements when compared for the three concentration ranges evaluated (Table 3). Within the crevasse splays, 31.4% had no chlorite, 27.6% contained low chlorite concentrations (<P_{50}), and 41.1% had high chlorite concentrations (>P_{50}). The distribution for the channel fills was very similar, with 29.4% lacking chlorite, 29.9% having low chlorite concentrations and 40.7% having high chlorite concentrations. When compared against lithology, high concentrations (above 1.3%) of chlorite were found in 41.0% of the sandstones, while the low concentrations were in 30.5%. There were 28.5% of the sandstones that lacked chlorite. The occurrence of high concentrations of chlorite varied stratigraphically, from 0.1% in Zone 2 to 60.4% in Zone 10, with an increasing-downward trend from Zone 1 through Zone 5 (Figure 16C). There was no discernible pattern of occurrence below Zone 5. High concentrations (≥7%) of potassium feldspar were only shown to exist in 0.36% of the sandstones, and the low concentrations (< 7%) were only in 0.19%. The potassium feldspar concentrations were not analyzed stratigraphically or by architectural-element type, due to such low occurrences.

KEY RESULTS AND DISCUSSION

The eight key lithofacies and three main architectural elements observed are similar to those previously documented in the basin (Cole and Cumella, 2005; Pranter et al., 2009; Hewlett, 2010; Sloan, 2012). The sandstone proportions (net-to-gross ratios) are within previously-observed ranges: middle Williams Fork Formation net-to-gross is 58.3%, compared to 50-80%, and upper Williams Fork Formation net-to-gross is 48.5%, compared to 15-60% (Hewlett, 2010). Crevasse-splay and channel-fill architectural

Table 3: Chlorite Distribution by Architectural Element Type		No VCHL	Low VCHL <1.3%	**High VCHL >1.3%**	Total
Percentage of total architectural elements (Weighted by proportion of crevasse splays and channel fills)	Channel Fill	27.4%	27.9%	38.0%	93.4%
	Crevasse Splays	2.1%	1.8%	2.7%	6.6%
	Channel Fill and Crevasse Splays	29.5%	29.8%	40.7%	100.0%
	Crevasse Splays	31.4%	27.6%	**41.1%**	100.0%
	Channel Fill	29.4%	29.9%	**40.7%**	100.0%

Table 3: The table summarizes chlorite distribution by architectural-element type. There was no significant difference between the architectural-element type (crevasse splays and channel fills) and the distribution of chlorite.

elements can be identified from wells logs, with crevasse splays showing a general upward-coarsening in the gamma-ray or v-shale logs, and channel fills showing a general upward-fining in the same logs. The stratigraphic variations in architectural elements were also comparable to previously established ranges: crevasse splays comprised 1-7% (compared to 1-20%) and channel fills comprised 18-75% (compared to 15-65%) of the total proportions (Hewlett, 2010). This additional dataset of net-to-gross ratios and architectural elements variations may allow for trend comparisons across fields, but data from additional fields within the basin are necessary to adequately characterize basin-wide trends. The decrease in observed crevasse splays from 20% in the middle Williams Fork Formation to 10% in the upper Williams Fork Formation and the increase in channel fills from 37% to 68% are both indications of a change in depositional style. There is possibly a transition from a meandering/anastamosing fluvial system with low aggradation to a braided fluvial system. However, determining depositional style was outside of the scope of this study and more work would be needed to conclusively determine such a change.

The two minerals investigated, chlorite and potassium feldspar, both averaged 1% within the overall study area, while having rare local measurements of up to 30%, calculated from the petrophysical model. These high proportions are not seen in the core data, and may be an artifact of limitations due to the petrophysical modeling or tool-measurement sensitivity. The highest percentages for chlorite (8.9%) and potassium feldspar (10%) from the cores were used as upper limits for subsequent modeling. Further investigation shows that 49.8% of the potassium feldspar from the petrophysical results (and contributing to the P_{50} value) occurs in the mudstone regions of the lithology model. These regions were excluded from the distribution modeling based on their v-clay log responses, and this exclusion is likely the cause of the low proportions calculated when compared to the P_{50} values. Adjusting the controls for calculating the v-shale in the intervals where potassium feldspar occurs as sand grains may result in more accurate lithology and proportion calculations in subsequent analysis.

The lowest stratigraphic zones of sand (zones 12 and14) were of particular interest in this study as they are directly above the completed intervals within the wells, and are possible targets for recompletions pending reevaluation of petrophysical models. When compared to the other zones, they exhibited the two highest percentages of sandstones containing chlorite: 84.5% of the sandstones in zone 12 and 96.5% of the sandstones in zone 14 had chlorite (Figure 16B). This is significant as relatively small amounts of iron-bearing chlorite increase water saturation calculations from well logs, and may indicate low-resistivity pay (Bates et al., 2004). This interval of the Williams Fork Formation has generally been considered part of the transition zone (<100% gas-saturated), and not historically completed due to higher calculated water saturations (Marc Connolly, personal communications, 2011). The transition zone could be an interval with bypassed pay in both existing and new wells if petrophysical and water-saturation models were not properly calibrated for low-resistivity minerals such as chlorite.

Although the architectural elements have different depositional controls, they are found in the same stratigraphic interval, and were subjected to the same post-depositional environment in terms of pressures and diagenetic fluids. As previously stated, there was no significant variation of chlorite distribution between channel-fill and crevasse-splay architectural elements. The lack of variation in distribution indicates that the chlorite is authigenic in nature, as has been previously suggested (Pitman et al., 1989; Crossey et al., 1992).

CONCLUSIONS

1. Eight lithofacies are identified in the middle and upper Williams Fork Formations from the core of the Cascade Creek 697-20-28 well: contorted mudstone (F_C), laminated mudstone (F_L), contorted sandstone (S_C), planar-laminated sandstone (S_L), ripple-laminated sandstone (S_R), wavy-laminated sandstone (S_{WL}) structureless sandstone (S_S), and coal (C). Examination of the core indicates that each lithofacies has distinct grain size, sedimentary structures, and contact styles.
2. Four architectural elements are identified in the core, each exhibiting distinct assemblages of lithofacies: channel fill, crevasse splay, floodplain, and coal. Each of the architectural elements indicates a different environment of deposition.
3. Net-to-gross ratios vary stratigraphically, from 8% to 88%. There is a higher average ratio in the middle Williams Fork Formation (58.3%) than in the upper Williams Fork Formation (48.5%). The proportions of crevasse splays (1-7%) and channel fills (18-75%) vary stratigraphically, and the ratio of channel fills to crevasse splays (CF:CS) is much lower in the middle Williams Fork Formation (1.9:1) than in the upper Williams Fork Formation (6.7:1). The control for the variations in both net-to-gross and CF:CS ratio is interpreted to be a change in depositional style.
4. The occurrence and distribution of chlorite and potassium feldspar can be estimated from limited core and well-log data. While the average proportions of chlorite and

potassium feldspars are both <1%, with P_{50} values of 1.3% and 7%, intervals of higher concentrations in the middle Williams Fork Formation exist directly above completed intervals. Saturation models in these intervals need to account for the occurrence of chlorite in order to correct for adverse effects on calculated water saturations such as artificially high calculations of water saturation and artificially low calculations of gas saturation.

5. Chlorite does not vary significantly between reservoir architectural elements, specifically channel fills and crevasse splays.
6. The occurrence of almost 50% of the potassium feldspar in mudstones indicates a need to re-evaluate the use of gamma-ray logs for lithology calculations, especially in intervals where the potassium feldspar occurs as sand-sized grains instead of clay particles. Doing so will result in more accurate shale and sand volume calculations.
7. The overall bottom-up increase in formation water resistivity (R_w) suggests an overall decrease in formation salinity, indicative of a landward shift in the depositional environment, where the formation water resistivity is less influenced by saltwater and more influenced by fresh water.
8. The results of this study demonstrate that petrophysical analysis of a reservoir should focus on factors that could artificially influence saturation models.

REFERENCES

Asquith, G., and D. Krygowski, 2004, Basic Well Log Analysis: AAPG Methods in Exploration 16, p.31-35.

Bates, T.G., J.W. Hankla, T.E. Voytovich and G. Hall, 2004, Identifying low resistivity pay in the Cotton Valley sand using a pulse neutron tool: Annual Meeting Expanded Abstracts - American Association of Petroleum Geologists, v. 13, 11 p.

Baytok, S., 2010, Three-dimensional seismic interpretation and discrete-fracture network modeling of the Williams Fork Formation, central Mamm Creek Field, Piceance Basin, Colorado: Master's Thesis, University of Colorado, Boulder, CO, 227 p.

Blakey, R. C., 2010, Paleogeographic and Paleotectonic Maps - Use, Construction, Interpretation, and Example, RMAG Short Course CD, January 28, 2010.

Bowen, D.G., 2005, Formation Evaluation and Petrophysics: Core Labs Manual, 273 p.

Burger, B.J., 2007, A new late Paleocene vertebrate fauna from the Ohio Creek Formation of Western Colorado: The Mountain Geologist, v. 44, p. 141-150.

Cantwell, J., 2010-2011. Personal communications.

Carroll, C. J., E. Robeck, G. Hunt, and W. Koontz, 2004, Structural implications of underground coal mining in the Mesaverde Group in the Somerset coal field, Delta and Gunnison counties, Colorado; field trips in the southern Rocky Mountains, USA. GSA Field Guide, 5, p. 41-58.

Cluff, R.M., and A.P. Byrnes, 2010, Relative permeability in tight gas sandstone reservoirs – the "permeability jail" model: SPWLA 51st Annual Logging Symposium, June 19-23, 16 p.

Cole, R. and S. Cumella, 2003, Stratigraphic architecture and reservoir characteristics of the Mesaverde Group, southern Piceance Basin, Colorado, in K.M. Peterson, T.M. Olsen, and D.S. Anderson, eds., Piceance Basin 2003 guidebook: Rocky Mountain Association of Geologists, p. 385-442.

Cole, R.D. and S.P. Cumella, 2005, Sand-Body Architecture in the Lower Williams Fork Formation (Upper Cretaceous), Coal Canyon, Colorado, with Comparison to the Piceance Basin Subsurface: The Mountain Geologist, v. 42, no. 3, p. 85-106.

Crain, E.R., 1986, The Log Analysis Handbook, Volume 1: Quantitative Log Analysis Methods, Pennwell Books, Tulsa, 684 p.

Crossey, I. J., and D. Larsen, 1992, Authigenic mineralogy of sandstones intercalated with organic-rich mudstones: Integrating diagenesis and burial history of the Mesaverde Group, Piceance Basin, northwest Colorado, in D. W. Houseknecht and E. D. Pittman, eds., Origin, diagenesis and petrophysics of clay minerals in sandstones: SEPM Special Publication 47, p. 125–144.

DeCelles, P. G., 2004, Late Jurassic to Eocene evolution of the Cordilleran thrust belt and foreland basin system, western U.S.A.: American Journal of Science, 304(2), p. 105-168.

Discovery Group Inc, Mesaverde Tight Gas Sandstones from Western US Basins, online report, http://www.discovery-group.com/projects_doe.htm, accessed April 2014.

Durand, C.L., E. Brosse, and A. Cerepi, 2001, Effect of pore-lining chlorite on petrophysical properties of low-resistivity sandstone reservoirs: SPE Reservoir Evaluation & Engineering Journal, Vol 5, no. 3, June 2001, p. 231-239.

German, Q. A., 2006, Analysis of fluvial sandstone-body characteristics and architecture in a high net-to-gross system: Upper Williams Fork Formation, Plateau Creek Canyon, Piceance Basin, Colorado: Master's Thesis, University of Colorado, Boulder, CO, 151 p.

Grose, L. T., 1972, Tectonics: Geologic Atlas of the Rocky Mountain Region: RMAG, p. 35-44.

Hemborg, H.T., 2000, Gas production characteristics of the Rulison, Grand Valley, Mamm Creek, and Parachute fields, Garfield County, Colorado: turning marginally economic basin-centered tight-gas sands into profitable reservoirs in the southern Piceance Basin: Report 39, 30 p.

Hettinger, R.D. and M.A. Kirschbaum, 2002, Stratigraphy of the Upper Cretaceous Mancos Shale (upper part) and Mesaverde Group in the southern part of the Uinta and Piceance basins, Utah and Colorado: Report I-2764, 21 p.

Hettinger, R.D. and M.A. Kirschbaum, 2003, Stratigraphy of the Upper Cretaceous Mancos shale (Upper Part) and Mesaverde Group in the southern part of the of the Uinta and Piceance basins, Utah and Colorado (Chapter 12), in Petroleum systems and geologic assessment of oil and gas in the Uinta-Piceance province, Utah and Colorado: United States Geological Survey Digital Data Series DDS-69-B, 25 p.

Hewlett, A.C., 2010, Analysis and modeling of the fluvial architecture and static connectivity of the Williams Fork Formation, central Mamm Creek Field, Piceance Basin, Colorado: Master's thesis, University of Colorado, Boulder, CO, 211 p.

Hoak, T. E., and A. L. Klawitter, 1997, Prediction of fractured reservoir production trends and compartmentalization using an integrated analysis of basement structures in the Piceance Basin, western Colorado, in T. E. Hoak, A. L. Klawitter, and P. K. Blomquist, eds., Fractured reservoirs, characterization and modeling: Denver, Colorado, Rocky Mountain Association of Geologists, p. 67–102.

Johnson, R.C., 1989, Geologic history and hydrocarbon potential of Late Cretaceous-age, low permeability reservoirs, Piceance Basin, Western Colorado: U.S. Geological Survey Bulletin 1787-E, 51 p.

Johnson, R.C., and Flores, R.M., 2003, History of the Piceance Basin from Latest Cretaceous through Early Eocene and the characterization of Lower Tertiary sandstone reservoirs, in K. M. Peterson, T. M. Olson, and D. S. Anderson eds., Piceance Basin 2003 guidebook: RMAG, p. 21-61.

Johnson, R.C., and May, F., 1980, A Study of the Cretaceous-Tertiary Unconformity in the Piceance Creek Basin, Colorado: The underlying Ohio Creek Formation (Upper Cretaceous) Redefined as a Member of the Hunter Canyon or Mesaverde Formation: Geological Survey Bulletin 1482-B.

Keeton, G.I., 2012, Sedimentological and stratigraphic characteristics of fluvial sandstones based on outcrop spectral-gamma-ray data and borehole images, Williams Fork Formation, Piceance Basin, Colorado: Master's Thesis, University of Colorado, Boulder, 142 p.

Law, B.E., 2002, Basin-centered Gas Systems: AAPG Bulletin, v. 86, no. 11, p. 1891-1919.

Lee, W.T., 1909, The Grand Mesa Coal field, Colorado: U.S. Geological Survey Bulletin 341, pt. 2, p. 316-334.

Lorenz, J.C., and Rutledge, A.K., 1987, Late Cretaceous Mesaverde Group outcrops at Rifle Gap, Piceance Creek basin, northwestern Colorado, in, Beus, S.S. (ed.), Rocky Mountain Section, Geological Society of America, Centennial Field Guide, v. 2, p.307-310.

Ozkan, A., Cumella, S. P., Milliken, K. L., & Laubach, S. E., 2011, Prediction of lithofacies and reservoir quality using well logs, late Cretaceous Williams Fork Formation, Mamm Creek field, Piceance Basin, Colorado. AAPG Bulletin, 95(10), 1699-1723.

Patterson, P.E., K. Kronmueller, and T.D. Davies, 2003, Sequence stratigraphy of the Mesaverde Group and Ohio Creek Conglomerate, northern Piceance Basin, Colorado, in K. M. Peterson, T. M. Olson, and D. S. Anderson eds., Piceance Basin 2003 guidebook: RMAG, p. 115-129.

Pitman, J. K., C. W. Spencer, and R. M. Pollastro, 1989, Petrography, mineralogy, and reservoir characteristics of the upper Cretaceous Mesaverde Group in the east-central Piceance Basin, Colorado: U.S.G.S. Bulletin, v. 1787-G, 31 p.

Pranter, M.J., A.I. Ellison, R.D. Cole, and P.E. Patterson, 2007, Analysis and modeling of intermediate-scale reservoir heterogeneity based on a fluvial point-bar outcrop analog, Williams Fork Formation, Piceance Basin, Colorado: AAPG Bulletin, v. 91, no.7, p. 1025-1051.

Pranter, M.J., Vargas, M.F., and Davis, T.L., 2008, Characterization and 3-D reservoir modeling of fluvial sandstones of the Williams Fork Formation, Rulison field, Piceance Basin, Colorado, U.S.A.: Journal of Geophysics and Engineering, v. 5, p. 158-172.

Pranter, M.J., R.D. Cole, H. Panjaitan, and N.K. Sommer, 2009, Sandstone-body dimensions in a lower coastal-plain depositional setting: Lower Williams Fork Formation, Coal Canyon, Piceance Basin, Colorado: AAPG Bulletin, v. 93, no. 10, p. 1379-1401.

Pranter, M.J., and Sommer, N.K., 2011, Static connectivity of fluvial sandstones in a lower coastal-plain setting: An example from the Upper Cretaceous lower Williams Fork Formation, Piceance Basin, Colorado: AAPG Bulletin, v. 95, no. 6 (June 2011), p. 899–923.

Rider, M. 2002, “Facies, sequences and depositional environments from logs” (Chapter 14), in M. H. Rider, The Geological Interpretation of Well Logs, 2nd edition: Rider-French Consulting Ltd., 288 p.

Ryer, T.A., and M. McPhillips, 1983, Early Late Cretaceous paleogeography of east/central Utah in Reynolds, M.W. and Dolly, E.D., eds., Mesozoic Paleogeography of the west-central United States: Society of Economic Paleontologists and Mineralogists, Rocky Mountain Paleogeography Symposium 2, p. 253-272.

Schlumberger. 2009, Log Interpretation Charts, 2009 Edition, 310 p.

Shaak, R.V., 2010, Stratigraphic architecture of shallow-marine to coastal-plain strata: Lower Williams Fork Formation, southeastern Piceance Basin, Colorado: Master’s Thesis, University of Colorado, Boulder, CO, 176 p.

Sloan, A.D., 2012, Stratigraphic architecture and connectivity of a low net-to-gross fluvial system: Combining outcrop analogs and multiple-point geostatistical modeling, lower Williams Fork Formation, Piceance Basin, Colorado: Master’s Thesis, University of Colorado, Boulder, CO, 266 p.

Tyler, R., and R. McMurray, 1995, Genetic stratigraphy, coal occurrence, and regional cross section of the Williams Fork Formation, Mesaverde Group, Piceance Basin, northwestern Colorado: Colorado Geological Survey Open File Report 95-2, 42 p.

Tweto, O., 1975, Laramide (late Cretaceous–early Tertiary) orogeny in the southern Rocky Mountains, in Curtis, B.F., ed., Cenozoic history of the southern Rocky Mountains: Geological Society of America Memoir 144, p. 1–44.

Tweto, O., 1977, Tectonic history of west-central Colorado, *in* Veal, H.K., ed., Exploration frontiers of the central and southern Rockies: Rocky Mountain Association of Geologists 1977 Symposium, p. 11-22.

Appendix

Appendix A

Expanded Discussion of Tectonic and Stratigraphic Setting

The paleogeography of the region which is now the Piceance Basin was controlled primarily by Cordilleran orogenic activity, beginning in late Jurassic time due to the Pacific oceanic plate subducting under the North American continental plate (DeCelles, 2004). The Cordilleran orogeny included the formation of the Sevier thrust belt, an area of active uplift in central Utah and southwestern Wyoming from Jurassic through early Cenozoic time (Tweto, 1977). The Sevier Thrust Belt was approximately 185 mi (300 km) wide in northern Utah, and extended from southern California to Alaska, coincident to the convergent margin along western North America (DeCelles, 2004). Thin-skinned, low-angle thrust faults decoupled Paleozoic and Mesozoic strata from basement rocks and created the highlands in central Utah during the Sevier Orogeny from Early Cretaceous into Eocene time (DeCelles, 2004). The Williams Fork Formation is composed of sediments from the Sevier highlands (Hemborg, 2000; Hettinger and Kirschbaum, 2002, 2003).

The Piceance Basin is an asymmetrical northwest-southeast-elongated basin bounded by numerous uplifts which developed during the Laramide Orogeny from Late Cretaceous through the Eocene (~75-40 Ma): the Axial Arch on the north, the White River Uplift on the east, the Sawatch Uplift and Elk Mountains on the southeast, the Gunnison Uplift on the south, the Uncompahgre Uplift on the southwest, the Douglas Arch on the west, and the Uinta Mountain Uplift on the northwest (Appendix B) (Tweto, 1975; Johnson, 1989). Basement-cored, high-angle reverse-fault uplifts during the

Laramide orogeny partitioned the larger Rocky Mountain Foreland Basin system into the multiple basins present today (Johnson and Flores, 2003; DeCelles, 2004).

The maximum extent of the Western Interior Seaway was reached during the early portion of the Late Cretaceous (~94-89 Ma) at which time the shoreline was located as far west as central Utah (Appendix C). During late Cretaceous time (97-95 Ma), the study area was located east of the Sevier Orogenic Belt, along the western shoreline of the Western Interior Seaway, within the Rocky Mountain Foreland Basin (Appendix D) (Hettinger and Kirschbaum, 2002, 2003). Sediments shed from the Sevier highlands in the west were transported towards the seaway by fluvial systems within alluvial- and coastal-plain settings (Hettinger and Kirschbaum, 2002, 2003).

The Mesaverde Group was deposited during Campanian time along the western margin of an epeiric seaway bisecting North America, running from northern Canada to the Gulf of Mexico (Johnson, 1989), and contains, in stratigraphic order, the Iles Formation, Williams Fork Formation, and Ohio Creek Member (Figure 2). Underlying and intertounging with the Mesaverde Group is the Mancos Shale, a marine shale deposited during major incursions of the Western Interior Seaway. The Mesaverde Group was deposited in an overall regression of the Western Interior Seaway as clastic sediments began to fill the basin, pushing the shoreline eastward (Johnson, 1989). Higher-order transgressive-regressive cycles are observed within the Mesaverde strata through detailed outcrop work and well-log analysis (Hettinger and Kirschbaum, 2002; Cole and Cumella, 2005; Shaak, 2010).

The Iles Formation is composed of multiple regressive marine sandstones of the Corcoran, Cozzette, and Rollins sandstone members, separated by tongues of the

Mancos Shale (Young, 1955; Johnson, 1989; Hettinger and Kirschbaum, 2002). The Williams Fork Formation, overlying the Iles Formation, is composed primarily of strata deposited by fluvial systems in the western portion of the Piceance Basin, with decreasing marine influence over time and towards the west. The Williams Fork Formation is approximately 5000 ft (1524 m) thick near the Grand Hogback on the eastern margin of the basin and thins to approximately 1200 ft (365 m) thick at the Colorado-Utah state line (Hettinger and Kirschbaum, 2002, 2003).The Williams Fork Formation is divided into the lower (sandstone-poor), middle and upper (sandstone-rich) Williams Fork Formations (Cole and Cumella, 2005). In certain localities within the basin, the lower Williams Fork Formation is further subdivided into the Bowie Shale Member and the unconformably overlying Paonia Shale Member (Lee, 1909). The uppermost portion of the Williams Fork Formation includes the Ohio Creek Member (or Conglomerate), identified as a white kaolinitic zone which may or may not contain conglomeratic lenses (Johnson and May, 1980). The Ohio Creek Member is separated from the rest of the Williams Fork Formation by an extensive unconformity, and has been interpreted as lowstand deposits formed by braided-fluvial rivers (Patterson et al., 2003).

The lower Williams Fork Formation was deposited within anastomosing to meandering river systems within a coastal-plain setting (Lorenz, 1987; Johnson, 1989; Hemborg, 2000; Patterson et al., 2003; Cole and Cumella, 2005). In the southeastern Piceance Basin near Mamm Creek Field, the lower Williams Fork Formation consists of offshore, distal to proximal lower shoreface and upper shoreface strata deposited during multiple transgressive-regressive cycles (Shaak, 2010). The middle and upper Williams

Fork Formations are interpreted as having been deposited by a low-to-moderate sinuosity braided river system within an alluvial-plain setting (Patterson et al., 2003; Cole and Cumella, 2005; German, 2006). This interpretation has primarily been based on: (1) the low-to-moderate range of paleocurrents, the paucity of sandstones with distinct lateral accretion surfaces, and the relatively higher net-to-gross ratio for the middle and upper Williams Fork Formations as well as the observations that the sandstones are highly amalgamated and sheetlike with high width-to-thickness ratios (8:1–100:1; average: 34:1) (German, 2006). Keeton (2012) recognized deposits in outcrop (Plateau Creek Canyon) that support dividing the upper Williams Fork formation into a lower meandering-fluvial system (Flaco interval) and an overlying braided-fluvial system (Ges interval).

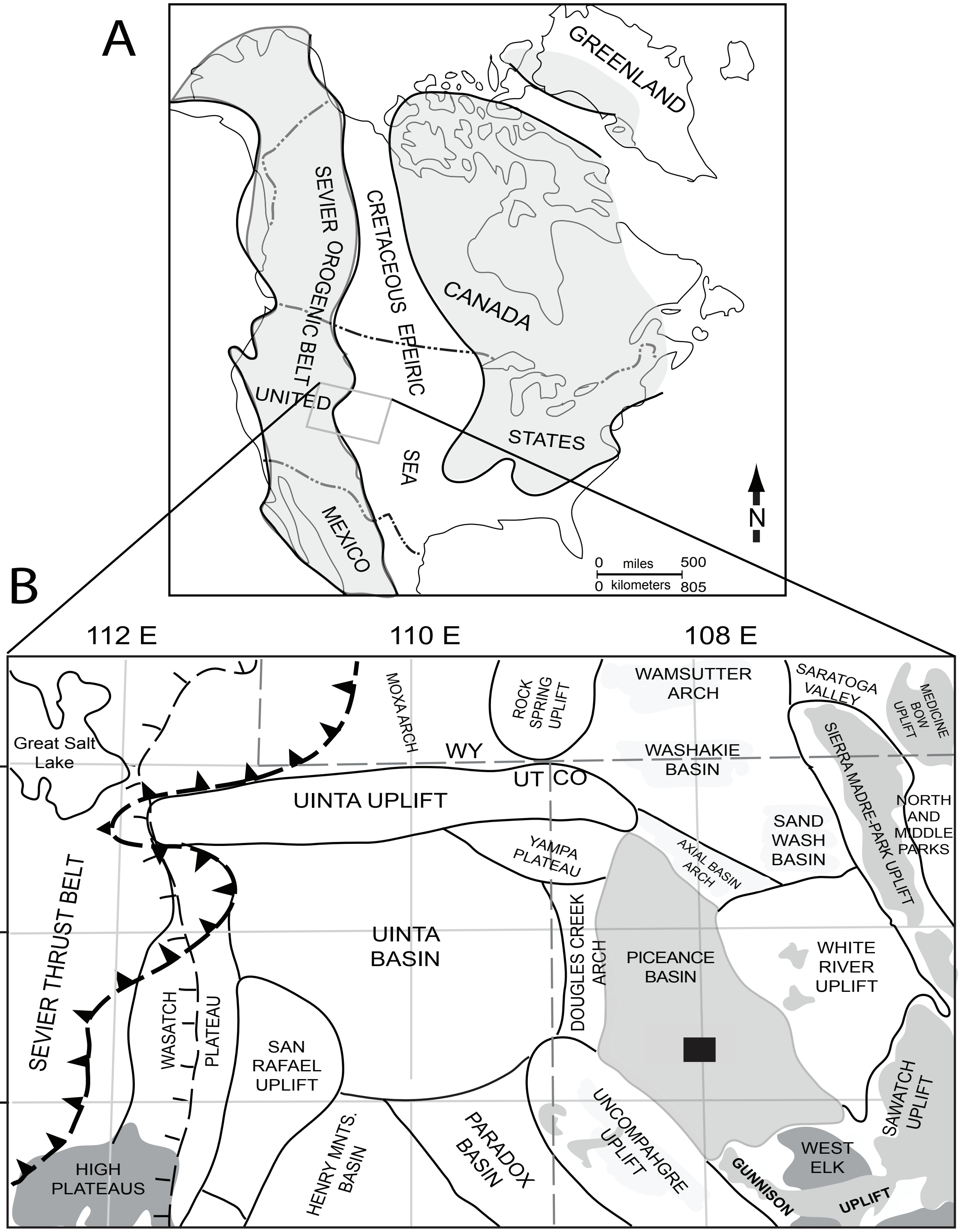

Appendix B

A) Generalized map of the Cretaceous Epeiric Seaway, Sevier orogenic belt, and Piceance Basin during the late Cretaceous. Modified from Johnson (1989) B) Generalized structural map of the Laramide tectonic elements in the eastern Utah and western Colorado. Modified from Grose (1972) and Patterson et al. (2003). Black box denotes study area.

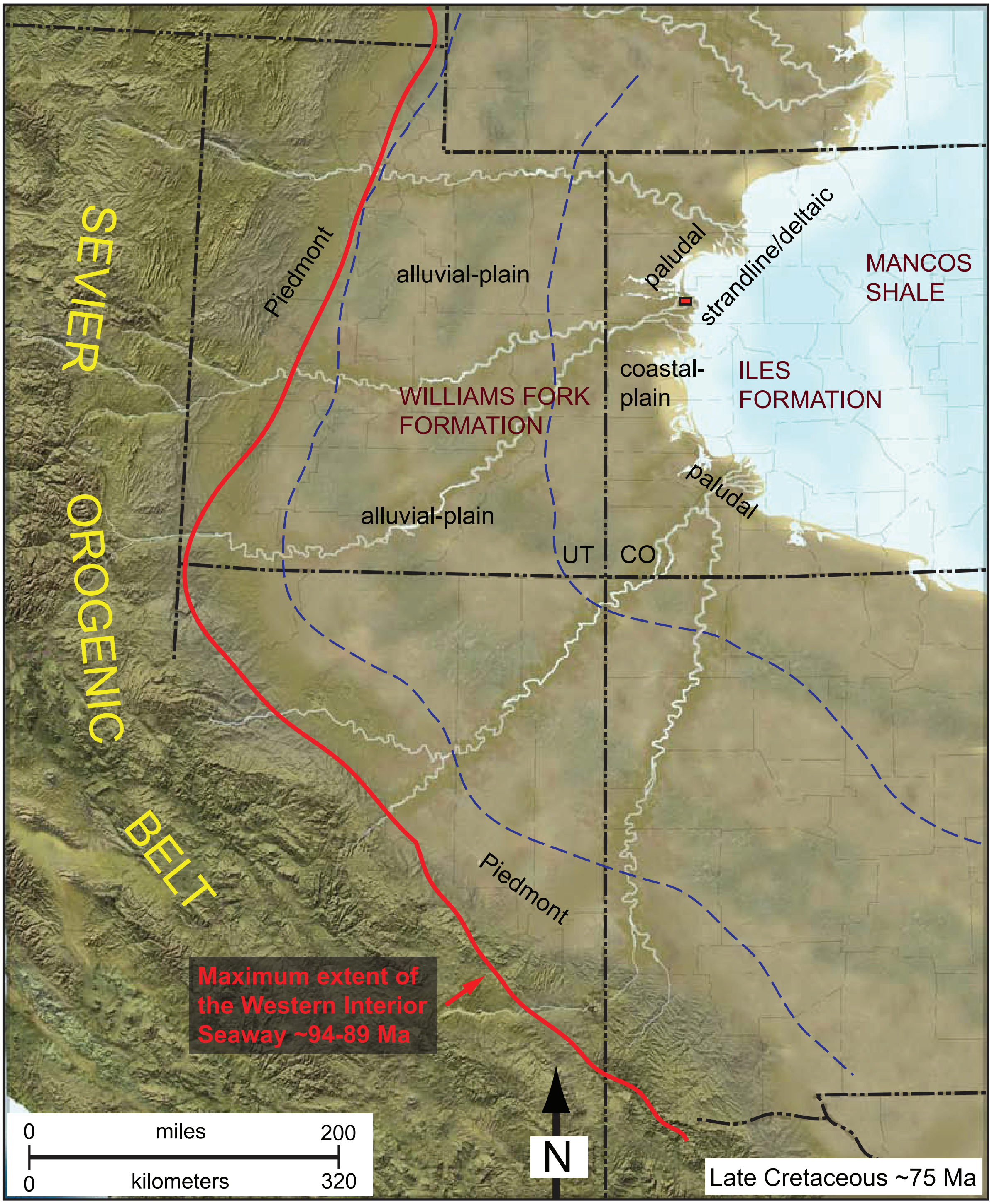

Appendix C
Late Cretaceous (~75 Ma) paleogeography of Western North America. Maximum extent of the Western Interior coastline during the early Late Cretaceous (~94-89 Ma) is shown in red, and study area is shown by red box near shoreline. Modified from Blakey (2010) and Baytok (2010).

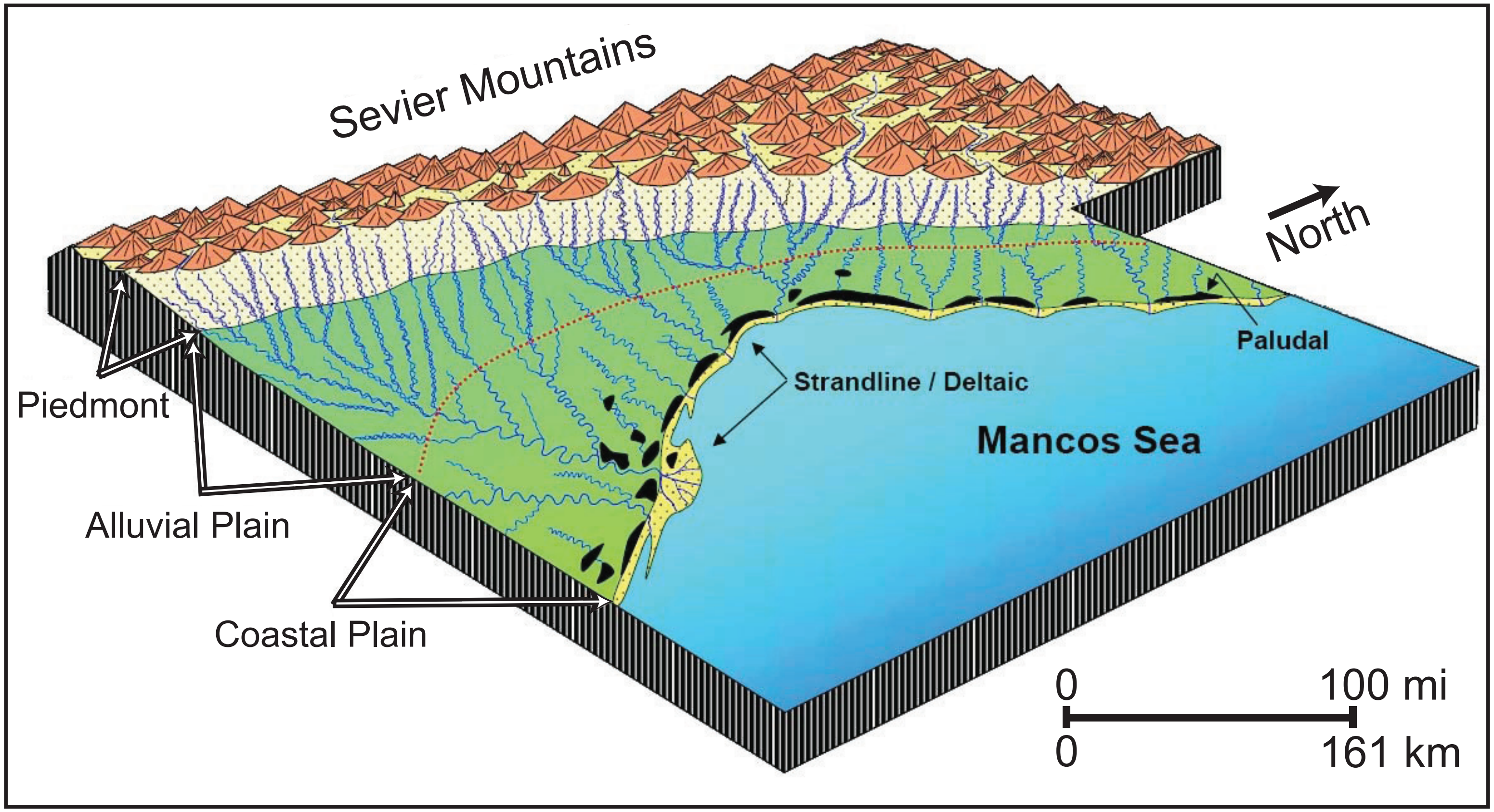

Appendix D. Idealized depiction of the Late Cretaceous depositional environment in Utah and western Colorado. From Cole and Cumella (2003). Modified from Ryer and McPhillips (1963).

Appendix E

List of select geophysical logs for the 27 wells

used in the petrophysical modeling.

Well logs were measured (Blue) or calculated (Green).

API	UWI	GR (Gamma Ray)	RHOB (Bulk Density)	RILD (Resistivity)	PHIN (Neutron Porosity)	VCHL (Chlorite Volume)	VKSP (Potassium Feldspar Volume)	VSH (Shale Volume)	PHIND (Neutron-Density Porosity)	BVW (Bulk Volume Water)	PHIE (Effective Porosity)
05045100100000	GM424-2	x	x	x	x	x	x	x	x	x	x
05045101330000	GM534-3	x	x	x	x	x	x	x	x	x	x
05045102210000	GM522-3	x	x	x	x	x	x	x	x	x	x
05045106420000	GM313-3	x	x	x	x	x	x	x	x	x	x
05045108710000	GM22-36	x	x	x	x	x	x	x	x	x	x
05045115980000	GM333-35	x	x	x	x	x	x	x	x	x	x
05045116000000	GM433-35	x	x	x	x	x	x	x	x	x	x
05045116010000	GM543-35	x	x	x	x	x	x	x	x	x	x
05045116030000	GM443-35	x	x	x	x	x	x	x	x	x	x
05045116040000	GM442-35	x	x	x	x	x	x	x	x	x	x
05045116090000	GM432-35	x	x	x	x	x	x	x	x	x	x
05045119370000	GM432-4	x	x	x	x	x	x	x	x	x	x
05045119580000	GM443-4	x	x	x	x	x	x	x	x	x	x
05045121330000	GM524-35	x	x	x	x	x	x	x	x	x	x
05045121360000	GM23-35	x	x	x	x	x	x	x	x	x	x
05045122650000	GM512-4	x	x	x	x	x	x	x	x	x	x
05045122660000	GM412-4	x	x	x	x	x	x	x	x	x	x
05045128270000	GM314-33	x	x	x	x	x	x	x	x	x	x
05045128320000	GM511-33	x	x	x	x	x	x	x	x	x	x
05045130490000	GM521-36	x	x	x	x	x	x	x	x	x	x
05045130660000	GM541-36	x	x	x	x	x	x	x	x	x	x
05045130710000	GM432-36	x	x	x	x	x	x	x	x	x	x
05045141340000	GM433-36	x	x	x	x	x	x	x	x	x	x
05045141350000	GM43-36	x	x	x	x	x	x	x	x	x	x
05045144690000	GM423-1	x	x	x	x	x	x	x	x	x	x
05045172090000	GM332-33	x	x	x	x	x	x	x	x	x	x
05045172100000	GM411-34	x	x	x	x	x	x	x	x	x	x

Appendix F

List of select geophysical logs for the 329 wells used in the lithology and architectural element modeling. Logs were provided by Occidental Petroleum Company (Blue) or interpreted (Green).

API	UWI	Smoothed GR (Gamma Ray)	Normalized NPHI (Neutron Porosity)	Normalized RHOB (Bulk Density)	VCL (Clay Volume)	Coal Flag	Lithology	Architectural Element
05045064820000	MV39906	x	x	x	x	x	x	x
05045065220000	MV40150	x	x	x	x	x	x	x
05045065710000	MV33-34	x	x	x	x	x	x	x
05045066150000	MV40029	x	x	x	x	x	x	x
05045066200000	GV19-36	x	x	x	x	x	x	x
05045066230000	GV12693	x	x	x	x	x	x	x
05045066250000	GV40150	x	x	x	x	x	x	x
05045066310000	GV24-36	x	x	x	x	x	x	x
05045066400000	GV23-34	x	x	x	x	x	x	x
05045066480000	GV21-35	x	x	x	x	x	x	x
05045067850000	MV39-3	x	x	x	x	x	x	x
05045068010000	GR43-3V	x	x	x	x	x	x	x
05045068020000	GR21-3V	x	x	x	x	x	x	x
05045068040000	GR44-33V	x	x	x	x	x	x	x
05045068090000	MV41-33	x	x	x	x	x	x	x
05045068270000	GM12389	x	x	x	x	x	x	x
05045068380000	GR24-35	x	x	x	x	x	x	x
05045068530000	GR21-4	x	x	x	x	x	x	x
05045068630000	DOE2-M-36	x	x	x	x	x	x	x
05045068920000	GM13-33	x	x	x	x	x	x	x
05045068980000	GM41-4	x	x	x	x	x	x	x
05045070470000	GM14-2	x	x	x	x	x	x	x
05045070500000	GM34-2	x	x		x	x	x	x
05045070560000	GM13-1	x	x	x	x	x	x	x
05045070580000	GM21-2	x	x		x	x	x	x
05045070590000	GM24-2	x	x	x	x	x	x	x
05045070610000	GM44-2	x	x	x	x	x	x	x
05045070620000	GM43-33	x	x	x	x	x	x	x
05045070920000	GM14-35	x	x	x	x	x	x	x
05045071020000	GM42-3	x	x	x	x	x	x	x
05045071040000	GM24-33	x	x	x	x	x	x	x
05045071050000	GM12359	x	x	x	x	x	x	x
05045071130000	GM31-3	x	x	x	x	x	x	x
05045071150000	GM13-2	x	x	x	x	x	x	x
05045071160000	GM40119	x	x	x	x	x	x	x

API	UWI	Smoothed GR (Gamma Ray)	Normalized NPHI (Neutron Porosity)	Normalized RHOB (Bulk Density)	VCL (Clay Volume)	Coal Flag	Lithology	Architectural Element
05045071190000	GM201-4	x	x	x	x	x	x	x
05045071200000	GM203-33	x	x	x	x	x	x	x
05045071250000	GM202-33	x	x	x	x	x	x	x
05045071270000	GM22-2	x	x	x	x	x	x	x
05045071280000	GM33-2	x	x	x	x	x	x	x
05045071290000	GM43-2	x	x	x	x	x	x	x
05045071300000	GM41-3	x	x	x	x	x	x	x
05045071310000	GM42-4	x	x	x	x	x	x	x
05045071320000	GM42-33	x	x	x	x	x	x	x
05045071330000	GM13-34	x	x	x	x	x	x	x
05045071470000	GM22-1	x	x	x	x	x	x	x
05045071720000	MV102-3	x	x	x	x	x	x	x
05045071730000	GM22-3	x	x	x	x	x	x	x
05045071890000	GR1-33R	x	x	x	x	x	x	x
05045071900000	GM34-3	x	x	x	x	x	x	x
05045071910000	GM44-3	x	x	x	x	x	x	x
05045071920000	GM33-3	x	x	x	x	x	x	x
05045072220000	GM24-34	x	x	x	x	x	x	x
05045072380000	GM32-2	x	x	x	x	x	x	x
05045072590000	GM24-1	x	x	x	x	x	x	x
05045072710000	GM40118	x	x	x	x	x	x	x
05045072720000	GM40148	x	x	x	x	x	x	x
05045073080000	GM231-34	x	x	x	x	x	x	x
05045073150000	GM33-4	x	x	x	x	x	x	x
05045073160000	GM32-4	x	x	x	x	x	x	x
05045073700000	GM42-1	x	x	x	x	x	x	x
05045073710000	GM33-1	x	x	x	x	x	x	x
05045073720000	GM43-1	x	x	x	x	x	x	x
05045073730000	GM32-1	x	x	x	x	x	x	x
05045073950000	GM269-3	x	x	x	x	x	x	x
05045073980000	GM33-34	x	x		x	x	x	x
05045074110000	GM14-4	x	x	x	x	x	x	x
05045074180000	GM14-1	x	x	x	x	x	x	x
05045074190000	GM12724	x	x	x	x	x	x	x
05045074420000	GM259-2	x	x	x	x	x	x	x

API	UWI	Smoothed GR (Gamma Ray)	Normalized NPHI (Neutron Porosity)	Normalized RHOB (Bulk Density)	VCL (Clay Volume)	Coal Flag	Lithology	Architectural Element
05045074430000	GM250-1	x	x		x	x	x	x
05045074440000	GM31-1	x	x	x	x	x	x	x
05045074640000	GM265-2	x	x	x	x	x	x	x
05045074680000	GM255-2	x	x	x	x	x	x	x
05045074730000	GM263-2	x			x	x	x	x
05045074890000	GM243-1	x	x	x	x	x	x	x
05045074900000	GM244-1	x	x	x	x	x	x	x
05045074990000	GM22-33	x	x	x	x	x	x	x
05045075000000	GM22-34	x	x	x	x	x	x	x
05045075020000	GM24-36	x	x	x	x	x	x	x
05045075030000	GM223-33	x	x	x	x	x	x	x
05045075080000	GM34-1	x	x	x	x	x	x	x
05045075230000	GM258-2	x			x	x	x	x
05045075310000	GM260-2	x			x	x	x	x
05045075430000	GM235-34	x			x	x	x	x
05045075700000	GM42-35	x			x	x	x	x
05045075760000	GM21-1	x	x	x	x	x	x	x
05045075770000	GM23-33	x	x	x	x	x	x	x
05045075960000	GM267-3	x	x	x	x	x	x	x
05045076020000	GM31-33	x	x	x	x	x	x	x
05045076080000	GM23-36	x	x	x	x	x	x	x
05045076350000	GM34-34	x	x	x	x	x	x	x
05045076870000	GM261-2	x			x	x	x	x
05045076880000	GM230-34	x			x	x	x	x
05045076890000	GM264-2	x			x	x	x	x
05045077110000	GM23-34	x	x	x	x	x	x	x
05045077140000	GM232-34	x			x	x	x	x
05045077300000	GM237-36	x	x	x	x	x	x	x
05045077310000	GM241-1	x	x	x	x	x	x	x
05045077320000	GM266-3	x			x	x	x	x
05045077420000	GM246-1	x	x	x	x	x	x	x
05045077430000	GM251-2	x	x	x	x	x	x	x
05045077450000	GM249-1	x	x	x	x	x	x	x
05045077460000	GM248-1	x	x	x	x	x	x	x
05045077480000	GM245-1	x	x	x	x	x	x	x

API	UWI	Smoothed GR (Gamma Ray)	Normalized NPHI (Neutron Porosity)	Normalized RHOB (Bulk Density)	VCL (Clay Volume)	Coal Flag	Lithology	Architectural Element
05045077560000	GM31-34	x	x	x	x	x	x	x
05045077800000	GM324-1	x			x	x	x	x
05045078310000	GM40151	x	x	x	x	x	x	x
05045078330000	GM14-33	x	x	x	x	x	x	x
05045078510000	GM33-35	x	x	x	x	x	x	x
05045078550000	GM43-35	x	x	x	x	x	x	x
05045078800000	GM543-33	x	x	x	x	x	x	x
05045078810000	GM443-33	x	x	x	x	x	x	x
05045078840000	GM434-33	x	x		x	x	x	x
05045078860000	GM544-33	x	x	x	x	x	x	x
05045078880000	GM444-33	x	x	x	x	x	x	x
05045079000000	GM433-33	x	x	x	x	x	x	x
05045079020000	GM534-33	x	x	x	x	x	x	x
05045079040000	GM533-33	x	x	x	x	x	x	x
05045079180000	GM238-36	x	x	x	x	x	x	x
05045079190000	GM333-36	x	x	x	x	x	x	x
05045079610000	GM254-2	x	x	x	x	x	x	x
05045079780000	GM257-2	x	x		x	x	x	x
05045079910000	GM256-2	x	x	x	x	x	x	x
05045080070000	GM12754	x	x	x	x	x	x	x
05045080090000	GM218-33	x	x	x	x	x	x	x
05045080280000	GM224-34	x	x	x	x	x	x	x
05045081020000	GM332-34	x	x		x	x	x	x
05045081030000	GM42-34	x	x		x	x	x	x
05045081040000	GM342-34	x	x		x	x	x	x
05045082040000	GM41-1	x	x	x	x	x	x	x
05045082050000	GM341-1	x			x	x	x	x
05045093860000	GM344-2	x	x	x	x	x	x	x
05045094220000	GM434-1	x	x	x	x	x	x	x
05045094230000	GM334-1	x	x	x	x	x	x	x
05045094720000	GM321-34	x			x	x	x	x
05045094790000	GM421-34				x	x	x	x
05045094800000	GM431-34				x	x	x	x
05045095000000	GM314-1				x	x	x	x
05045095550000	GM422-33				x	x	x	x

API	UWI	Smoothed GR (Gamma Ray)	Normalized NPHI (Neutron Porosity)	Normalized RHOB (Bulk Density)	VCL (Clay Volume)	Coal Flag	Lithology	Architectural Element
05045095560000	GM522-33				x	x	x	x
05045095630000	GM424-1				x	x	x	x
05045095770000	GM524-1				x	x	x	x
05045098000000	GM414-2				x	x	x	x
05045098010000	GM514-2				x	x	x	x
05045098740000	GM432-3				x	x	x	x
05045098750000	GM532-3				x	x	x	x
05045099390000	GM443-3				x	x	x	x
05045099400000	GM343-3				x	x	x	x
05045099670000	GM216-33	x			x	x	x	x
05045099700000	GM544-3				x	x	x	x
05045099710000	GM531-33	x			x	x	x	x
05045099720000	GM431-33	x			x	x	x	x
05045099730000	GM344-3				x	x	x	x
05045099740000	GM444-3				x	x	x	x
05045099750000	GM511-3	x	x	x	x	x	x	x
05045099760000	GM311-3				x	x	x	x
05045099770000	GM411-3				x	x	x	x
05045100050000	GM512-3				x	x	x	x
05045100060000	GM312-3				x	x	x	x
05045100070000	GM412-3				x	x	x	x
05045100100000	GM424-2				x	x	x	x
05045100200000	GM524-2				x	x	x	x
05045101130000	GM14-3	x	x	x	x	x	x	x
05045101160000	GM414-3				x	x	x	x
05045101190000	GM314-3				x	x	x	x
05045101200000	GM514-3	x			x	x	x	x
05045101250000	GM334-3				x	x	x	x
05045101320000	GM434-3	x			x	x	x	x
05045101330000	GM534-3				x	x	x	x
05045101760000	GM532-4				x	x	x	x
05045101810000	GM433-4				x	x	x	x
05045101820000	GM333-4				x	x	x	x
05045102060000	GM542-4				x	x	x	x
05045102070000	GM442-4				x	x	x	x

API	UWI	Smoothed GR (Gamma Ray)	Normalized NPHI (Neutron Porosity)	Normalized RHOB (Bulk Density)	VCL (Clay Volume)	Coal Flag	Lithology	Architectural Element
05045102090000	GM342-4				x	x	x	x
05045102130000	GM434-2				x	x	x	x
05045102140000	GM534-2				x	x	x	x
05045102150000	GM323-3				x	x	x	x
05045102160000	GM423-3	x		x	x	x	x	x
05045102170000	GM523-3				x	x	x	x
05045102210000	GM522-3				x	x	x	x
05045102220000	GM422-3				x	x	x	x
05045102230000	GM322-3				x	x	x	x
05045102440000	GM413-1	x		x	x	x	x	x
05045102450000	GM513-1	x		x	x	x	x	x
05045103740000	GM443-34				x	x	x	x
05045103750000	GM543-34				x	x	x	x
05045103760000	GM234-34	x	x	x	x	x	x	x
05045103770000	GM643-34	x			x	x	x	x
05045103800000	GM421-1	x		x	x	x	x	x
05045103810000	GM332-1	x		x	x	x	x	x
05045103820000	GM521-1	x	x		x	x	x	x
05045104650000	GM233-34				x	x	x	x
05045104660000	GM434-34				x	x	x	x
05045104670000	GM534-34				x	x	x	x
05045104830000	GM412-1	x	x	x	x	x	x	x
05045104840000	GM511-1	x		x	x	x	x	x
05045105270000	GM324-3				x	x	x	x
05045105280000	GM424-3				x	x	x	x
05045105290000	GM524-3				x	x	x	x
05045106350000	GM41-35				x	x	x	x
05045106390000	GM311-36				x	x	x	x
05045106400000	GM513-3	x		x	x	x	x	x
05045106410000	GM413-3				x	x	x	x
05045106420000	GM313-3				x	x	x	x
05045108590000	GM421-4				x	x	x	x
05045108600000	GM521-4				x	x	x	x
05045108610000	GM321-4				x	x	x	x
05045108680000	GM321-3				x	x	x	x

API	UWI	Smoothed GR (Gamma Ray)	Normalized NPHI (Neutron Porosity)	Normalized RHOB (Bulk Density)	VCL (Clay Volume)	Coal Flag	Lithology	Architectural Element
05045108710000	GM22-36	x	x	x	x	x	x	x
05045108720000	GM312-36				x	x	x	x
05045109210000	GM442-34	x	x		x	x	x	x
05045109220000	GM542-34	x	x	x	x	x	x	x
05045109230000	GM532-34	x	x	x	x	x	x	x
05045109240000	GM432-34	x	x	x	x	x	x	x
05045113620000	GM413-34	x		x	x	x	x	x
05045113630000	GM312-34	x	x	x	x	x	x	x
05045113640000	GM512-34	x	x	x	x	x	x	x
05045113650000	GM412-34	x	x	x	x	x	x	x
05045113960000	GM511-36	x	x	x	x	x	x	x
05045113970000	GM422-36	x	x	x	x	x	x	x
05045113980000	GM512-36	x	x	x	x	x	x	x
05045113990000	GM412-36	x	x	x	x	x	x	x
05045114000000	GM421-36	x	x	x	x	x	x	x
05045114250000	GM614-35	x		x	x	x	x	x
05045114260000	GM414-35				x	x	x	x
05045114270000	GM514-35				x	x	x	x
05045115020000	GM253-2	x		x	x	x	x	x
05045115030000	GM421-2				x	x	x	x
05045115050000	GM411-2				x	x	x	x
05045115060000	GM511-2				x	x	x	x
05045115980000	GM333-35				x	x	x	x
05045115990000	GM332-35				x	x	x	x
05045116000000	GM433-35	x	x	x	x	x	x	x
05045116010000	GM543-35	x	x	x	x	x	x	x
05045116020000	GM343-35				x	x	x	x
05045116030000	GM443-35	x	x	x	x	x	x	x
05045116040000	GM442-35	x	x	x	x	x	x	x
05045116050000	GM331-35				x	x	x	x
05045116090000	GM432-35	x	x	x	x	x	x	x
05045116100001	GM22-35R	x	x	x	x	x	x	x
05045116110000	GM342-35				x	x	x	x
05045116120000	GM341-35				x	x	x	x
05045116950000	GM441-3	x	x	x	x	x	x	x

API	UWI	Smoothed GR (Gamma Ray)	Normalized NPHI (Neutron Porosity)	Normalized RHOB (Bulk Density)	VCL (Clay Volume)	Coal Flag	Lithology	Architectural Element
05045116960000	GM541-3				x	x	x	x
05045119190000	GM433-3				x	x	x	x
05045119240000	GM333-3	x	x	x	x	x	x	x
05045119370000	GM432-4				x	x	x	x
05045119390000	GM533-4				x	x	x	x
05045119570000	GM343-4				x	x	x	x
05045119580000	GM443-4				x	x	x	x
05045120150000	GM513-2				x	x	x	x
05045120160000	GM413-2				x	x	x	x
05045120780000	GM422-2				x	x	x	x
05045120790000	GM423-2				x	x	x	x
05045121330000	GM524-35	x	x	x	x	x	x	x
05045121340000	GM424-35	x	x	x	x	x	x	x
05045121350000	GM324-35				x	x	x	x
05045121360000	GM23-35	x	x	x	x	x	x	x
05045122630000	GM322-4				x	x	x	x
05045122640000	GM312-4				x	x	x	x
05045122650000	GM512-4	x	x	x	x	x	x	x
05045122660000	GM412-4				x	x	x	x
05045124860000	GM532-2				x	x	x	x
05045124870000	GM432-2				x	x	x	x
05045124880000	GM542-2				x	x	x	x
05045124890000	GM442-2				x	x	x	x
05045124900000	GM441-2				x	x	x	x
05045124940000	GM444-4	x	x	x	x	x	x	x
05045124950000	GM434-4	x	x	x	x	x	x	x
05045126620000	GM643-35	x	x	x	x	x	x	x
05045126630000	GM227-35				x	x	x	x
05045126640000	GM34-35				x	x	x	x
05045126660000	GM544-35	x	x	x	x	x	x	x
05045127830000	GM441-4				x	x	x	x
05045127840000	GM431-4				x	x	x	x
05045128270000	GM314-33				x	x	x	x
05045128280000	GM324-33				x	x	x	x
05045128290000	GM424-33	x	x	x	x	x	x	x

API	UWI	Smoothed GR (Gamma Ray)	Normalized NPHI (Neutron Porosity)	Normalized RHOB (Bulk Density)	VCL (Clay Volume)	Coal Flag	Lithology	Architectural Element
05045128300000	GM411-33	x	x	x	x	x	x	x
05045128320000	GM511-33	x	x	x	x	x	x	x
05045130480000	GM21-36				x	x	x	x
05045130490000	GM521-36	x	x	x	x	x	x	x
05045130500000	GM321-36				x	x	x	x
05045130520000	GM541-35	x	x	x	x	x	x	x
05045130650000	GM531-36	x	x	x	x	x	x	x
05045130660000	GM541-36				x	x	x	x
05045130670000	GM442-36	x	x	x	x	x	x	x
05045130690000	GM431-36	x	x	x	x	x	x	x
05045130700000	GM342-36				x	x	x	x
05045130710000	GM432-36	x	x	x	x	x	x	x
05045130720000	GM341-36				x	x	x	x
05045130730000	GM441-36	x	x	x	x	x	x	x
05045130860000	GM31-35				x	x	x	x
05045130870000	GM411-36	x	x	x	x	x	x	x
05045133360000	GM444-1				x	x	x	x
05045133370000	GM344-1	x	x	x	x	x	x	x
05045133380000	GM544-1				x	x	x	x
05045134410000	GM443-1	x			x	x	x	x
05045134420000	GM543-1	x		x	x	x	x	x
05045134740000	GM442-1	x		x	x	x	x	x
05045134750000	GM542-1	x		x	x	x	x	x
05045135480000	GM228-34	x			x	x	x	x
05045135490000	GM422-34	x			x	x	x	x
05045139800000	GM424-36	x	x	x	x	x	x	x
05045139810000	GM225-36				x	x	x	x
05045139820000	GM513-36	x	x	x	x	x	x	x
05045141330000	GM44-36				x	x	x	x
05045141340000	GM433-36	x	x	x	x	x	x	x
05045141350000	GM43-36	x	x	x	x	x	x	x
05045141360000	GM444-36	x	x	x	x	x	x	x
05045141370000	GM434-36	x	x	x	x	x	x	x
05045142610000	GM441-1	x		x	x	x	x	x
05045142620000	GM344-36				x	x	x	x

API	UWI	Smoothed GR (Gamma Ray)	Normalized NPHI (Neutron Porosity)	Normalized RHOB (Bulk Density)	VCL (Clay Volume)	Coal Flag	Lithology	Architectural Element
05045144670000	GM411-1	x	x	x	x	x	x	x
05045144680000	GM512-1	x	x	x	x	x	x	x
05045144690000	GM423-1	x	x	x	x	x	x	x
05045146910000	GM423-36	x	x	x	x	x	x	x
05045146920000	GM323-36				x	x	x	x
05045146930000	GM239-36	x	x	x	x	x	x	x
05045146940000	GM413-36	x	x	x	x	x	x	x
05045172040000	GM432-33	x	x	x	x	x	x	x
05045172050000	GM442-33	x	x	x	x	x	x	x
05045172060000	GM441-33	x	x	x	x	x	x	x
05045172070000	GM532-33	x	x	x	x	x	x	x
05045172080000	GM342-33	x	x	x	x	x	x	x
05045172090000	GM332-33	x	x	x	x	x	x	x
05045172100000	GM411-34	x	x	x	x	x	x	x

Appendix G

Description for the Cascade Creek 697-20-28 core

Modified from Core Labs

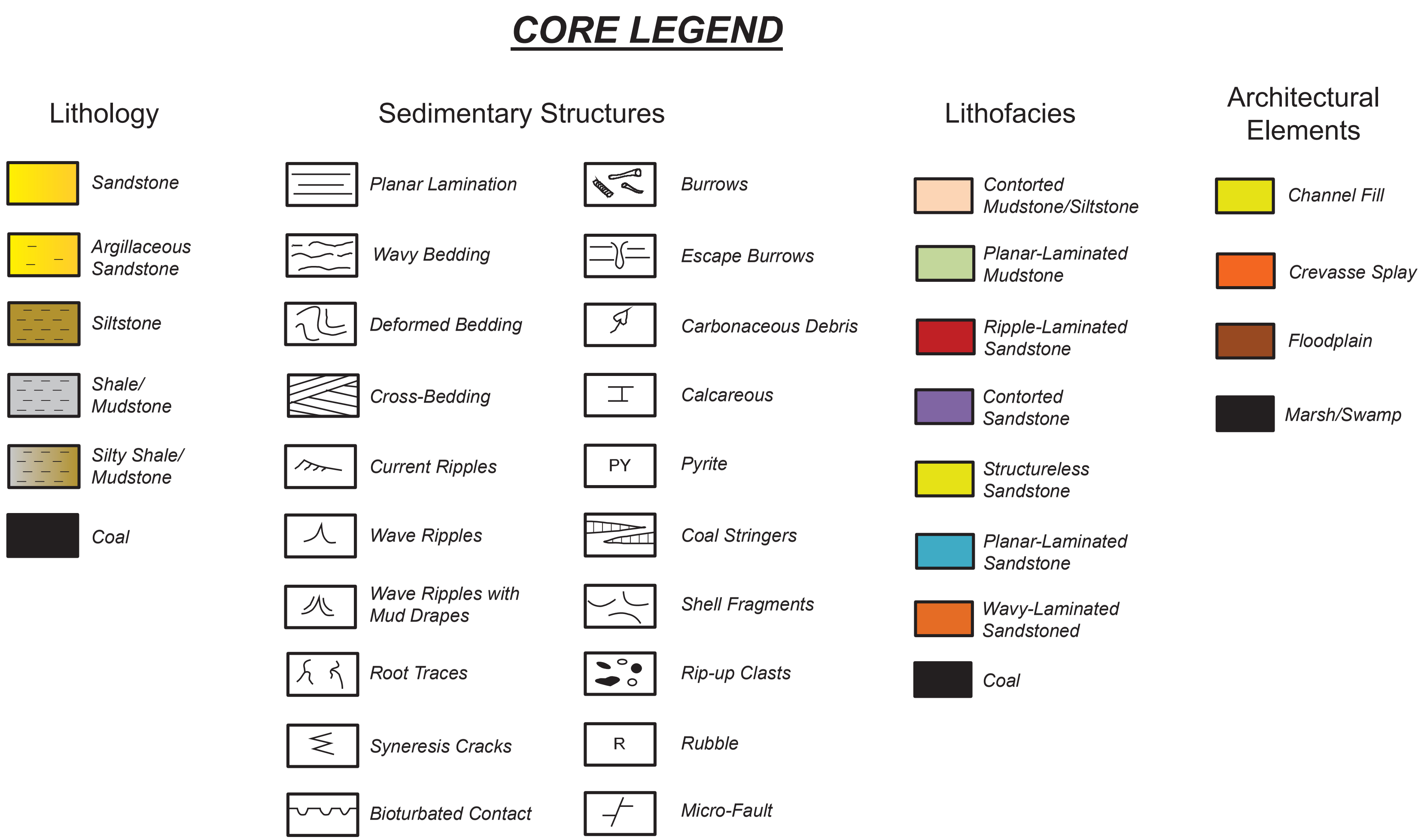

Legend describing key lithologies, sedimentary structures, lithofacies and architectural elements interpreted in the core from the Cascade Creek 697-20-28 well (Appendix D). Modified from Core Labs.

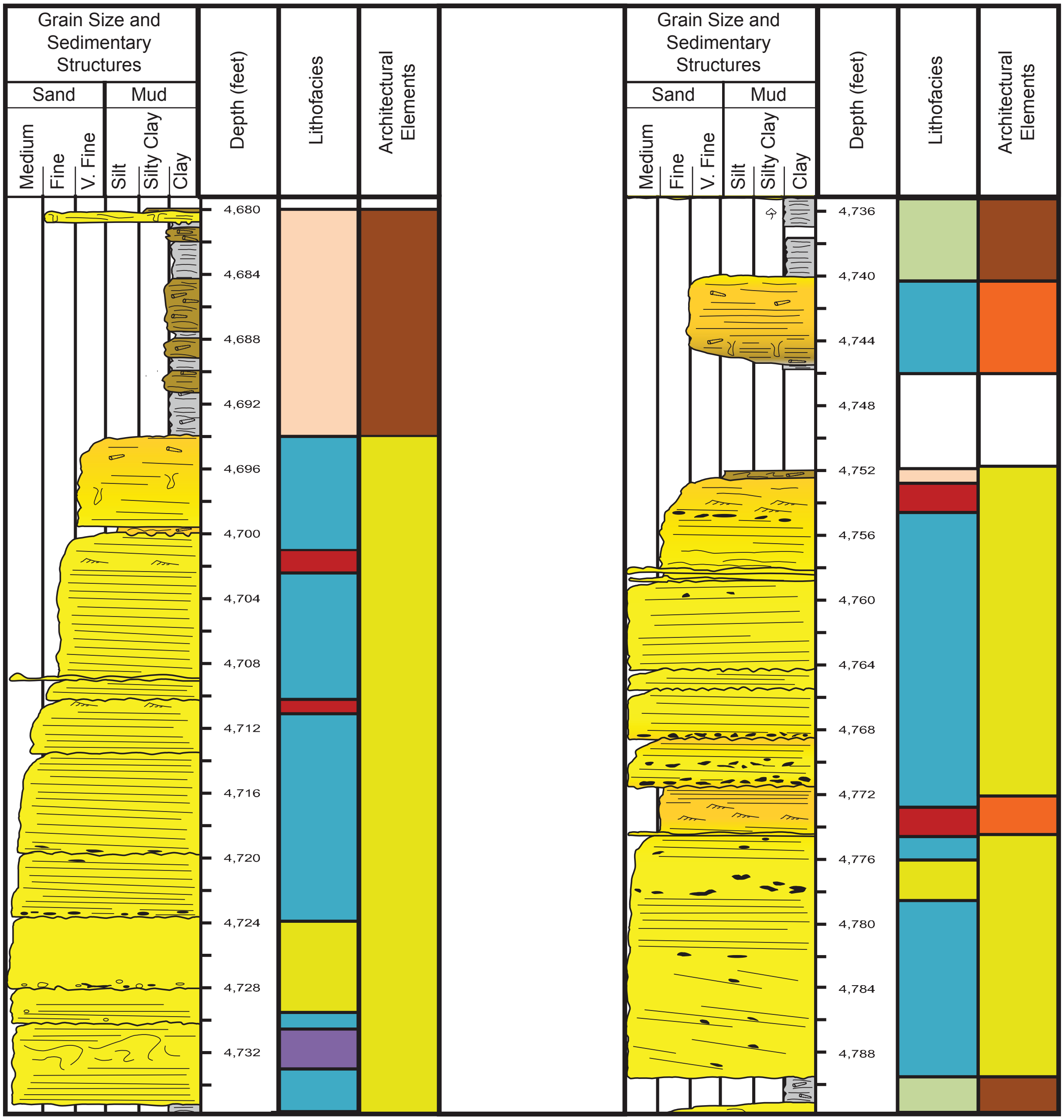

Upper Williams Fork Formation

Plate 1 of 2

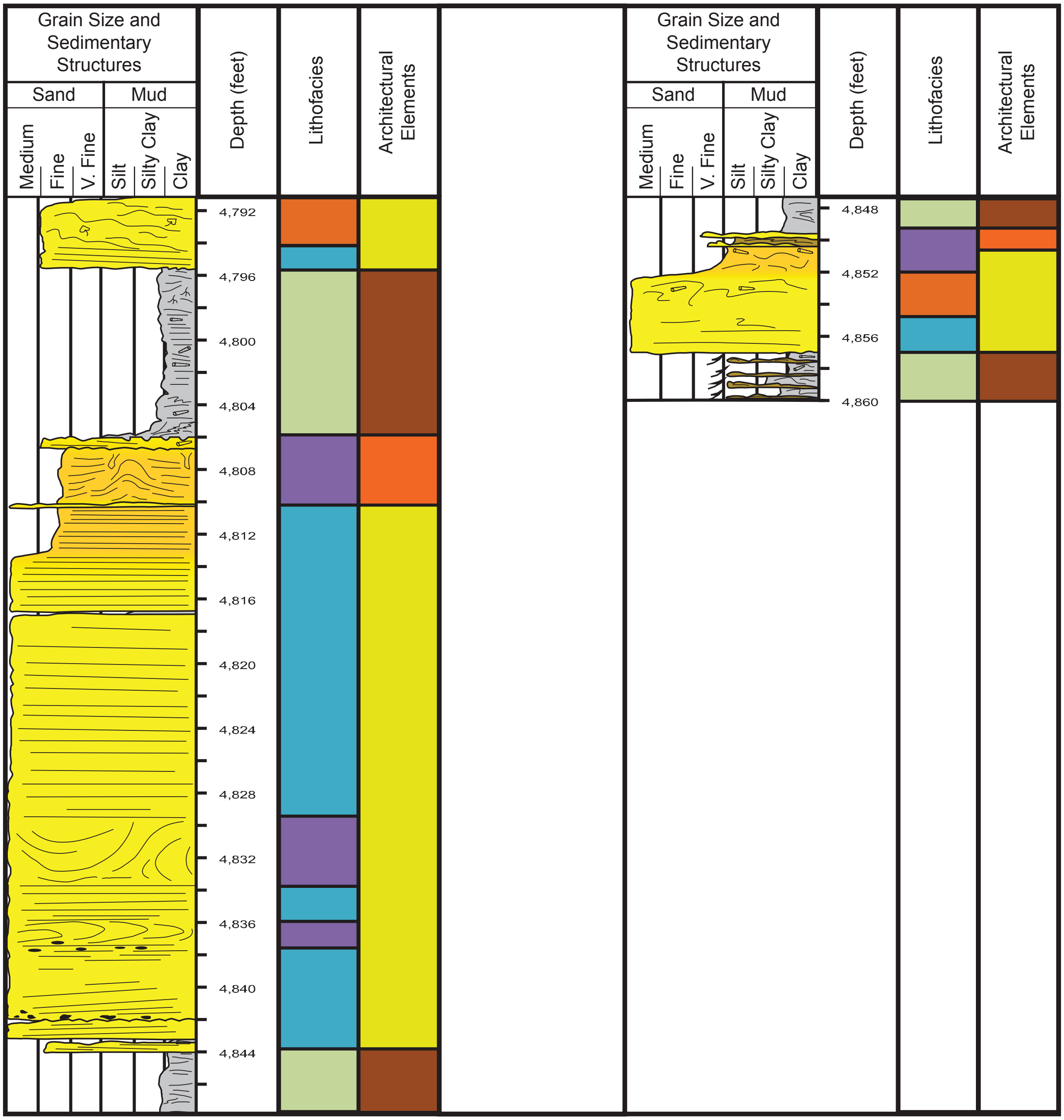

Upper Williams Fork Formation

Plate 2 of 2

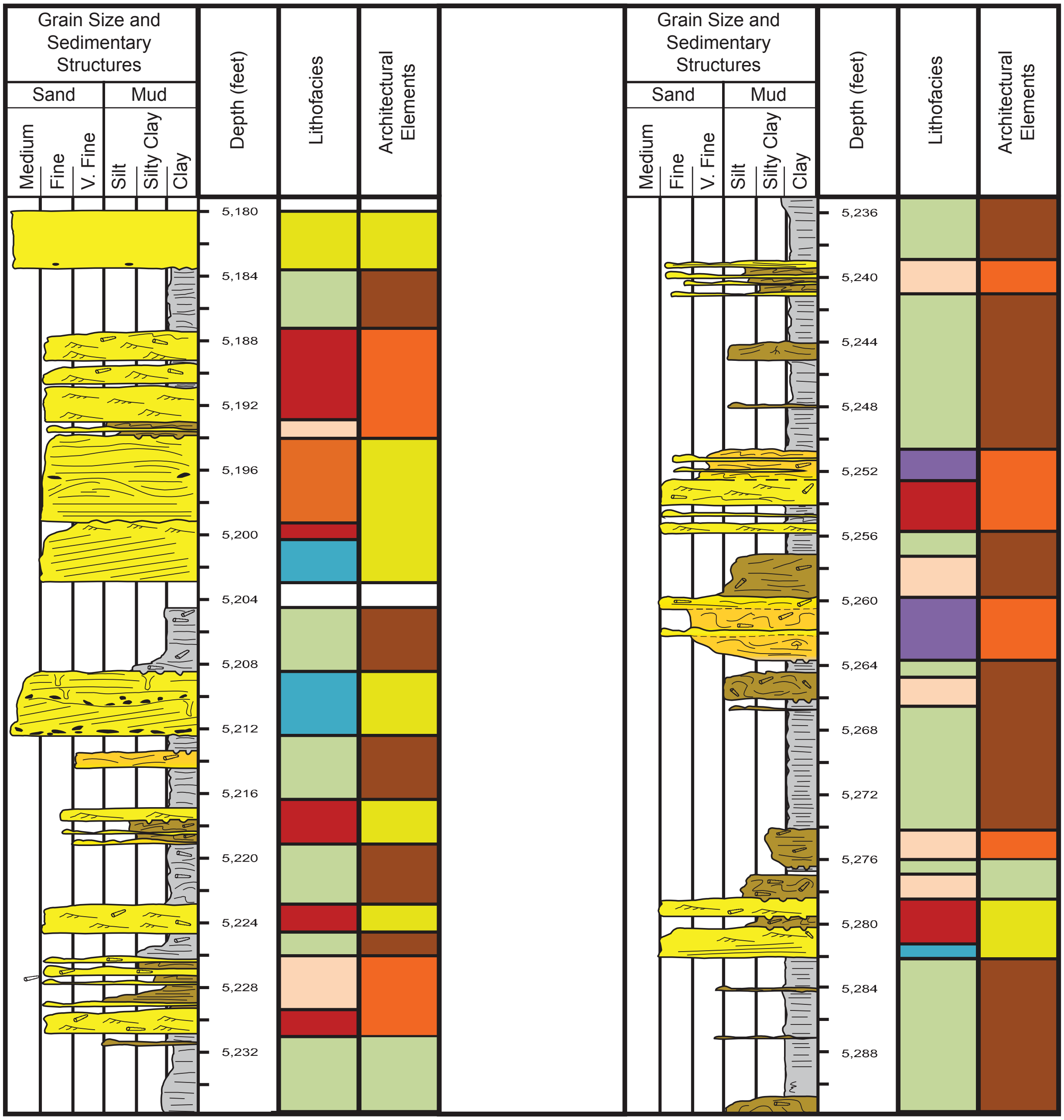

Middle Williams Fork Formation

Plate 1 of 2

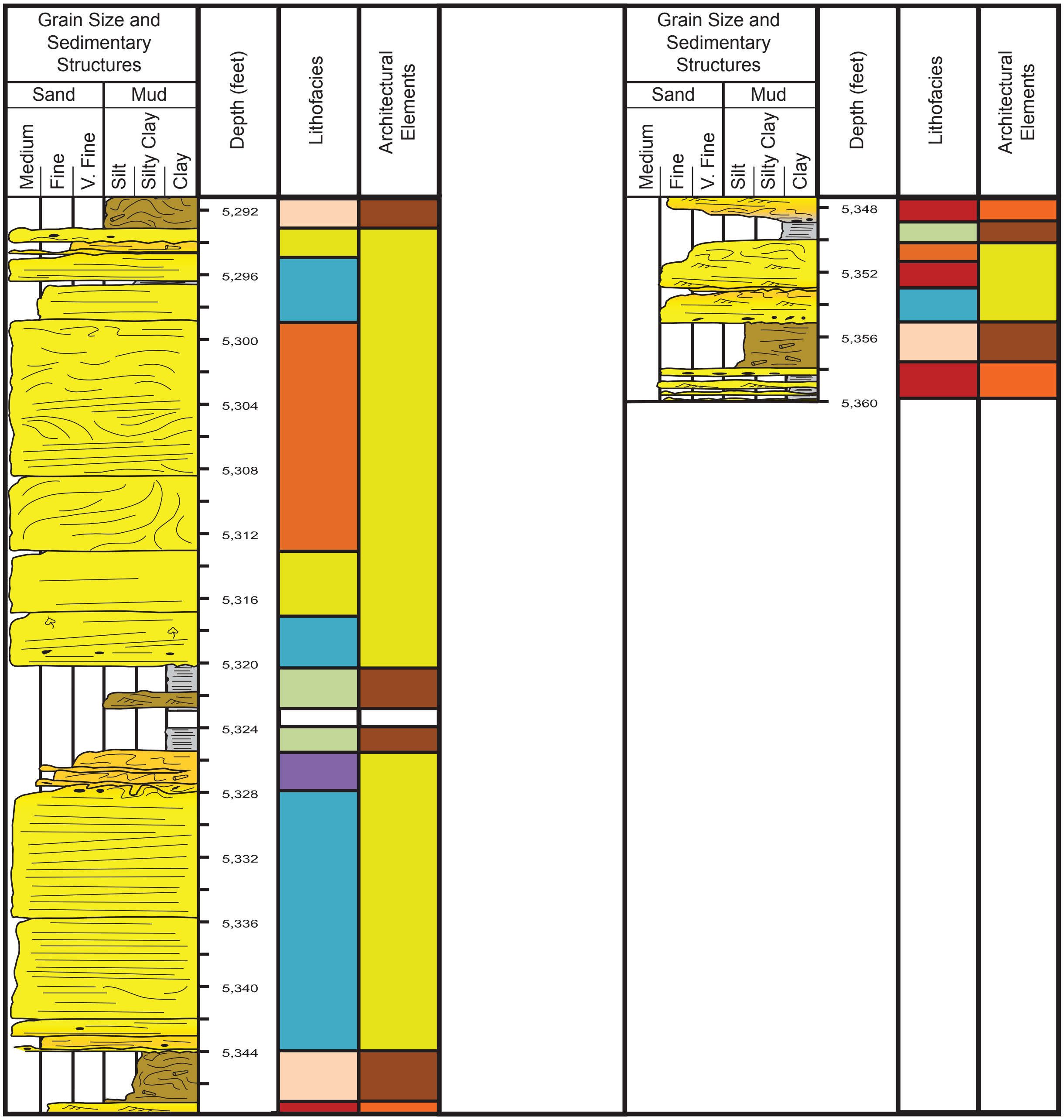

Middle Williams Fork Formation

Plate 2 of 2

Appendix H

Measured Depth (in feet) for Surfaces Modeled

In the Three-Dimensional Study

Well API	Well UWI	Top of Mesaverde	Top of Sand 700	Top of Mud 600	Top of Sand 600	Top of Mud 500	Top of Sand 500	Top of Mud 400	Top of Sand 400	Top of Mud 300	Top of Sand 300	Top of Mud 200	Top of Sand 200	Top of Mud 100	Top of Sand 100	Base of Middle Williams Fork
050450648200000	MV39906	3453	3473	3512	3556	3655	4006	4164	4317	4380	4428	4597	4652	4703	4727	4833
050450652200000	MV40150	3664	3684	3724	3768	3869	4231	4395	4556	4622	4671	4849	4906	4960	4984	5095
050450657100000	MV33-34	3610	3630	3671	3716	3818	4181	4345	4505	4570	4619	4796	4853	4907	4931	5042
050450661500000	MV40029	3765	3785	3824	3867	3964	4310	4465	4617	4679	4726	4893	4948	4998	5022	5127
050450662000000	GV19-36	3764	3785	3826	3871	3974	4340	4505	4665	4731	4780	4957	5015	5068	5093	5204
050450662300000	GV12693	3327	3347	3387	3431	3531	3888	4048	4204	4269	4317	4489	4545	4597	4621	4729
050450662500000	GV40150	3426	3445	3484	3526	3622	3963	4116	4265	4327	4373	4537	4591	4641	4664	4767
050450663100000	GV24-36	3723	3744	3786	3831	3935	4305	4471	4634	4700	4750	4928	4987	5041	5065	5178
050450664000000	GV23-34	3501	3521	3560	3602	3699	4044	4199	4350	4412	4459	4626	4680	4730	4754	4858
050450664800000	GV21-35	3608	3629	3670	3716	3820	4192	4359	4521	4588	4638	4818	4876	4930	4955	5068
050450678500000	MV39-3	3649	3668	3706	3748	3843	4182	4334	4483	4544	4589	4753	4806	4856	4878	4981
050450680100000	GR43-3V	3381	3401	3441	3485	3584	3939	4098	4253	4317	4365	4535	4591	4642	4666	4773
050450680200000	GR21-3V	3387	3407	3448	3492	3593	3953	4115	4273	4338	4386	4560	4617	4670	4694	4803
050450680400000	GR44-33V	3364	3384	3426	3471	3575	3944	4109	4271	4337	4387	4565	4623	4677	4702	4813
050450680900000	MV41-33	3515	3535	3575	3618	3717	4070	4229	4384	4447	4495	4666	4721	4773	4797	4904
050450682700000	GM12389	3629	3650	3691	3737	3841	4209	4375	4536	4603	4652	4830	4888	4942	4967	5078
050450683800000	GR24-35	3542	3562	3602	3646	3745	4100	4259	4415	4479	4526	4698	4754	4805	4829	4937
050450685300000	GR21-4	3454	3475	3516	3562	3666	4036	4203	4365	4432	4482	4660	4718	4772	4797	4910
050450686300000	DOE2-M-36	4386	4408	4450	4497	4603	4982	5153	5319	5387	5438	5622	5681	5737	5762	5877
050450689200000	GM13-33	3649	3669	3710	3756	3859	4225	4389	4550	4616	4665	4842	4900	4953	4978	5089
050450689800000	GM41-4	3308	3329	3370	3415	3517	3882	4045	4205	4270	4319	4496	4553	4606	4631	4741
050450704700000	GM14-2	3336	3355	3394	3437	3535	3882	4038	4190	4252	4299	4467	4522	4572	4596	4701
050450705000000	GM34-2	3231	3251	3291	3335	3435	3790	3950	4105	4169	4217	4388	4444	4496	4519	4627
050450705600000	GM13-1	3693	3713	3753	3798	3899	4257	4418	4575	4640	4688	4861	4918	4970	4994	5103
050450705800000	GM21-2	3370	3390	3430	3475	3575	3933	4093	4250	4314	4362	4534	4591	4643	4667	4775
050450705900000	GM24-2	3265	3284	3324	3367	3466	3817	3974	4128	4191	4238	4408	4463	4515	4538	4650
050450706100000	GM44-2	3213	3233	3274	3318	3418	3776	3937	4094	4159	4207	4380	4436	4488	4512	4621
050450706200000	GM43-33	3380	3401	3442	3488	3591	3957	4122	4283	4349	4399	4576	4633	4687	4712	4823
050450709200000	GM14-35	3492	3511	3550	3593	3690	4036	4191	4342	4404	4450	4617	4671	4721	4744	4849
050450710200000	GM42-3	3293	3312	3352	3396	3495	3847	4005	4160	4223	4271	4441	4496	4548	4571	4678
050450710400000	GM24-33	3708	3729	3771	3817	3921	4294	4461	4624	4691	4741	4921	4979	5034	5059	5172
050450710500000	GM12359	3466	3487	3528	3574	3678	4048	4214	4376	4443	4493	4671	4730	4784	4809	4921
050450711300000	GM31-3	3307	3327	3368	3412	3514	3875	4038	4196	4261	4310	4484	4540	4593	4617	4727
050450711500000	GM13-2	3237	3257	3296	3340	3438	3788	3946	4099	4162	4209	4378	4433	4484	4508	4614
050450711600000	GM40119	3365	3384	3424	3467	3565	3914	4071	4224	4286	4333	4502	4557	4608	4631	4737
050450711900000	GM201-4	3496	3516	3558	3604	3707	4076	4242	4404	4470	4520	4698	4756	4810	4835	4947
050450712000000	GM203-33	3615	3636	3678	3725	3830	4206	4374	4539	4606	4657	4839	4898	4952	4978	5092
050450712500000	GM202-33	3349	3369	3411	3456	3559	3927	4092	4254	4320	4369	4547	4605	4658	4683	4795
050450712700000	GM22-2	3274	3295	3335	3380	3481	3840	4002	4159	4224	4272	4446	4502	4555	4579	4688
050450712800000	GM33-2	3258	3278	3317	3361	3460	3812	3971	4125	4189	4236	4407	4462	4514	4537	4645
050450712900000	GM43-2	3318	3338	3378	3422	3521	3875	4034	4189	4252	4300	4471	4526	4578	4602	4709
050450713000000	GM41-3	3289	3308	3347	3390	3487	3832	3988	4139	4201	4248	4415	4469	4520	4543	4648
050450713100000	GM42-4	3588	3609	3650	3695	3797	4163	4327	4487	4552	4601	4778	4835	4889	4913	5024
050450713200000	GM42-33	3431	3451	3490	3534	3632	3984	4142	4296	4360	4407	4577	4632	4684	4707	4814
050450713300000	GM13-34	3411	3431	3471	3515	3615	3972	4132	4288	4352	4400	4572	4628	4680	4704	4812
050450714700000	GM22-1	3700	3721	3761	3806	3907	4266	4427	4585	4649	4698	4871	4927	4980	5004	5113

Well API	Well UWI	Top of Mesaverde	Top of Sand 700	Top of Mud 600	Top of Sand 600	Top of Mud 500	Top of Sand 500	Top of Mud 400	Top of Sand 400	Top of Mud 300	Top of Sand 300	Top of Mud 200	Top of Sand 200	Top of Mud 100	Top of Sand 100	Base of Middle Williams Fork
050450717200000	MV102-3	3323	3343	3382	3425	3522	3869	4024	4176	4238	4285	4452	4506	4557	4580	4685
050450717300000	GM22-3	3476	3495	3532	3573	3666	3998	4146	4291	4351	4395	4555	4607	4656	4678	4778
050450718900000	GR1-33R	3395	3416	3457	3502	3604	3969	4132	4292	4358	4407	4583	4640	4694	4718	4829
050450719000000	GM34-3	3534	3554	3592	3634	3729	4068	4220	4369	4430	4475	4639	4692	4742	4765	4868
050450719100000	GM44-3	3393	3413	3451	3494	3592	3937	4092	4243	4305	4352	4518	4572	4623	4646	4750
050450719200000	GM33-3	3457	3477	3516	3558	3655	3999	4154	4305	4367	4414	4580	4635	4685	4708	4813
050450722200000	GM24-34	3301	3321	3361	3404	3503	3856	4015	4169	4233	4280	4451	4506	4558	4582	4689
050450723800000	GM32-2	3338	3358	3397	3441	3540	3894	4053	4208	4271	4319	4489	4545	4596	4620	4727
050450725900000	GM24-1	3283	3303	3344	3389	3492	3857	4021	4182	4247	4297	4473	4531	4584	4609	4720
050450727100000	GM40118	3795	3815	3856	3900	4002	4364	4527	4685	4750	4799	4974	5031	5084	5108	5218
050450727200000	GM40148	3751	3771	3811	3856	3957	4316	4478	4635	4700	4748	4922	4978	5031	5055	5164
050450730800000	GM231-34	3383	3403	3444	3488	3589	3949	4110	4267	4332	4381	4554	4611	4663	4687	4796
050450731500000	GM33-4	3616	3636	3676	3720	3820	4176	4336	4492	4556	4604	4775	4831	4883	4907	5015
050450731600000	GM32-4	3305	3326	3367	3412	3515	3881	4045	4206	4271	4321	4497	4555	4608	4633	4744
050450737000000	GM42-1	3521	3542	3583	3628	3731	4096	4260	4421	4486	4536	4712	4770	4823	4848	4959
050450737100000	GM33-1	3624	3644	3685	3731	3833	4199	4364	4524	4590	4639	4816	4874	4927	4952	5063
050450737200000	GM43-1	3442	3462	3504	3549	3652	4019	4184	4345	4411	4461	4638	4696	4750	4775	4886
050450737300000	GM32-1	3664	3684	3726	3771	3874	4241	4406	4567	4633	4682	4860	4917	4971	4996	5107
050450739500000	GM269-3	3455	3475	3514	3556	3654	4000	4155	4307	4369	4415	4582	4637	4687	4711	4815
050450739800000	GM33-34	3477	3497	3538	3583	3684	4046	4208	4367	4432	4481	4656	4713	4766	4791	4901
050450741100000	GM14-4	3466	3487	3528	3574	3678	4048	4215	4376	4443	4493	4671	4729	4783	4808	4920
050450741800000	GM14-1	3386	3407	3447	3491	3592	3952	4113	4271	4336	4384	4558	4614	4667	4691	4800
050450741900000	GM12724	3723	3744	3785	3830	3933	4299	4464	4624	4690	4740	4917	4975	5029	5053	5165
050450744200000	GM259-2	3314	3334	3373	3417	3515	3864	4021	4174	4237	4284	4453	4508	4559	4582	4688
050450744300000	GM250-1	3385	3406	3446	3491	3592	3954	4116	4275	4340	4388	4563	4619	4672	4696	4805
050450744400000	GM31-1	3655	3676	3718	3764	3870	4244	4413	4577	4644	4694	4875	4934	4988	5014	5127
050450746400000	GM265-2	3217	3237	3276	3320	3419	3771	3929	4083	4147	4194	4364	4420	4471	4495	4602
050450746800000	GM255-2	3274	3294	3333	3377	3476	3827	3985	4139	4203	4250	4420	4475	4527	4550	4657
050450747300000	GM263-2	3347	3366	3405	3447	3544	3889	4044	4195	4258	4304	4471	4525	4576	4599	4704
050450748900000	GM243-1	3734	3754	3794	3839	3939	4296	4457	4614	4678	4726	4899	4955	5007	5031	5139
050450749000000	GM244-1	3814	3834	3875	3920	4023	4387	4550	4709	4775	4824	5000	5057	5110	5135	5245
050450749900000	GM22-33	3433	3453	3493	3538	3639	3999	4160	4318	4382	4431	4604	4661	4713	4737	4846
050450750000000	GM22-34	3577	3598	3639	3685	3789	4160	4327	4490	4556	4606	4786	4844	4898	4923	5036
050450750200000	GM24-36	3723	3744	3787	3833	3939	4316	4485	4651	4718	4769	4951	5010	5065	5091	5205
050450750300000	GM223-33	3350	3370	3411	3456	3558	3921	4085	4244	4309	4358	4534	4591	4644	4669	4779
050450750800000	GM34-1	3655	3676	3718	3763	3867	4237	4403	4566	4632	4682	4861	4919	4973	4998	5110
050450752300000	GM258-2	3380	3401	3442	3487	3589	3953	4116	4275	4340	4389	4564	4620	4673	4697	4807
050450753100000	GM260-2	3218	3238	3278	3322	3422	3778	3938	4095	4159	4207	4379	4435	4487	4511	4619
050450754300000	GM235-34	3494	3514	3553	3597	3696	4048	4207	4362	4425	4472	4643	4698	4750	4774	4881
050450757000000	GM42-35	4144	4165	4206	4250	4352	4711	4872	5029	5094	5142	5315	5371	5424	5448	5557
050450757600000	GM21-1	3689	3710	3752	3797	3901	4269	4435	4596	4663	4712	4890	4948	5002	5027	5139
050450757700000	GM23-33	3632	3653	3695	3741	3845	4218	4386	4549	4617	4667	4847	4906	4961	4986	5099
050450759600000	GM267-3	3282	3302	3341	3383	3481	3826	3981	4132	4194	4241	4407	4462	4512	4535	4639
050450760200000	GM31-33	3475	3495	3534	3578	3678	4032	4191	4345	4409	4457	4627	4683	4734	4758	4865
050450760800000	GM23-36	3887	3908	3951	3998	4104	4482	4651	4817	4885	4936	5118	5178	5233	5258	5373
050450763500000	GM34-34	3335	3356	3397	3442	3544	3907	4070	4229	4294	4343	4518	4575	4628	4652	4762

Well API	Well UWI	Top of Mesaverde	Top of Sand 700	Top of Mud 600	Top of Sand 600	Top of Mud 500	Top of Sand 500	Top of Mud 400	Top of Sand 400	Top of Mud 300	Top of Sand 300	Top of Mud 200	Top of Sand 200	Top of Mud 100	Top of Sand 100	Base of Middle Williams Fork
050450768700000	GM261-2	3245	3265	3305	3350	3450	3809	3970	4127	4192	4240	4413	4470	4522	4546	4655
050450768800000	GM230-34	3368	3388	3429	3473	3575	3937	4099	4258	4323	4372	4547	4603	4656	4681	4791
050450768900000	GM264-2	3198	3218	3258	3302	3403	3761	3922	4079	4143	4192	4365	4421	4474	4498	4607
050450771100000	GM23-34	3410	3429	3469	3513	3612	3966	4125	4280	4343	4391	4562	4618	4669	4693	4801
050450771400000	GM232-34	3401	3421	3461	3506	3606	3962	4122	4277	4341	4388	4559	4615	4666	4690	4797
050450773000000	GM237-36	3734	3755	3796	3841	3944	4311	4476	4637	4702	4752	4929	4987	5040	5065	5176
050450773100000	GM241-1	3606	3626	3667	3713	3815	4181	4346	4506	4572	4621	4799	4856	4910	4935	5046
050450773200000	GM266-3	3293	3312	3352	3395	3493	3843	4000	4153	4216	4263	4432	4487	4538	4562	4668
050450774200000	GM246-1	3553	3573	3615	3660	3763	4130	4295	4456	4522	4572	4749	4807	4861	4886	4997
050450774300000	GM251-2	3691	3711	3751	3796	3896	4253	4413	4569	4633	4682	4854	4910	4962	4986	5094
050450774500000	GM249-1	3700	3721	3762	3807	3909	4275	4439	4599	4665	4714	4891	4948	5002	5026	5137
050450774600000	GM248-1	3595	3616	3657	3703	3807	4176	4341	4503	4569	4619	4797	4855	4909	4934	5046
050450774800000	GM245-1	3543	3564	3605	3650	3753	4119	4283	4444	4509	4559	4735	4793	4846	4871	4982
050450775600000	GM31-34	3697	3718	3759	3804	3908	4275	4440	4601	4667	4716	4894	4952	5005	5030	5141
050450778000000	GM324-1	3351	3372	3415	3461	3568	3947	4114	4275	4341	4391	4568	4625	4679	4703	4814
050450783100000	GM40151	3420	3441	3482	3528	3633	4001	4165	4326	4391	4441	4618	4676	4730	4754	4865
050450783300000	GM14-33	3754	3776	3819	3866	3975	4354	4522	4685	4752	4802	4981	5039	5093	5118	5230
050450785100000	GM33-35	4099	4119	4159	4204	4306	4667	4829	4987	5052	5101	5276	5332	5385	5410	5519
050450785500000	GM43-35	4099	4119	4159	4204	4306	4667	4829	4987	5052	5101	5275	5332	5385	5409	5519
050450788000000	GM543-33	3384	3405	3446	3491	3595	3962	4126	4285	4351	4400	4575	4632	4685	4710	4820
050450788100000	GM443-33	3391	3411	3451	3496	3597	3955	4116	4273	4337	4385	4557	4613	4665	4689	4798
050450788400000	GM434-33	3695	3716	3758	3804	3908	4277	4442	4602	4668	4717	4894	4951	5005	5029	5140
050450788600000	GM544-33	3402	3423	3464	3509	3610	3973	4135	4294	4359	4408	4582	4639	4691	4716	4825
050450788800000	GM444-33	3367	3387	3428	3473	3575	3938	4101	4259	4325	4373	4548	4605	4658	4683	4792
050450790000000	GM433-33	3505	3525	3566	3610	3711	4071	4232	4388	4452	4500	4672	4728	4780	4804	4912
050450790200000	GM534-33	3594	3615	3656	3701	3805	4172	4337	4498	4564	4614	4791	4849	4902	4927	5038
050450790400000	GM533-33	3399	3419	3460	3505	3607	3968	4130	4288	4353	4402	4576	4633	4686	4710	4819
050450791800000	GM238-36	3729	3749	3791	3836	3940	4310	4476	4638	4704	4754	4932	4990	5044	5069	5181
050450791900000	GM333-36	3794	3815	3858	3905	4012	4391	4561	4727	4795	4846	5028	5087	5142	5167	5281
050450796100000	GM254-2	3313	3333	3372	3416	3516	3871	4031	4187	4250	4298	4470	4525	4577	4601	4709
050450797800000	GM257-2	3373	3393	3435	3480	3583	3953	4119	4280	4346	4396	4572	4630	4683	4708	4819
050450799100000	GM256-2	3298	3318	3358	3402	3503	3859	4019	4175	4239	4287	4459	4515	4567	4591	4700
050450800700000	GM12754	3528	3549	3591	3637	3742	4115	4283	4447	4514	4564	4744	4803	4857	4883	4996
050450800900000	GM218-33	3541	3562	3604	3650	3754	4125	4290	4451	4517	4567	4744	4801	4855	4880	4991
050450802800000	GM224-34	3745	3766	3808	3855	3960	4336	4506	4671	4739	4790	4972	5031	5086	5112	5226
050450810200000	GM332-34	3601	3622	3663	3708	3811	4179	4346	4507	4574	4623	4801	4859	4912	4937	5049
050450810300000	GM42-34	3625	3646	3688	3734	3838	4211	4380	4544	4611	4661	4840	4897	4951	4975	5086
050450810400000	GM342-34	3604	3624	3664	3708	3809	4170	4334	4493	4557	4606	4780	4836	4889	4913	5021
050450820400000	GM41-1	3762	3783	3826	3872	3978	4351	4518	4681	4748	4798	4978	5036	5090	5115	5228
050450820500000	GM341-1	3730	3752	3796	3844	3952	4337	4508	4674	4742	4793	4976	5035	5091	5116	5231
050450938600000	GM344-2	3280	3301	3342	3388	3491	3858	4024	4184	4250	4299	4474	4530	4583	4607	4716
050450942200000	GM434-1	3672	3693	3735	3781	3886	4260	4427	4590	4657	4707	4887	4945	4999	5024	5137
050450942300000	GM334-1	3662	3684	3726	3772	3878	4253	4421	4585	4652	4702	4882	4941	4996	5021	5134
050450947200000	GM321-34	3647	3667	3708	3753	3855	4217	4380	4539	4604	4653	4828	4885	4937	4962	5072
050450947900000	GM421-34	3681	3702	3743	3789	3892	4260	4425	4585	4651	4700	4877	4934	4988	5013	5124
050450948000000	GM431-34	3830	3850	3891	3936	4039	4403	4567	4727	4793	4842	5018	5076	5129	5154	5264

Well API	Well UWI	Top of Mesaverde	Top of Sand 700	Top of Mud 600	Top of Sand 600	Top of Mud 500	Top of Sand 500	Top of Mud 400	Top of Sand 400	Top of Mud 300	Top of Sand 300	Top of Mud 200	Top of Sand 200	Top of Mud 100	Top of Sand 100	Base of Middle Williams Fork
050450950000000	GM314-1	3455	3476	3517	3563	3668	4038	4203	4363	4429	4478	4655	4713	4766	4791	4902
050450955500000	GM422-33	3612	3633	3673	3717	3818	4177	4338	4495	4560	4608	4781	4838	4890	4914	5023
050450955600000	GM522-33	3564	3585	3625	3670	3771	4132	4294	4452	4517	4565	4740	4796	4849	4873	4983
050450956300000	GM424-1	3350	3370	3412	3457	3560	3923	4086	4243	4308	4356	4529	4585	4638	4662	4770
050450957700000	GM524-1	3449	3471	3515	3563	3673	4057	4227	4390	4456	4506	4684	4742	4795	4820	4931
050450980000000	GM414-2	3345	3365	3404	3447	3545	3895	4052	4205	4268	4315	4484	4538	4589	4613	4718
050450980100000	GM514-2	3338	3358	3397	3440	3538	3887	4044	4196	4259	4306	4474	4529	4580	4603	4708
050450987400000	GM432-3	3583	3603	3642	3685	3782	4130	4286	4438	4500	4547	4715	4770	4821	4844	4949
050450987500000	GM532-3	3687	3707	3747	3791	3890	4239	4395	4547	4609	4655	4822	4876	4926	4949	5052
050450993900000	GM443-3	3382	3402	3441	3484	3583	3934	4092	4245	4308	4356	4525	4581	4632	4656	4762
050450994000000	GM343-3	3420	3440	3480	3524	3624	3979	4138	4293	4357	4405	4575	4631	4682	4706	4813
050450996700000	GM216-33	3494	3513	3552	3595	3692	4039	4194	4346	4408	4455	4622	4676	4727	4750	4855
050450997000000	GM544-3	3399	3419	3458	3500	3598	3943	4099	4250	4312	4359	4525	4580	4630	4653	4758
050450997100000	GM531-33	3543	3564	3606	3651	3755	4125	4291	4453	4519	4569	4746	4804	4857	4882	4993
050450997200000	GM431-33	3548	3569	3611	3657	3762	4135	4303	4466	4533	4583	4762	4820	4874	4899	5011
050450997300000	GM344-3	3432	3452	3491	3534	3633	3982	4139	4291	4353	4400	4567	4622	4672	4696	4800
050450997400000	GM444-3	3402	3422	3461	3504	3602	3951	4108	4260	4323	4370	4538	4593	4643	4667	4773
050450997500000	GM511-3	3461	3481	3522	3566	3668	4029	4191	4350	4415	4464	4639	4696	4749	4773	4883
050450997600000	GM311-3	3427	3447	3487	3530	3630	3984	4144	4299	4363	4410	4581	4637	4689	4713	4820
050450997700000	GM411-3	3461	3482	3524	3570	3674	4047	4213	4375	4441	4490	4667	4724	4777	4802	4913
050451000500000	GM512-3	3675	3695	3733	3776	3872	4216	4371	4521	4583	4630	4796	4850	4900	4923	5028
050451000600000	GM312-3	3728	3748	3789	3835	3937	4302	4466	4626	4692	4741	4918	4975	5028	5053	5164
050451000700000	GM412-3	3656	3675	3714	3756	3852	4194	4347	4497	4559	4605	4770	4823	4873	4896	5000
050451001000000	GM424-2	3275	3295	3335	3378	3478	3832	3991	4146	4210	4258	4429	4485	4536	4560	4667
050451002000000	GM524-2	3257	3277	3317	3360	3460	3815	3975	4130	4194	4242	4414	4470	4522	4546	4654
050451011300000	GM14-3	3815	3835	3873	3915	4011	4348	4498	4645	4705	4750	4911	4964	5012	5035	5136
050451011600000	GM414-3	3750	3769	3807	3848	3942	4276	4427	4573	4634	4679	4840	4893	4942	4965	5066
050451011900000	GM314-3	3786	3805	3843	3885	3980	4317	4467	4614	4674	4720	4882	4934	4983	5006	5108
050451012000000	GM514-3	3833	3852	3890	3932	4026	4362	4513	4661	4721	4766	4929	4982	5031	5054	5156
050451012500000	GM334-3	3537	3556	3595	3637	3733	4074	4227	4377	4438	4484	4649	4703	4753	4776	4879
050451013200000	GM434-3	3579	3598	3636	3677	3772	4109	4260	4408	4469	4514	4677	4730	4779	4802	4904
050451013300000	GM534-3	3601	3621	3662	3706	3807	4165	4323	4475	4538	4585	4752	4807	4857	4880	4985
050451017600000	GM532-4	3698	3719	3760	3805	3908	4270	4432	4590	4655	4703	4877	4933	4986	5010	5119
050451018100000	GM433-4	3638	3658	3698	3742	3843	4201	4361	4518	4583	4631	4804	4860	4913	4937	5045
050451018200000	GM333-4	3687	3707	3747	3791	3892	4250	4411	4568	4633	4681	4854	4910	4963	4987	5095
050451020600000	GM542-4	3604	3625	3666	3711	3814	4181	4345	4505	4571	4620	4797	4854	4908	4932	5043
050451020700000	GM442-4	3609	3630	3672	3718	3822	4193	4360	4523	4590	4640	4819	4878	4932	4957	5070
050451020900000	GM342-4	3657	3678	3720	3766	3870	4241	4408	4570	4637	4687	4865	4924	4978	5003	5115
050451021300000	GM434-2	3295	3315	3355	3399	3499	3852	4010	4165	4228	4276	4447	4502	4554	4578	4685
050451021400000	GM534-2	3277	3297	3339	3385	3490	3861	4024	4181	4246	4294	4467	4523	4575	4600	4708
050451021500000	GM323-3	3588	3608	3646	3688	3784	4124	4277	4426	4487	4533	4698	4751	4801	4824	4927
050451021600000	GM423-3	3551	3571	3610	3653	3749	4095	4249	4400	4462	4508	4675	4729	4779	4803	4907
050451021700000	GM523-3	3536	3555	3593	3636	3732	4074	4228	4378	4440	4486	4651	4705	4755	4778	4881
050451022100000	GM522-3	3547	3566	3605	3647	3744	4086	4239	4388	4449	4495	4659	4713	4762	4785	4888
050451022200000	GM422-3	3506	3525	3562	3604	3698	4035	4187	4335	4396	4441	4604	4657	4706	4729	4831
050451022300000	GM322-3	3563	3583	3622	3664	3761	4103	4256	4406	4467	4513	4678	4731	4781	4804	4907

Well API	Well UWI	Top of Mesaverde	Top of Sand 700	Top of Mud 600	Top of Sand 600	Top of Mud 500	Top of Sand 500	Top of Mud 400	Top of Sand 400	Top of Mud 300	Top of Sand 300	Top of Mud 200	Top of Sand 200	Top of Mud 100	Top of Sand 100	Base of Middle Williams Fork
050451024400000	GM413-1	3416	3436	3477	3521	3623	3984	4146	4304	4368	4417	4591	4648	4700	4724	4834
050451024500000	GM513-1	3396	3416	3456	3500	3601	3959	4120	4277	4342	4390	4563	4620	4672	4696	4805
050451037400000	GM443-34	3540	3559	3599	3642	3740	4087	4242	4394	4456	4502	4669	4723	4774	4797	4901
050451037500000	GM543-34	3522	3542	3581	3625	3724	4077	4235	4389	4453	4500	4670	4726	4777	4801	4908
050451037600000	GM234-34	3573	3593	3632	3676	3775	4124	4281	4433	4496	4543	4711	4765	4816	4839	4945
050451037700000	GM643-34	3562	3582	3621	3665	3763	4113	4270	4422	4485	4532	4700	4754	4805	4828	4934
050451038000000	GM421-1	3651	3672	3714	3761	3866	4239	4407	4569	4636	4686	4865	4923	4977	5002	5114
050451038100000	GM332-1	3632	3652	3694	3740	3844	4215	4382	4544	4611	4661	4839	4897	4951	4976	5088
050451038200000	GM521-1	3614	3634	3675	3720	3823	4187	4351	4511	4577	4626	4802	4859	4912	4937	5047
050451046500000	GM233-34	3354	3375	3416	3461	3564	3930	4094	4254	4320	4369	4546	4603	4657	4682	4793
050451046600000	GM434-34	3349	3369	3410	3454	3556	3915	4077	4235	4299	4348	4522	4578	4631	4655	4764
050451046700000	GM534-34	3379	3400	3442	3488	3593	3964	4131	4293	4359	4409	4587	4645	4699	4724	4836
050451048300000	GM412-1	3761	3781	3822	3867	3969	4333	4496	4656	4721	4770	4945	5002	5055	5080	5190
050451048400000	GM511-1	3787	3807	3848	3893	3995	4358	4522	4680	4745	4793	4968	5025	5077	5102	5211
050451052700000	GM324-3	3703	3723	3761	3804	3901	4245	4399	4550	4611	4657	4822	4876	4926	4949	5052
050451052800000	GM424-3	3660	3679	3717	3759	3855	4197	4351	4501	4563	4609	4774	4828	4878	4901	5005
050451052900000	GM524-3	3667	3686	3725	3767	3864	4206	4360	4510	4572	4618	4783	4837	4887	4910	5014
050451063500000	GM41-35	4205	4226	4267	4312	4413	4775	4938	5096	5161	5210	5385	5442	5495	5519	5629
050451063900000	GM311-36	4058	4078	4119	4165	4267	4633	4797	4957	5023	5072	5247	5305	5358	5382	5493
050451064000000	GM513-3	3711	3731	3770	3813	3911	4257	4410	4559	4621	4666	4831	4884	4934	4957	5060
050451064100000	GM413-3	3637	3656	3695	3737	3834	4176	4330	4480	4541	4587	4752	4806	4856	4879	4983
050451064200000	GM313-3	3638	3657	3696	3739	3836	4182	4337	4488	4549	4596	4762	4816	4866	4890	4994
050451085900000	GM421-4	3471	3492	3534	3580	3685	4058	4225	4388	4455	4505	4684	4742	4797	4822	4934
050451086000000	GM521-4	3476	3496	3538	3583	3686	4052	4216	4376	4442	4491	4667	4725	4778	4803	4914
050451086100000	GM321-4	3504	3525	3568	3614	3721	4097	4266	4430	4497	4548	4729	4788	4842	4868	4981
050451086800000	GM321-3	3426	3446	3488	3534	3639	4009	4174	4333	4399	4448	4623	4680	4733	4757	4867
050451087100000	GM22-36	4045	4067	4112	4161	4273	4664	4837	5005	5073	5125	5308	5368	5423	5449	5564
050451087200000	GM312-36	3963	3985	4027	4074	4181	4556	4723	4885	4951	5001	5179	5237	5291	5316	5427
050451092100000	GM442-34	3953	3974	4016	4062	4167	4532	4696	4856	4921	4970	5145	5202	5255	5279	5388
050451092200000	GM542-34	3830	3851	3894	3941	4047	4416	4581	4741	4806	4855	5030	5087	5140	5164	5274
050451092300000	GM532-34	3622	3643	3685	3731	3835	4205	4371	4532	4598	4647	4824	4881	4935	4959	5070
050451092400000	GM432-34	3587	3608	3648	3693	3794	4156	4318	4477	4542	4591	4766	4823	4876	4901	5011
050451136200000	GM413-34	3463	3484	3527	3573	3679	4055	4224	4389	4456	4507	4689	4748	4803	4828	4942
050451136300000	GM312-34	3712	3734	3777	3825	3932	4310	4478	4643	4710	4760	4941	4999	5054	5079	5192
050451136400000	GM512-34	3501	3522	3565	3611	3716	4089	4256	4419	4486	4536	4715	4773	4828	4853	4965
050451136500000	GM412-34	3542	3563	3605	3651	3757	4129	4296	4459	4525	4575	4754	4812	4866	4891	5003
050451139600000	GM511-36	4007	4029	4072	4120	4227	4600	4766	4927	4993	5042	5219	5277	5331	5355	5466
050451139700000	GM422-36	4037	4059	4104	4153	4264	4652	4824	4990	5059	5110	5292	5352	5407	5432	5547
050451139800000	GM512-36	3903	3924	3966	4013	4119	4496	4664	4828	4895	4945	5125	5184	5238	5264	5377
050451139900000	GM412-36	3883	3903	3945	3991	4096	4468	4635	4797	4864	4914	5093	5151	5205	5230	5342
050451140000000	GM421-36	3977	3998	4041	4088	4196	4573	4743	4908	4975	5026	5206	5264	5318	5343	5456
050451142500000	GM614-35	3536	3555	3594	3637	3734	4078	4232	4383	4445	4491	4657	4711	4761	4784	4888
050451142600000	GM414-35	3482	3501	3540	3583	3681	4028	4184	4337	4399	4446	4614	4668	4719	4742	4848
050451142700000	GM514-35	3498	3517	3556	3598	3694	4036	4189	4339	4400	4446	4611	4665	4715	4738	4842
050451150200000	GM253-2	3469	3490	3532	3577	3681	4045	4208	4366	4431	4480	4654	4710	4763	4787	4896
050451150300000	GM421-2	3396	3417	3458	3503	3605	3968	4131	4290	4355	4404	4579	4635	4688	4713	4822

Well API	Well UWI	Top of Mesaverde	Top of Sand 700	Top of Mud 600	Top of Sand 600	Top of Mud 500	Top of Sand 500	Top of Mud 400	Top of Sand 400	Top of Mud 300	Top of Sand 300	Top of Mud 200	Top of Sand 200	Top of Mud 100	Top of Sand 100	Base of Middle Williams Fork
050451150500000	GM411-2	3396	3415	3455	3498	3595	3943	4099	4251	4313	4360	4527	4582	4632	4656	4761
050451150600000	GM511-2	3365	3385	3424	3467	3565	3916	4073	4227	4290	4337	4507	4562	4613	4637	4743
050451159800000	GM333-35	4264	4285	4327	4374	4479	4850	5016	5176	5242	5291	5468	5525	5579	5603	5714
050451159900000	GM332-35	4188	4208	4249	4294	4396	4761	4922	5079	5144	5192	5364	5420	5472	5496	5604
050451160000000	GM433-35	4163	4184	4225	4271	4374	4739	4903	5061	5126	5175	5349	5406	5459	5483	5593
050451160100000	GM543-35	4166	4187	4228	4274	4378	4747	4914	5076	5143	5192	5370	5427	5481	5505	5616
050451160200000	GM343-35	4127	4147	4188	4233	4334	4695	4858	5017	5082	5131	5306	5362	5415	5440	5549
050451160300000	GM443-35	4135	4155	4196	4242	4344	4711	4875	5035	5101	5150	5326	5384	5437	5461	5572
050451160400000	GM442-35	4130	4150	4191	4236	4337	4700	4862	5021	5086	5135	5309	5366	5419	5443	5552
050451160500000	GM331-35	4506	4527	4570	4617	4722	5090	5254	5414	5479	5528	5703	5760	5813	5837	5947
050451160900000	GM432-35	4199	4220	4261	4307	4410	4776	4940	5099	5164	5212	5386	5443	5496	5520	5629
050451161000010	GM22-35R	4455	4476	4517	4563	4666	5031	5193	5350	5415	5463	5637	5693	5745	5770	5878
050451161100000	GM342-35	4235	4255	4297	4343	4447	4815	4979	5137	5202	5251	5425	5481	5534	5558	5667
050451161200000	GM341-35	4343	4365	4407	4454	4559	4930	5094	5252	5317	5365	5538	5594	5647	5671	5779
050451169500000	GM441-3	3382	3402	3442	3487	3587	3941	4099	4252	4315	4362	4531	4586	4637	4660	4766
050451169600000	GM541-3	3335	3355	3395	3438	3536	3887	4044	4197	4260	4307	4475	4530	4581	4605	4710
050451191900000	GM433-3	3570	3590	3629	3671	3768	4109	4262	4412	4473	4519	4684	4738	4788	4811	4914
050451192400000	GM333-3	3489	3508	3546	3589	3685	4026	4179	4329	4391	4437	4602	4656	4706	4729	4833
050451193700000	GM432-4	3345	3366	3407	3452	3554	3917	4080	4237	4302	4350	4524	4581	4633	4658	4767
050451193900000	GM533-4	3488	3508	3549	3594	3696	4057	4217	4372	4436	4484	4656	4711	4763	4787	4895
050451195700000	GM343-4	3930	3951	3991	4035	4136	4493	4653	4808	4871	4919	5089	5144	5196	5219	5326
050451195800000	GM443-4	3811	3831	3870	3912	4009	4354	4509	4659	4721	4767	4933	4987	5037	5060	5164
050451201500000	GM513-2	3264	3284	3323	3366	3463	3810	3966	4118	4180	4227	4394	4449	4499	4523	4628
050451201600000	GM413-2	3325	3344	3384	3427	3525	3874	4030	4183	4245	4292	4459	4514	4564	4588	4692
050451207800000	GM422-2	3285	3305	3345	3389	3490	3846	4006	4162	4226	4274	4446	4502	4554	4578	4686
050451207900000	GM423-2	3342	3362	3403	3448	3549	3908	4068	4224	4288	4336	4508	4564	4615	4639	4747
050451213300000	GM524-35	3586	3606	3646	3690	3791	4148	4309	4465	4529	4578	4750	4806	4858	4882	4990
050451213400000	GM424-35	3650	3670	3711	3756	3858	4219	4381	4539	4603	4652	4825	4882	4934	4958	5067
050451213500000	GM324-35	3572	3592	3632	3676	3777	4133	4293	4448	4512	4560	4730	4786	4838	4862	4969
050451213600000	GM23-35	3695	3716	3758	3803	3906	4273	4437	4597	4662	4711	4886	4943	4996	5020	5130
050451226300000	GM322-4	3446	3467	3508	3553	3655	4018	4181	4340	4405	4454	4630	4687	4740	4765	4875
050451226400000	GM312-4	3534	3555	3597	3643	3748	4118	4283	4442	4507	4556	4731	4787	4840	4865	4974
050451226500000	GM512-4	3573	3594	3636	3683	3788	4155	4318	4476	4541	4589	4763	4819	4872	4896	5005
050451226600000	GM412-4	3529	3550	3593	3639	3743	4111	4275	4435	4500	4549	4725	4782	4835	4859	4969
050451248600000	GM532-2	3423	3444	3484	3529	3631	3990	4150	4306	4370	4418	4590	4646	4698	4721	4829
050451248700000	GM432-2	3342	3362	3402	3446	3546	3903	4063	4219	4283	4331	4503	4559	4611	4634	4742
050451248800000	GM542-2	3699	3719	3760	3805	3907	4269	4431	4589	4654	4702	4876	4933	4985	5010	5119
050451248900000	GM442-2	3677	3697	3738	3782	3883	4241	4401	4557	4622	4670	4842	4898	4951	4975	5083
050451249000000	GM441-2	3691	3711	3752	3797	3898	4258	4419	4576	4641	4689	4862	4918	4970	4995	5103
050451249400000	GM444-4	3817	3837	3877	3920	4019	4364	4518	4668	4729	4775	4940	4994	5044	5067	5170
050451249500000	GM434-4	3810	3830	3870	3915	4017	4378	4540	4697	4762	4810	4984	5040	5093	5117	5226
050451266200000	GM643-35	3654	3675	3717	3763	3867	4238	4403	4565	4631	4681	4858	4916	4970	4994	5106
050451266300000	GM227-35	3627	3647	3689	3735	3838	4208	4373	4535	4601	4650	4828	4885	4939	4964	5075
050451266400000	GM34-35	3617	3637	3679	3724	3828	4197	4362	4524	4590	4639	4817	4875	4929	4954	5066
050451266600000	GM544-35	3632	3653	3695	3741	3845	4215	4381	4542	4608	4658	4836	4894	4947	4972	5084
050451278300000	GM441-4	3584	3605	3648	3694	3800	4171	4336	4496	4562	4611	4786	4843	4896	4921	5031

Well API	Well UWI	Top of Mesaverde	Top of Sand 700	Top of Mud 600	Top of Sand 600	Top of Mud 500	Top of Sand 500	Top of Mud 400	Top of Sand 400	Top of Mud 300	Top of Sand 300	Top of Mud 200	Top of Sand 200	Top of Mud 100	Top of Sand 100	Base of Middle Williams Fork
050451278400000	GM431-4	3427	3448	3491	3538	3643	4018	4184	4346	4412	4461	4639	4697	4750	4775	4886
050451282700000	GM314-33	3807	3828	3871	3919	4026	4407	4577	4743	4810	4861	5042	5102	5156	5182	5296
050451282800000	GM324-33	3717	3738	3780	3826	3932	4307	4475	4639	4706	4756	4937	4996	5051	5076	5190
050451282900000	GM424-33	3731	3752	3794	3840	3944	4316	4482	4645	4711	4761	4940	4998	5052	5077	5189
050451283000000	GM411-33	3643	3664	3705	3750	3854	4220	4385	4546	4612	4661	4838	4896	4950	4974	5086
050451283200000	GM511-33	3619	3640	3682	3727	3831	4199	4365	4526	4593	4642	4821	4879	4932	4957	5069
050451304800000	GM21-36	4163	4183	4225	4271	4376	4747	4913	5073	5138	5187	5363	5420	5473	5497	5607
050451304900000	GM521-36	4190	4211	4253	4299	4404	4772	4937	5097	5162	5211	5385	5442	5494	5519	5628
050451305000000	GM321-36	4226	4247	4290	4336	4439	4806	4972	5133	5200	5249	5428	5486	5539	5563	5673
050451305200000	GM541-35	4372	4394	4439	4488	4599	4986	5158	5324	5391	5442	5620	5677	5730	5755	5864
050451306500000	GM531-36	4645	4667	4710	4758	4867	5247	5416	5581	5648	5698	5878	5937	5991	6016	6129
050451306600000	GM541-36	4506	4528	4571	4619	4726	5110	5283	5450	5518	5569	5752	5812	5867	5893	6007
050451306700000	GM442-36	4407	4428	4471	4518	4625	5006	5177	5344	5412	5463	5647	5707	5763	5788	5904
050451306900000	GM431-36	4563	4584	4626	4673	4778	5151	5317	5479	5545	5595	5772	5830	5884	5908	6020
050451307000000	GM342-36	4454	4476	4518	4565	4672	5051	5221	5386	5454	5504	5686	5746	5801	5826	5940
050451307100000	GM432-36	4448	4469	4513	4560	4668	5052	5224	5391	5460	5511	5695	5755	5811	5836	5952
050451307200000	GM341-36	4781	4804	4848	4898	5009	5397	5567	5733	5800	5851	6031	6090	6145	6170	6283
050451307300000	GM441-36	4617	4639	4684	4733	4845	5234	5407	5574	5643	5694	5878	5938	5993	6019	6134
050451308600000	GM31-35	4656	4678	4722	4771	4880	5258	5426	5588	5654	5704	5879	5936	5989	6013	6122
050451308700000	GM411-36	4047	4068	4108	4153	4255	4617	4780	4938	5003	5052	5227	5284	5337	5361	5471
050451333600000	GM444-1	3625	3645	3687	3733	3838	4209	4376	4539	4606	4656	4836	4895	4949	4974	5087
050451333700000	GM344-1	3758	3779	3820	3866	3969	4336	4501	4661	4727	4777	4954	5011	5065	5090	5201
050451333800000	GM544-1	3629	3650	3692	3738	3842	4214	4381	4544	4610	4660	4840	4898	4952	4978	5090
050451344100000	GM443-1	3549	3570	3613	3660	3767	4145	4314	4477	4544	4594	4773	4831	4885	4909	5021
050451344200000	GM543-1	3469	3490	3532	3578	3682	4052	4218	4380	4447	4497	4675	4733	4787	4812	4924
050451347400000	GM442-1	3567	3587	3629	3674	3777	4144	4308	4468	4534	4583	4760	4817	4871	4895	5006
050451347500000	GM542-1	3598	3619	3660	3706	3810	4177	4342	4501	4567	4616	4792	4849	4902	4927	5037
050451354800000	GM228-34	3643	3664	3705	3751	3856	4224	4388	4548	4614	4663	4839	4896	4949	4974	5084
050451354900000	GM422-34	3613	3634	3676	3722	3826	4197	4363	4525	4592	4641	4820	4878	4932	4957	5069
050451398000000	GM424-36	3761	3782	3824	3871	3976	4350	4518	4681	4748	4799	4979	5037	5092	5117	5230
050451398100000	GM225-36	3888	3910	3952	3999	4105	4479	4645	4807	4873	4922	5100	5157	5211	5236	5347
050451398200000	GM513-36	3918	3939	3981	4028	4132	4502	4667	4827	4892	4941	5117	5174	5227	5252	5362
050451413300000	GM44-36	4037	4059	4103	4152	4262	4652	4825	4994	5063	5114	5299	5360	5415	5441	5557
050451413400000	GM433-36	3969	3991	4035	4083	4191	4574	4745	4910	4978	5029	5210	5269	5323	5349	5462
050451413500000	GM43-36	4096	4118	4163	4212	4323	4711	4883	5051	5119	5171	5355	5415	5470	5496	5611
050451413600000	GM444-36	4091	4115	4161	4211	4326	4723	4899	5070	5140	5192	5378	5438	5494	5520	5637
050451413700000	GM434-36	3733	3754	3796	3842	3947	4321	4490	4654	4722	4772	4953	5012	5067	5092	5206
050451426100000	GM441-1	3650	3670	3712	3758	3862	4231	4397	4558	4624	4674	4851	4908	4962	4987	5098
050451426200000	GM344-36	3841	3863	3908	3957	4068	4459	4632	4799	4868	4919	5102	5162	5217	5243	5357
050451446700000	GM411-1	3815	3836	3877	3922	4025	4391	4555	4715	4780	4830	5006	5063	5117	5141	5252
050451446800000	GM512-1	3933	3954	3996	4041	4145	4509	4671	4829	4894	4942	5116	5173	5225	5250	5359
050451446900000	GM423-1	3719	3739	3780	3825	3926	4287	4448	4606	4671	4720	4893	4950	5002	5026	5135
050451469100000	GM423-36	3935	3957	4000	4047	4155	4536	4706	4872	4940	4991	5173	5232	5287	5313	5427
050451469200000	GM323-36	3955	3977	4021	4069	4178	4568	4742	4910	4979	5031	5216	5276	5332	5358	5474
050451469300000	GM239-36	3955	3976	4018	4064	4169	4540	4706	4867	4933	4983	5160	5218	5272	5296	5408
050451469400000	GM413-36	4026	4047	4090	4136	4242	4616	4782	4944	5010	5059	5236	5294	5348	5372	5483

Well API	Well UWI	Top of Mesaverde	Top of Sand 700	Top of Mud 600	Top of Sand 600	Top of Mud 500	Top of Sand 500	Top of Mud 400	Top of Sand 400	Top of Mud 300	Top of Sand 300	Top of Mud 200	Top of Sand 200	Top of Mud 100	Top of Sand 100	Base of Middle Williams Fork
050451720400000	GM432-33	3698	3718	3758	3803	3903	4257	4416	4570	4633	4680	4850	4905	4956	4980	5086
050451720500000	GM442-33	3665	3686	3728	3775	3880	4250	4415	4576	4641	4691	4867	4925	4978	5003	5114
050451720600000	GM441-33	3613	3634	3675	3720	3823	4183	4342	4497	4561	4608	4779	4834	4886	4910	5017
050451720700000	GM532-33	3872	3893	3935	3980	4083	4441	4600	4754	4817	4864	5033	5089	5140	5164	5270
050451720800000	GM342-33	3735	3756	3797	3842	3944	4304	4464	4619	4683	4731	4903	4958	5010	5034	5142
050451720900000	GM332-33	3696	3716	3757	3801	3902	4257	4414	4568	4631	4678	4847	4902	4953	4976	5082
050451721000000	GM411-34	3735	3757	3800	3848	3956	4335	4504	4668	4735	4785	4964	5023	5077	5102	5214

Appendix I

Sandstone Proportion Maps by Net-to-Gross Zone

Zones and model area are defined in Figure 15

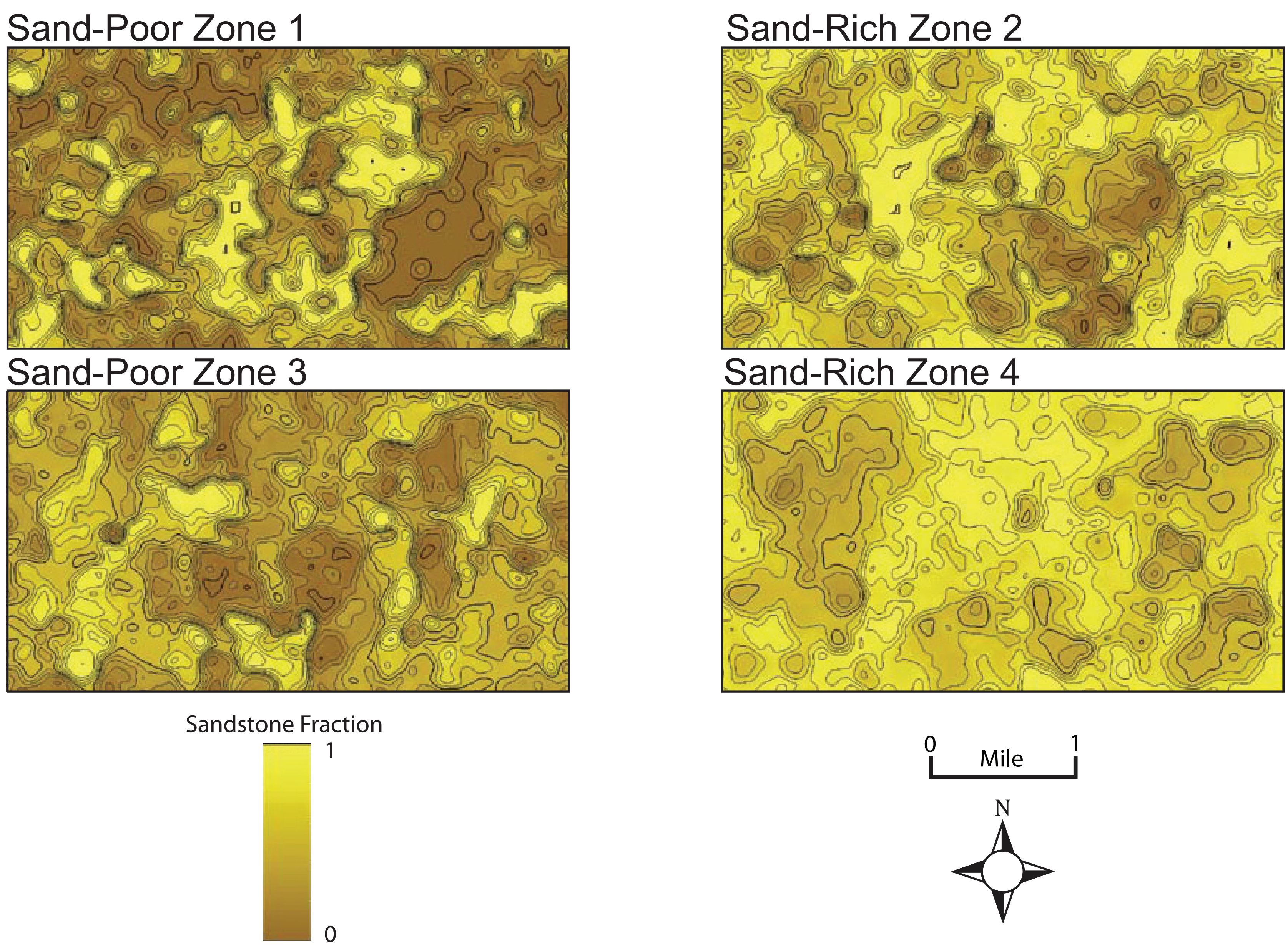
Sand-Poor Zone 1
Sand-Rich Zone 2
Sand-Poor Zone 3
Sand-Rich Zone 4
Sandstone Fraction
1
0
0
Mile
1
N

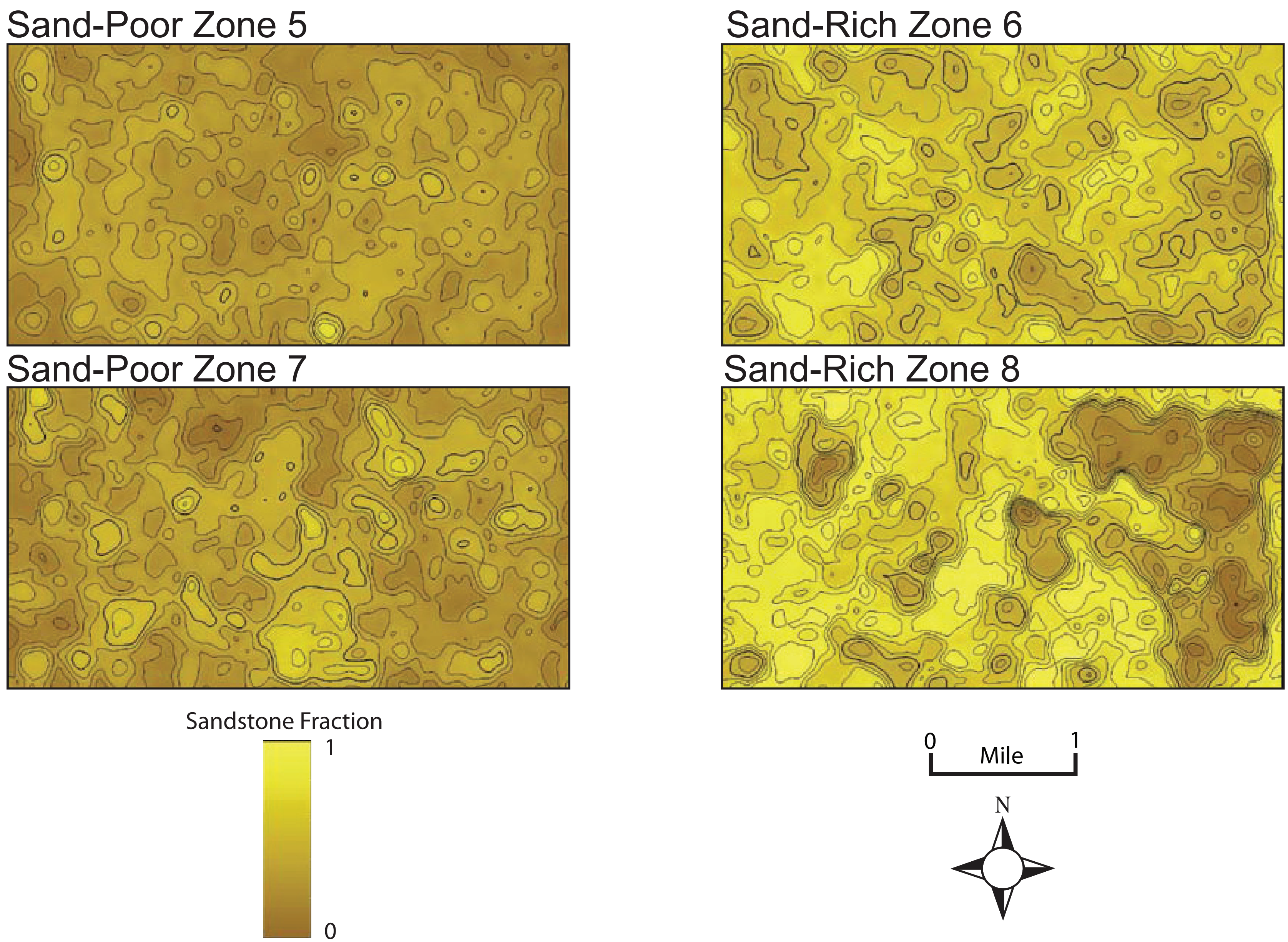
Sand-Poor Zone 5
Sand-Rich Zone 6
Sand-Poor Zone 7
Sand-Rich Zone 8
Sandstone Fraction
1
0
0
Mile
1
N

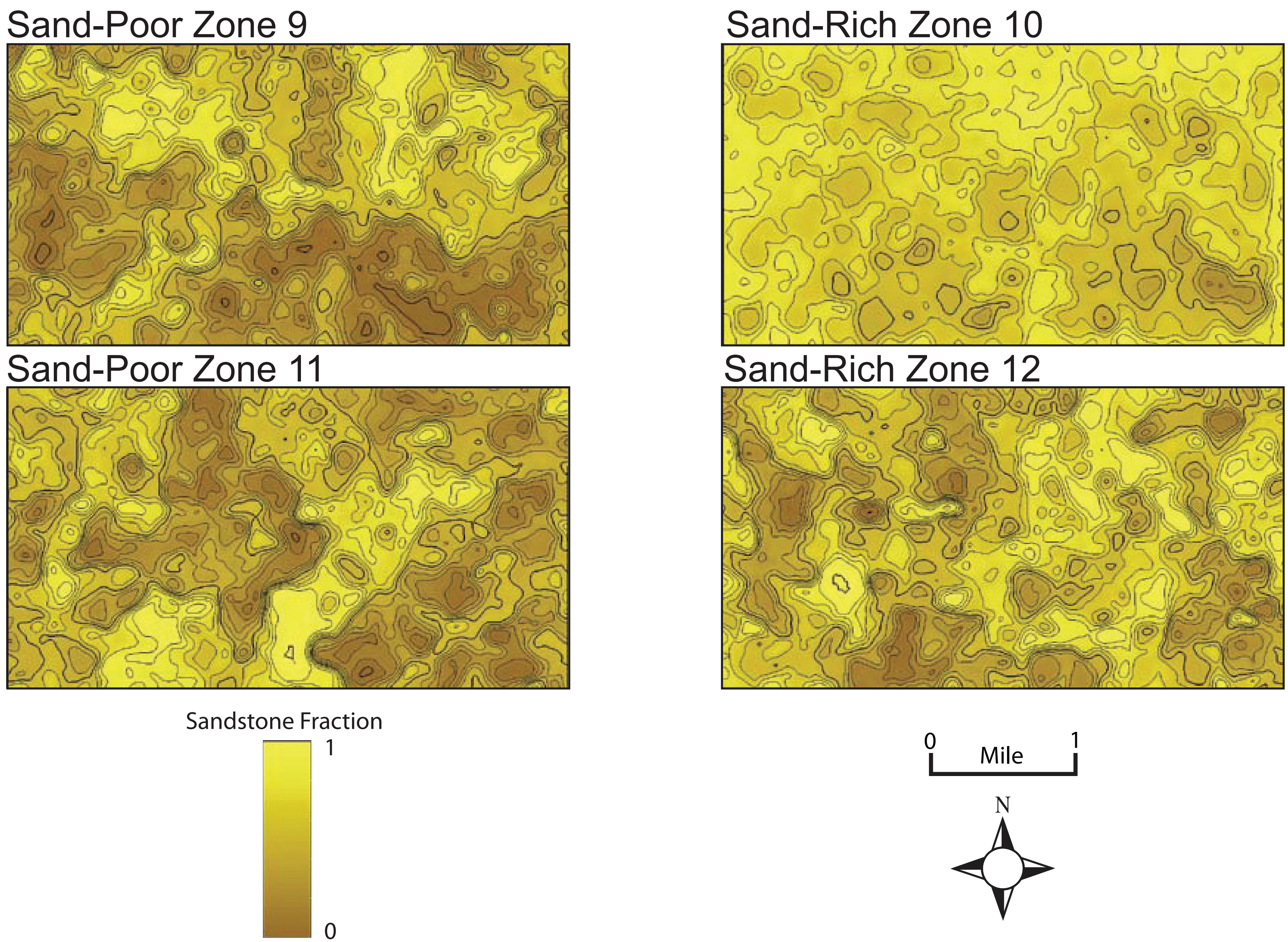
Sand-Poor Zone 9
Sand-Rich Zone 10
Sand-Poor Zone 11
Sand-Rich Zone 12
Sandstone Fraction
1
0
0
Mile
1
N

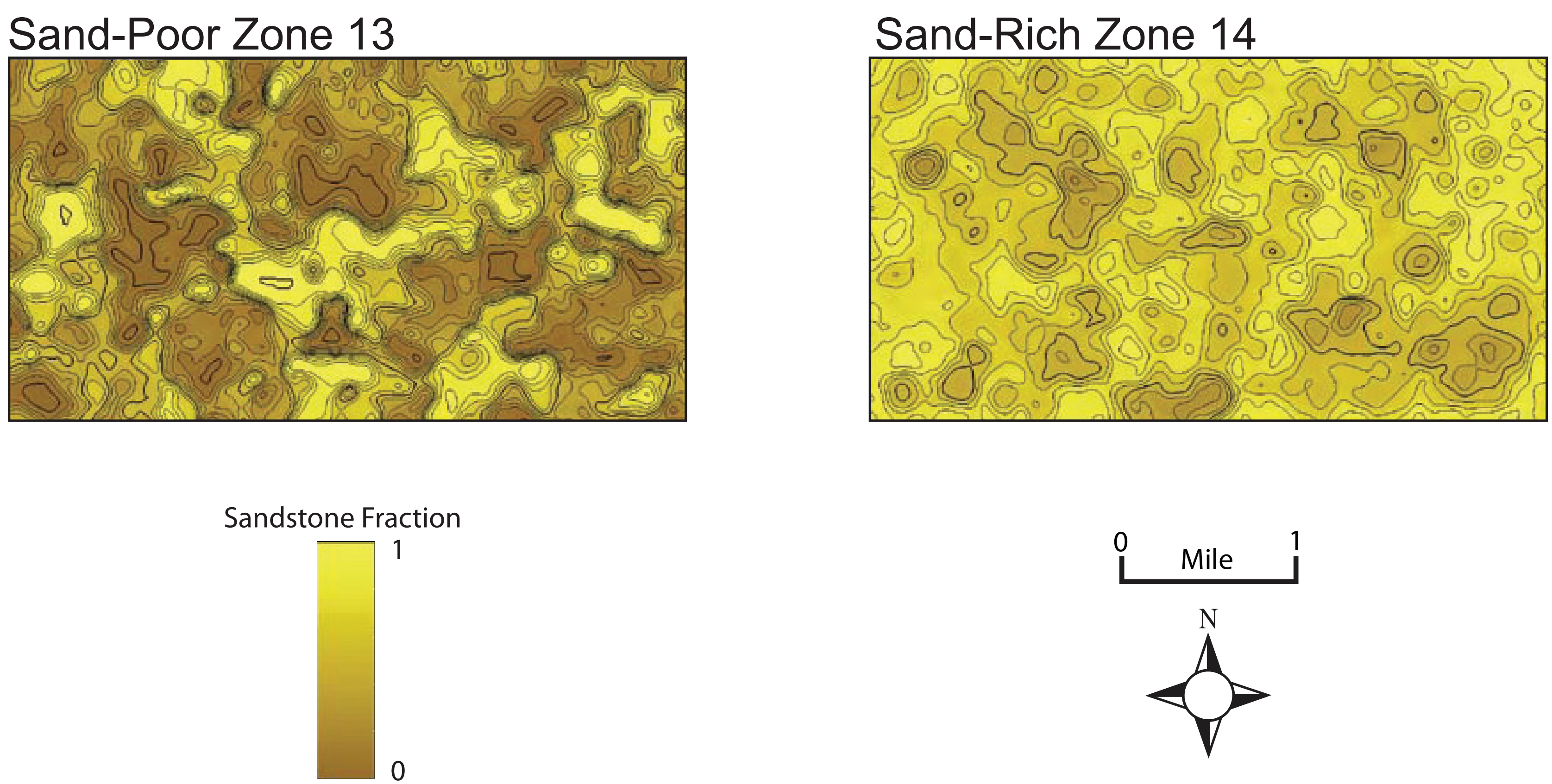

Sand-Poor Zone 13
Sand-Rich Zone 14
Sandstone Fraction
1
0
0
Mile
1
N

Appendix J

Chlorite Proportion Maps by Net-to-Gross Zone

Zones and model area are defined in Figure 15

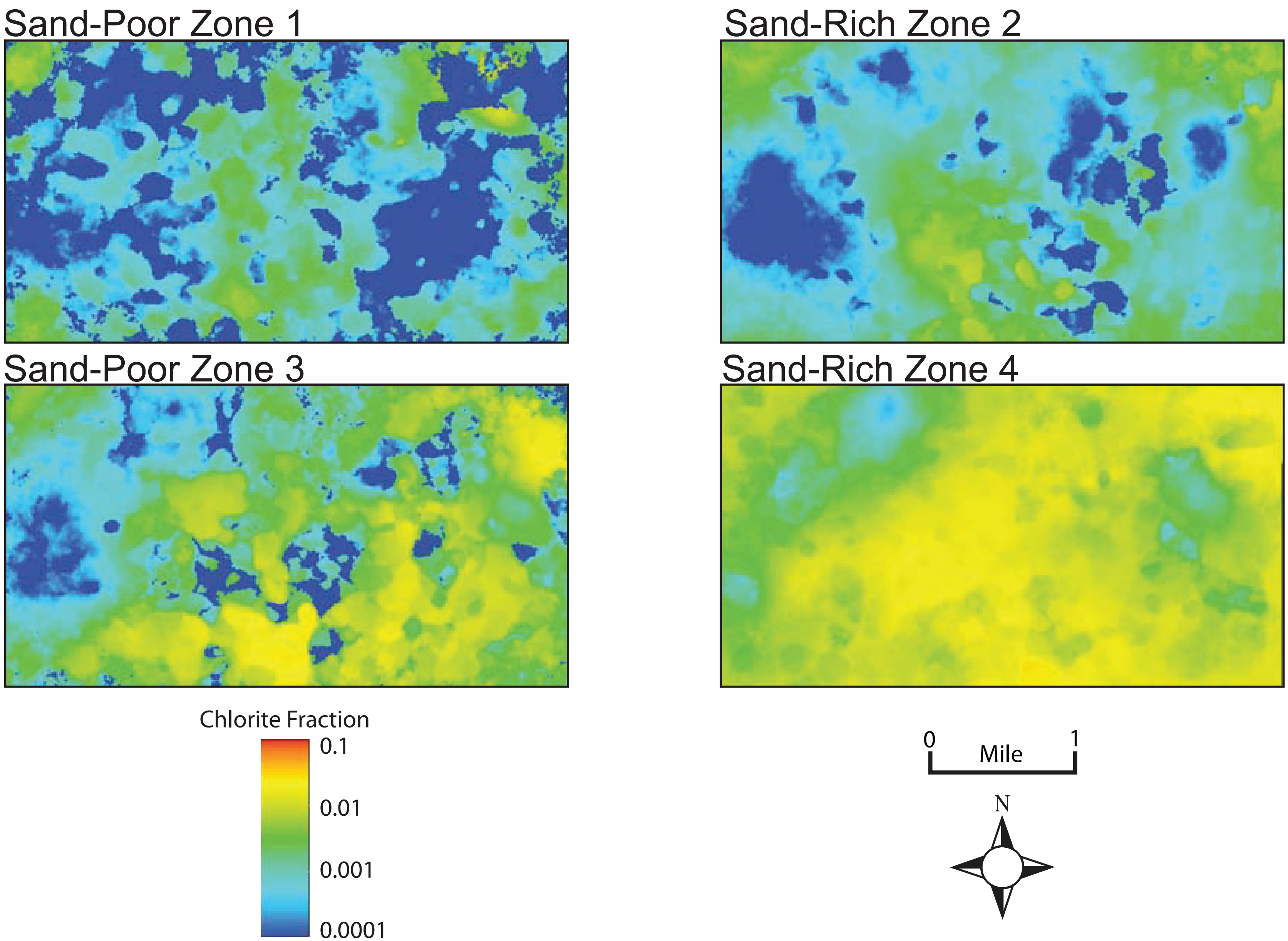
Sand-Poor Zone 1
Sand-Rich Zone 2
Sand-Poor Zone 3
Sand-Rich Zone 4
Chlorite Fraction
0.1
0.01
0.001
0.0001
0
Mile
1
N

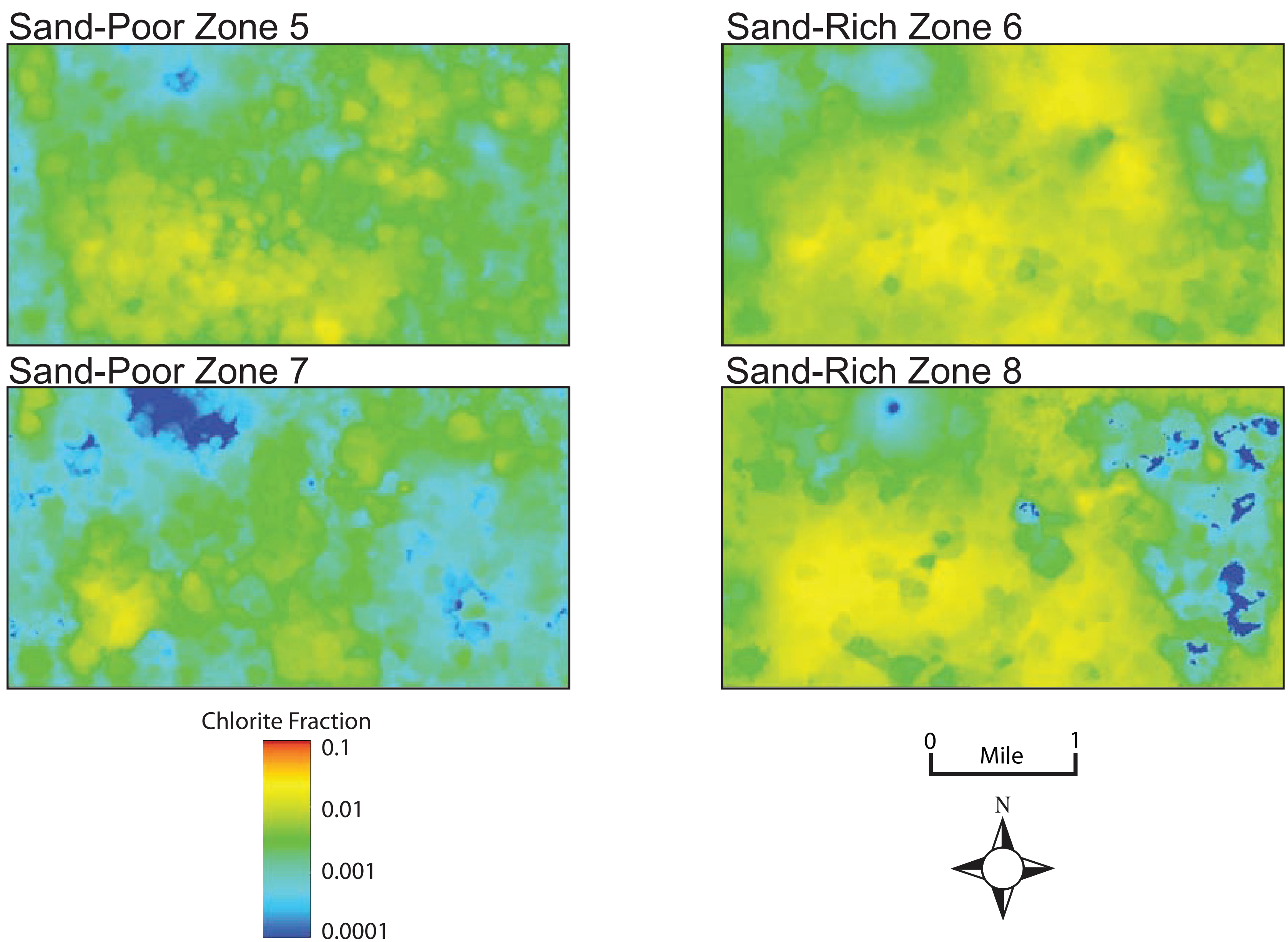
Sand-Poor Zone 5
Sand-Rich Zone 6
Sand-Poor Zone 7
Sand-Rich Zone 8
Chlorite Fraction
0.1
0.01
0.001
0.0001
0
Mile
1
N

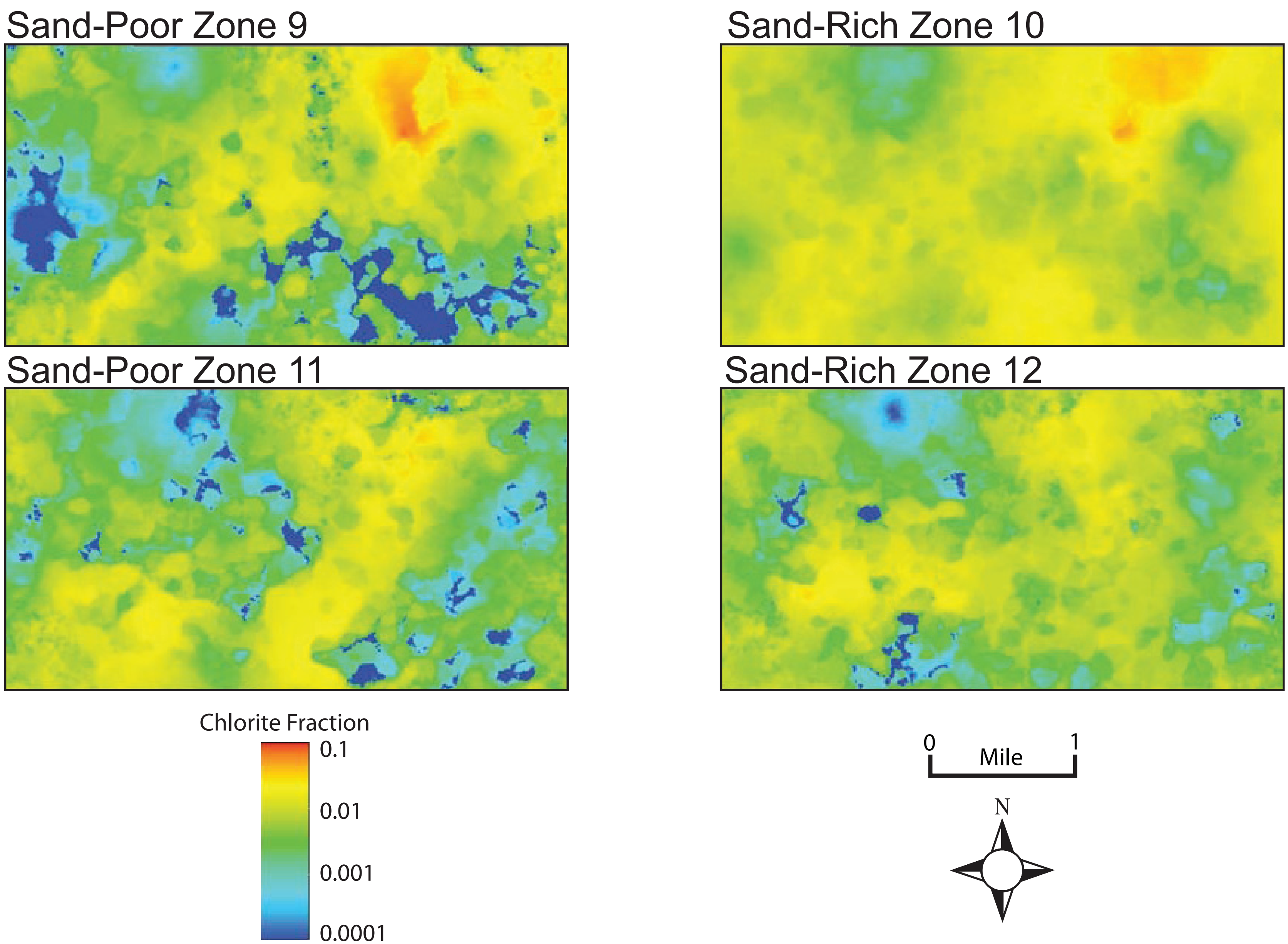
Sand-Poor Zone 9
Sand-Rich Zone 10
Sand-Poor Zone 11
Sand-Rich Zone 12
Chlorite Fraction
0.1
0.01
0.001
0.0001
0
Mile
1
N

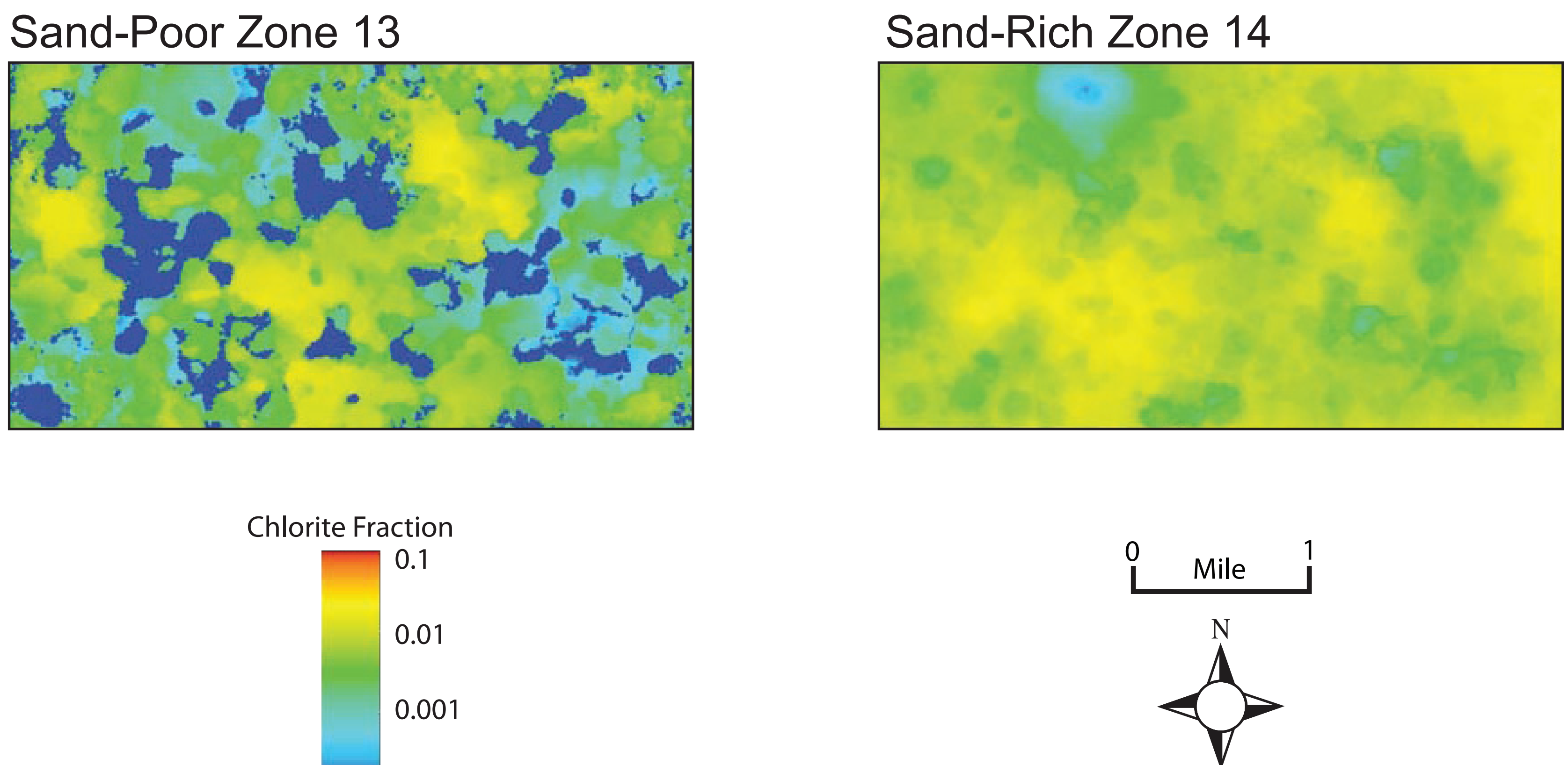
Sand-Poor Zone 13
Sand-Rich Zone 14
Chlorite Fraction
0.1
0.01
0.001
0.0001
0
Mile
1
N

Appendix K

Log Normalization and Results

Normalization is an iterative process in which a data-distribution histogram (in this case, for the gamma-ray and neutron-porosity logs) of a single well is compared to and, if necessary, adjusted to conform to the distribution of a standard well. The histogram and cumulative frequency curve are adjusted by first selecting a high and low reference line, both parallel to the y-axis of the histogram and creating a linear extrapolation between the reference lines. These reference lines are then individually moved along the x-axis, adjusting the distribution of the data within the linear extrapolation. Once a close match between the well and standard data has been established, a new log is created from the adjusted histogram and the label "_NM" is appended to the log name (GR_NM and PHIN_NM for the normalized gamma-ray and neutron-porosity logs, respectively). The process of log normalization changes the actual data values for a given log, and as such, was used sparingly and only on well-logs which exhibited large data ranges relative to the standard well. In this study, only the GR and PHIN logs were normalized. No other log data required normalization.

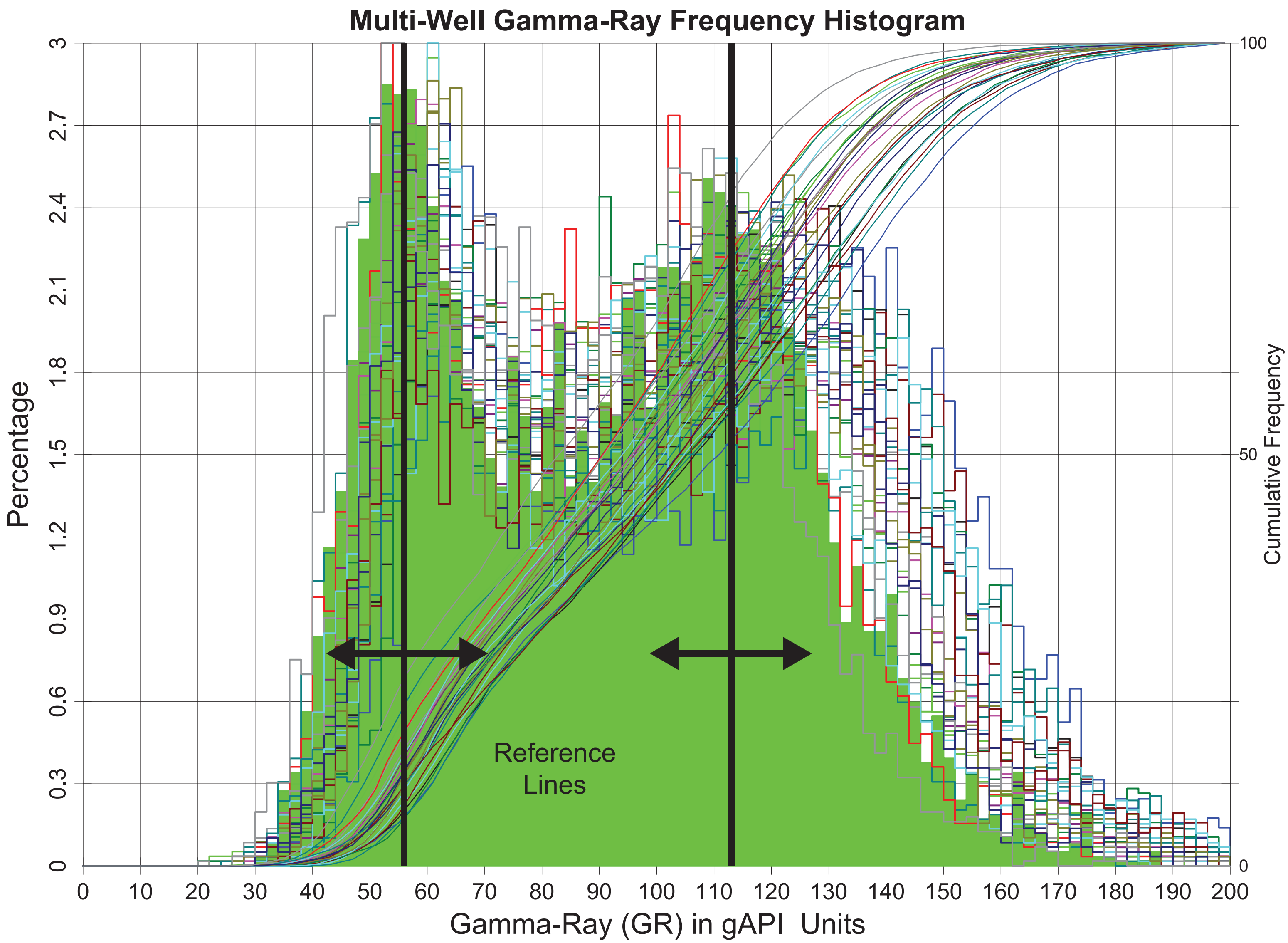

Multi-well histogram of gamma-ray distributions in the 27 wells used for petrophysical evaluation, prior to normalization. The standard well is shaded green. Cumulative frequency is also displayed. Gamma ray is displayed in gAPI units. The black reference lines allow for the data to be adjusted during normalization.

Multi-Well Normalized Gamma Ray Frequency Histogram

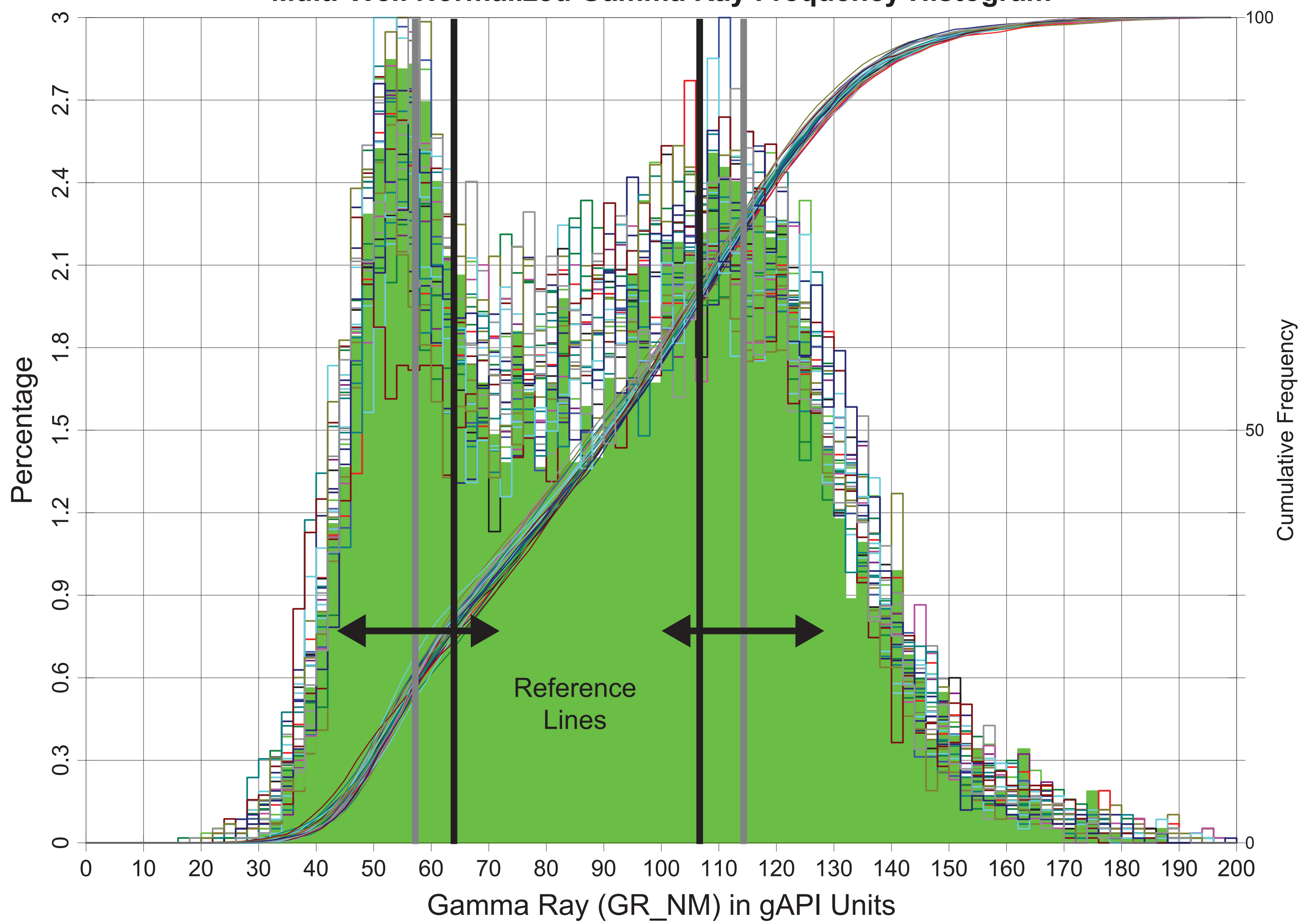

Multi-well histogram of gamma ray distributions in the 27 wells used for petrophysical evaluation, after normalization. The standard well is shaded green. Cumulative frequency is also displayed. Gamma ray is displayed in gAPI units. The black reference lines, and associated gamma ray values, have been adjusted during normalization from their original location along the grey lines.

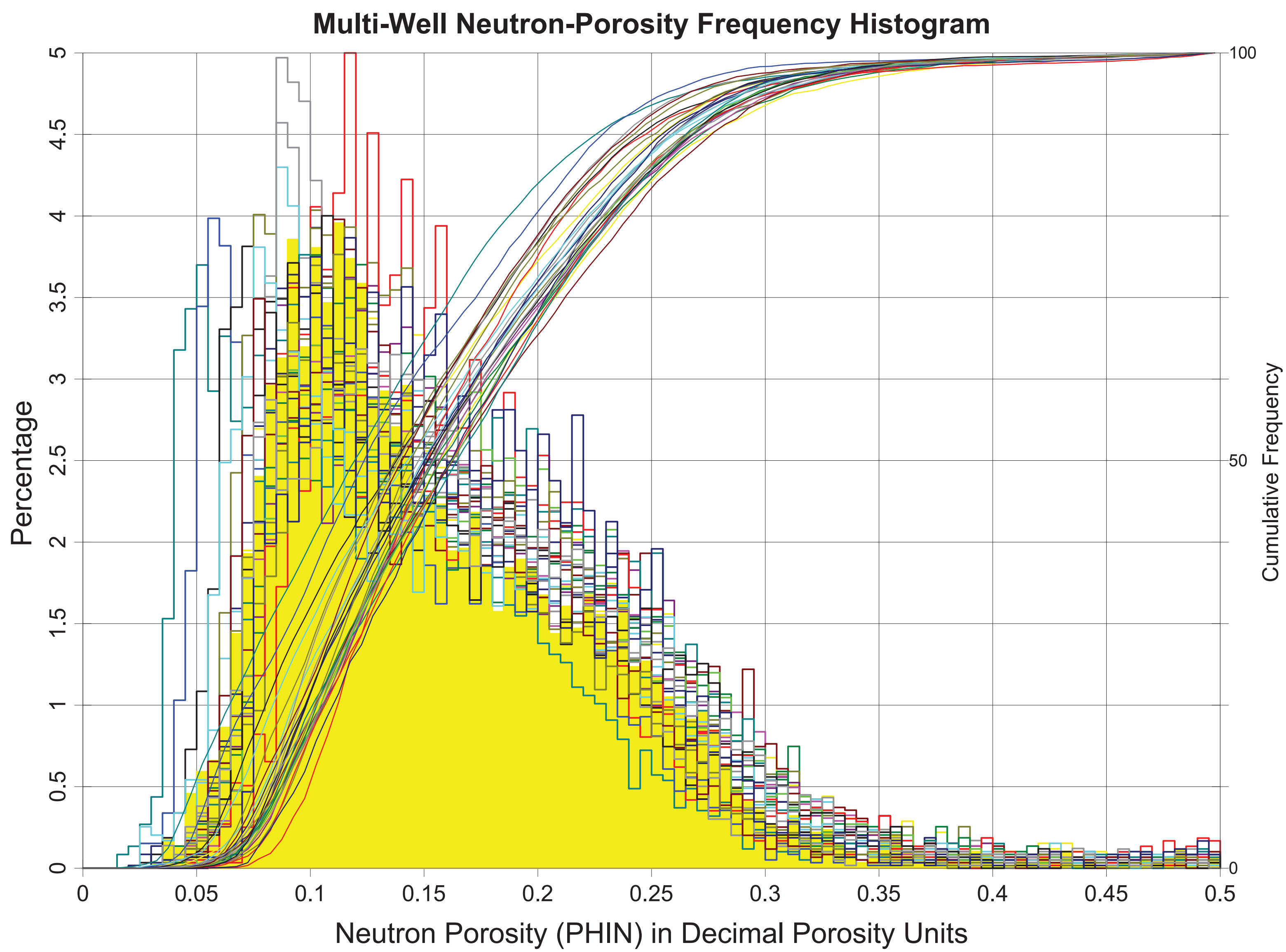

Multi-well histogram of neutron-porosity distributions in the 27 wells used for petrophysical evaluation, prior to normalization. The standard well is shaded yellow. Cumulative frequency is also displayed. Neutron porosity is displayed in decimal units.

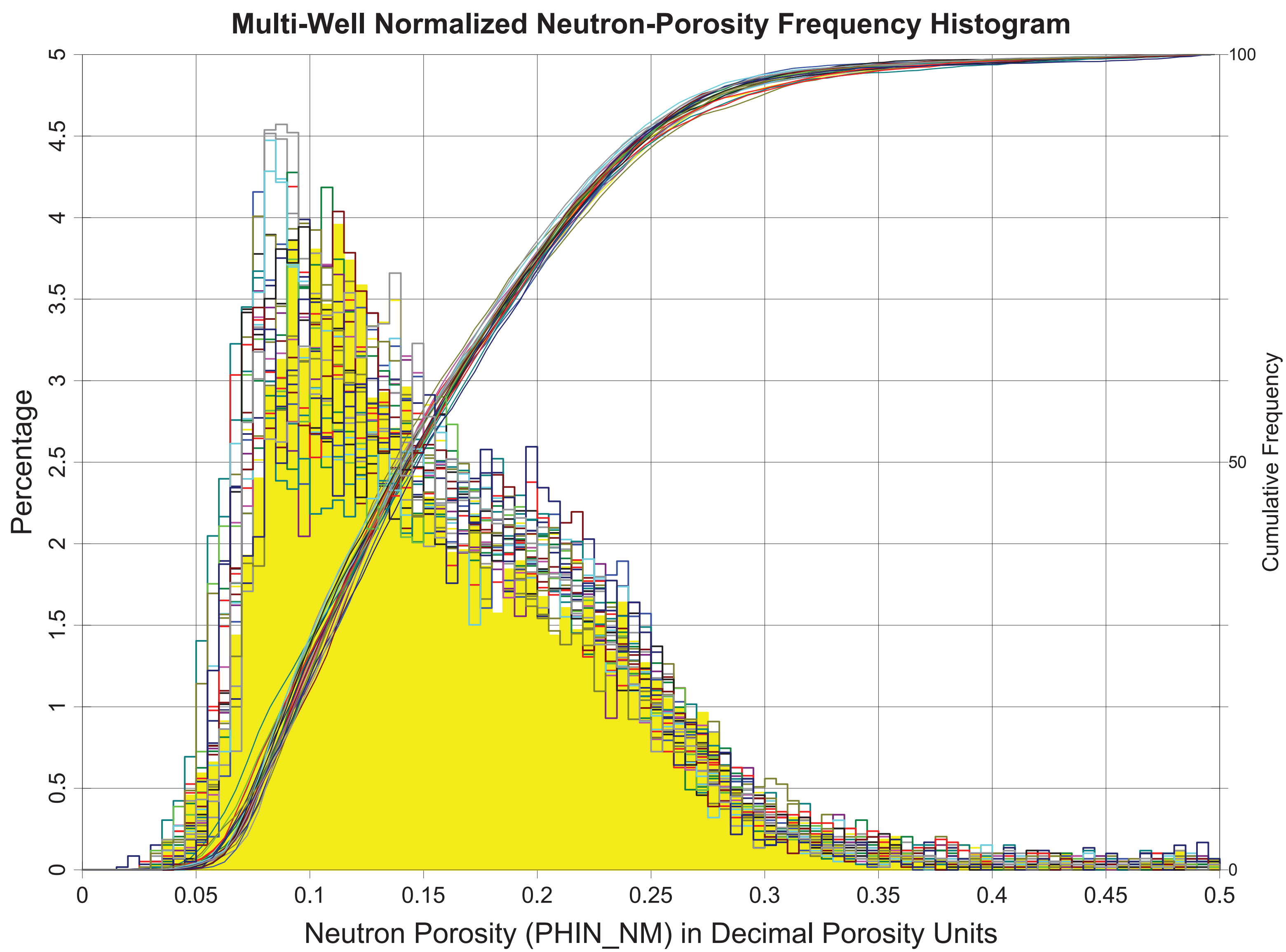

Multi-well histogram of neutron-porosity distributions in the 27 wells used for petrophysical evaluation, after normalization. The standard well is shaded yellow. Cumulative frequency is also displayed. Neutron-porosity is displayed in decimal units.

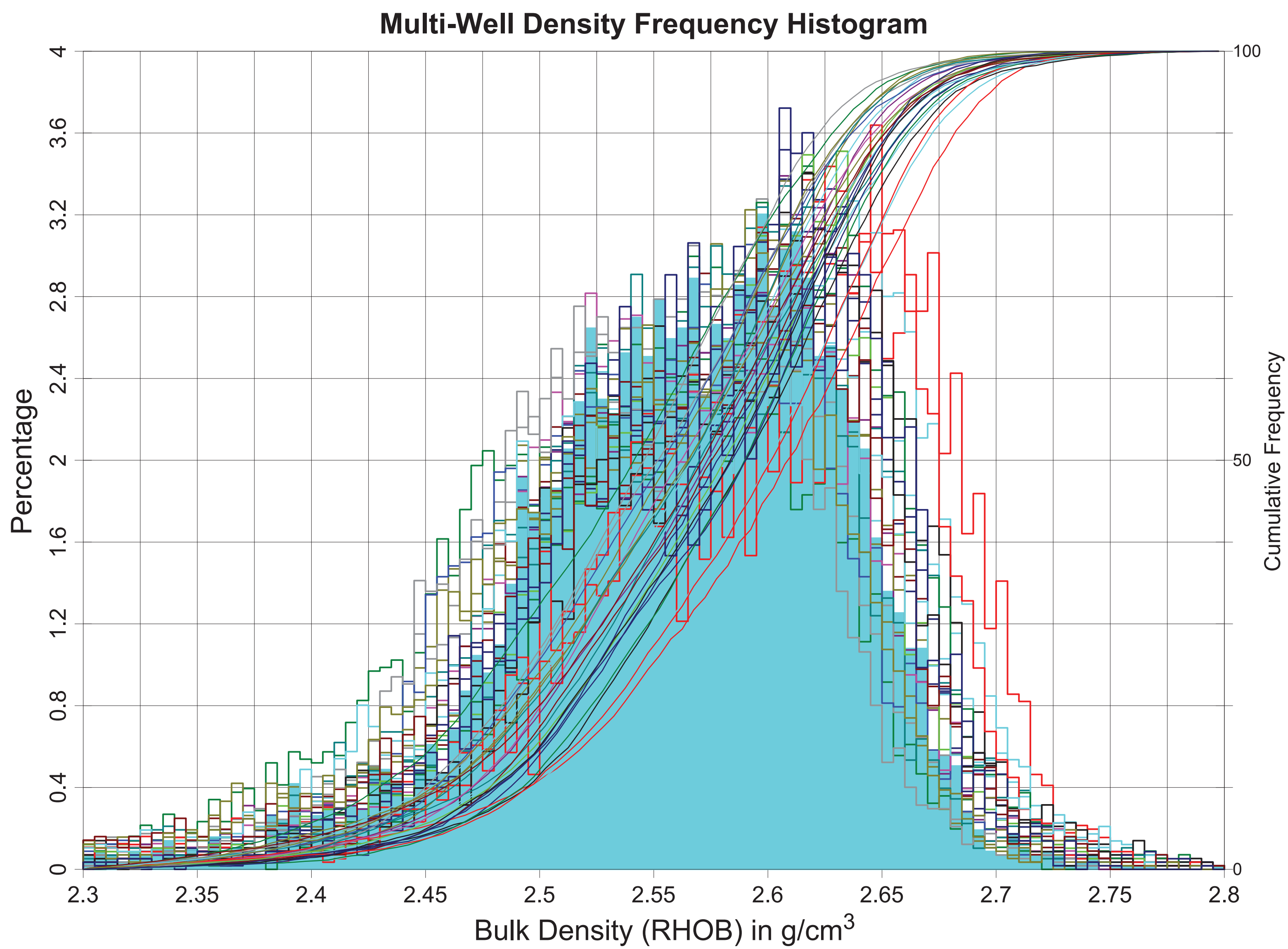

Multi-well histogram of bulk density distributions in the 27 wells used for petrophysical evaluation. An example well is shaded in blue. No normalization was conducted. Cumulative frequency is also displayed. Bulk density is displayed in g/cm^3.

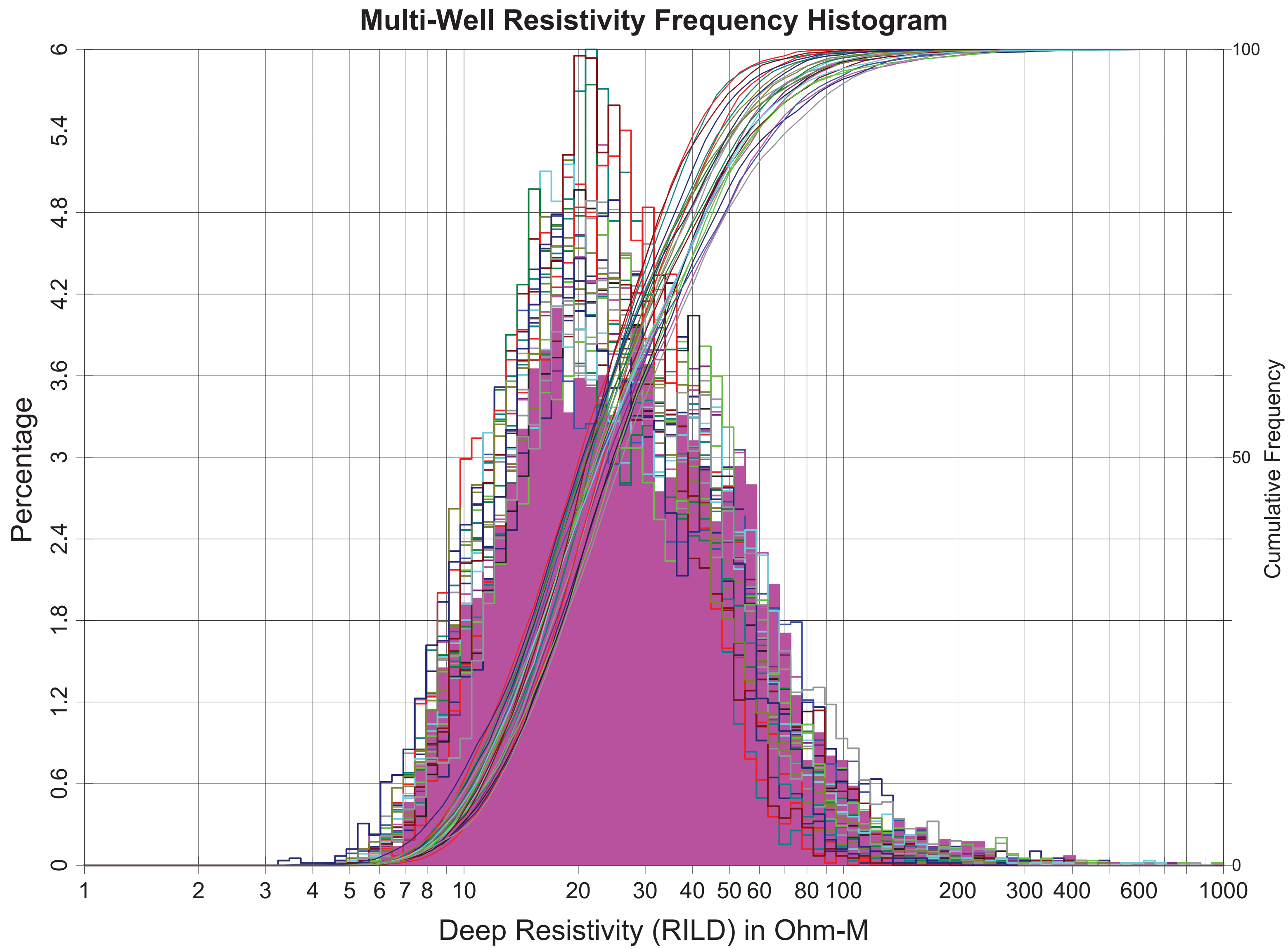

Multi-well histogram of deep resistivity distributions in the 27 wells used for petrophysical evaluation. An example well is shaded in purple. No normalization was conducted. Cumulative frequency is also displayed. Resistivity is displayed in Ohm-meters.

Appendix L

Equations in Petrophysical Modeling

Modified From

The Log Analysis Handbook (Quantitative Log Analysis Methods)

E. R. Crain

Calculation 1: Lithology

STEP 1: Calculate shale density and shale capture cross section (a constant for each zone):

$$1: RHOBSH = PHIDSH * KD1 + (1 – PHIDSH) * KD2$$

$$2: UmaSH = PESH * RHOBSH$$

NOTE: PHIDSH and DENSSH are constants for each zone, chosen from the density log in a 100% shale layer.

STEP 2: Convert density porosity to density units for each layer, if necessary:

$$3: RHOB = PHID * KD1 + (1 – PHID) * KD2$$

Where: KD1 = 1.00
KD2 = 2.65 for Sandstone scale
KD2 = 2.71 for Limestone scale

NOTE: Density data is needed in English units (g/cm^3), not fractional units.

STEP 3: Calculate matrix capture cross section for each layer:

$$4: Uma = (PE * RHOB – Vsh * UmaSH) / (1 – PHIe)$$

STEP 4: Calculate three mineral rock volumes from Uma and RHOMAND:

$$5: D = (Uma * (RHOMA2 – RHOMA1) + RHOMAND * (UMA1 – UMA2) + UMA2 * RHOMA1 – UMA1 * RHOMA2) / (UMA1 * (RHOMA3 – RHOMA2) + UMA2 * (RHOMA1 – RHOMA3) + UMA3 * (RHOMA2 – RHOMA1))$$

$$6: E = (D * (RHOMA3 – RHOMA1) – RHOMAND + RHOMA1) / (RHOMA1 – RHOMA2)$$

$$7: Min1 = MAX(0, 1 – D – E) / (MAX(0, 1 – D – E) + MAX(0, D) + MAX(0, E))$$

$$8: Min2 = MAX(0, E) / (MAX(0, 1 - D - E) + MAX(0, D) + MAX(0, E))$$

$$9: Min3 = 1 – Min1 – Min2$$

Where: RHOBSH = density log reading in 100% shale (g/cm^3 or Kg/m^3)
PHIDSH = density log reading in 100% shale (fractional)
KD1 = gas correction factor for density porosity (fractional)
KD2 = gas correction factor for density porosity in a sandstone or limestone matrix (fractional)
UmaSH = photoelectric absorption cross section in 100% shale ($barns/cm^3$)

PESH = photoelectric log reading in 100% shale (barns/electron)
RHOB = density log reading (g/cm^3 or Kg/m^3)
PHID = density porosity log reading (fractional)
Uma = computed matrix photoelectric absorption cross section (barns/cm^3)
UMA1 = photoelectric absorption cross section of 1st mineral (barns/cm^3)
UMA2 = photoelectric absorption cross section of 2nd mineral (barns/cm^3)
UMA3 = photoelectric absorption cross section of 3rd mineral (barns/cm^3)
PE = effective photoelectric cross section (barns/cm^3)
Vsh = shale volume from any method (fractional)
PHIe = effective porosity (fractional)
Min1 = volume of Mineral 1 (fractional)
Min2 = volume of Mineral 2 (fractional)
Min3 = volume of Mineral 3 (fractional)
RHOMA1 = density log reading in 1st mineral (g/cm^3 or Kg/m^3)
RHOMA2 = density log reading in 2nd mineral (g/cm^3 or Kg/m^3)
RHOMA3 = density log reading in 3rd mineral (g/cm^3 or Kg/m^3)
RHOMAND = calculated matrix density (g/cm^3 or Kg/m^3)
D = intermediate term in equation (unit-less)
E = intermediate term in equation (unit-less)
MAX(a, b) means to take the larger of a or b

Calculation 2: Porosity

Prior to calculations, convert density to density porosity units, if necessary:

$$\text{PHID} = (\text{RHOB} - \text{KD2}) / (\text{KD1} - \text{KD2})$$

Where: KD1 = 1.00 for English units
KD1 = 1000 for Metric units
KD2 = 2.65 for English units Sandstone log scale
KD2 = 2650 for Metric units Sandstone log scale
KD2 = 2.71 for English units Limestone log scale
KD2 = 2710 for Metric units Limestone log scale
KD2 = 2.87 for English units Dolomite log scale
KD2 = 2870 for Metric units Dolomite log scale

NOTE: The choice for KD2 must match the neutron log units – if neutron is in limestone units, KD2 must be 2.71 for g/cm^3 or 2710 for Kg/m^3 log scale.

STEP 1: Shale correct the density and neutron log data for each layer:

$$1: \text{PHIdc} = \text{PHID} - (\text{Vsh} * \text{PHIDSH})$$

$$2: \text{PHInc} = \text{PHIN} - (\text{Vsh} * \text{PHINSH})$$

Note: PHIDSH and PHINSH are constants for each zone, and are picked only once.

STEP 2: Check for gas crossover after shale corrections and calculate porosity for each layer from the correct equation:

3: IF $\text{PHInc} >= \text{PHIdc}$, there is no gas crossover
THEN $\text{PHIxdn} = (\text{PHInc} + \text{PHIdc}) / 2$

If gas is known to be present AND gas crossover occurs after shale corrections, apply the following gas correction:

4: IF $\text{PHInc} < \text{PHIdc}$, there is gas crossover
THEN $\text{PHIxdn} = ((\text{PHInc} \wedge 2 + \text{PHIdc} \wedge 2) / 2) \wedge 0.5$

The density neutron crossplot porosity, PHIxdn, after all corrections are applied, is called the effective porosity, PHIe.

Where: PHIdc = porosity from density log corrected for shale (fractional)
PHInc = neutron porosity corrected for shale (fractional)
PHID = density log reading (fractional)
PHIDSH = density log reading for 100% shale (fractional)
PHIN = neutron porosity log reading (fractional)
PHINSH = neutron log reading for 100% shale (fractional)

PHIxdn = porosity from density neutron crossplot (fractional)
PHIe = effective porosity (fractional)
BVWsh = bulk volume of water bound to 100 % shale (fractional)
PHIt = total porosity from any log (fractional)
PHID = density log reading (fractional)
PHIN = neutron porosity log reading (fractional)

Calculation 3: Material Balance for Porosity

Bad hole, high shale volume, and statistical variations can cause erratic results in both very low and high porosities. Values from any method used should be trimmed by the following:

1: IF PHIe < 0
THEN PHIe = 0

2: IF PHIe > PHIMAX * (1 - Vsh)
THEN PHImx = PHIMAX * (1 - Vsh)

AND PHIe = Min (PHIe, PHImx)

Where: PHIe = effective porosity (fractional)
PHIMAX = maximum expected porosity in clean rock (fractional)
PHImx = effective porosity from PHIMAX method (fractional)

Calculation 4: Water and Gas Saturation

STEP 1: Calculate water saturation:

1: PHIt = (PHID + PHIN) / 2

2: Rwa = (PHIt ^ M) * RILD / A

3: SWa = (Rw/ Rwa) ^ (1 / N)

4: Sw = SWa

The water saturation from the Archie method (SWa) is called the effective water saturation, Sw.

STEP 2: Calculate gas saturation:

5: Sg = 1 – Sw

Where: PHIt = total porosity from any log (fractional)
PHID = density log reading (fractional)
PHIN = neutron porosity log reading (fractional)
RWa = apparent water resistivity (ohm-m)
M = cementation exponent
RILD = deep resistivity log reading (ohm-m)
A = tortuosity factor
SWa = water saturation from Archie method (fractional)
Rw= water resistivity at formation temperature (ohm-m)
N = saturation exponent
Sw = calculated effective water saturation (fractional)
Sg = calculated gas saturation (fractional)

Appendix M

Petrophysical Model and Blind Study Correlation Results